TAMPEREEN TEKNILLINEN YLIOPISTO
TAMPERE UNIVERSITY OF TECHNOLOGY

JUSSI PEURALA

MODEL-BASED DESIGN, MODELLING AND SIMULATION OF DIGITAL HYDRAULIC GAS ADMISSION VALVE

Master of Science Thesis

Examiner: Adj. Prof. Matti Linjama
Examiner and topic were approved by the Faculty Council of the Faculty of Engineering sciences on 6th of March 2014

TIIVISTELMÄ

TAMPEREEN TEKNILLINEN YLIOPISTO
Konetekniikan koulutusohjelma
PEURALA, JUSSI: Model-Based Design, Modelling and Simulation of Digital Hydraulic Gas Admission Valve
Diplomityö, 132 sivua, 12 liitesivua
Toukokuu 2014
Pääaine: Hydrauliikka ja automatiikka, hydraulitekniikka
Tarkastaja: Dosentti Matti Linjama
Avainsanat Digitaalihydrauliikka, pneumatiikka, pääkaasuventtiili, mallipohjainen suunnittelu, CFD

Kaasumoottorin pääkaasuventtiili on strategisesti tärkeä komponentti. Hyvän venttiilin ominaisuuksiin kuuluvat esimerkiksi pieni vasteaika, suuri läpäisy, mahdollisuus toimia suurellakin paine-erolla ja vikasietoisuus. Nykyisen solenoidiohjatun pääkaasuventtiilin vasteaika on pieni ja virtauskapasiteetti suuri, mutta suurin ongelma on se, ettei venttiili avaudu jos paine-ero venttiilin yli on liian suuri.

Tämän työn tarkoituksena on suunnitella, mallintaa ja simuloida uudentyyppinen pääkaasuventtiili, joka hyödyntää digitaalisuuden periaatetta. Työn sovelluksessa imuventtiiliin on integroitu kaasu-urat, joiden kautta kaasu pääsee virtaamaan moottorin sylinteriin. Imuventtiilin ohjaus toteutetaan digitaalihydrauliikalla.

Työn toisena sovelluksena esitellään digitaalipneumaattinen pääkaasuventtiili. Digitaaliventtiili on toteutettu binäärikoodattuna digitaalisena tilavuusvirransäätöyksikkönä.

Kuten työn tulokset osoittavat, digitaalihydraulinen imuventtiili kaasu-urilla on realistinen konstruktio. Sekä virtaus- että simulointitulokset osoittavat, että konstruktio on toimiva ja valmistuskelpoinen.

Tämä diplomityö on tehty osana FIMECC EFFIMA -Digihybrid –tutkimusprojektia. FIMECCin tarkoituksena on lisätä ja syventää yhteistyötä yritysten, yliopistojen ja tutkimusinstituuttien tutkimus- ja kehitysosastojen välillä. EFFIMAn tarkoituksena on kehittää energiatehokkaita koneita ja laitteita ja energiatehokkuus on projektin avainsana. Tässä työssä energiatehokkuus on toteutettu älykkäällä ohjaustavalla säästäen energiaa.

ABSTRACT

TAMPERE UNIVERSITY OF TECHNOLOGY
Master's Degree Programme in Mechanical engineer
PEURALA, JUSSI: Model-Based Design, Modelling and Simulation of Digital Hydraulic Gas Admission Valve
Master of Science Thesis, 132 pages, 12 Appendix pages
May 2014
Major: Hydraulics and automation, fluid power
Examiner: Adj. Prof. Matti Linjama
Keywords: Digital hydraulics, pneumatics, gas admission valve, model-based design, CFD

Gas admission valve is strategically important component on gas engine. Short response time, large flow rate capacity through the valve, ability to work at large pressure difference and fault tolerant are characteristics that a good valve should be fulfilled. The solenoid based gas admission valve used at the moment has short response time and large flow rate capacity but the main problem is that if pressure difference over the valve is too large, the valve will not open.

The goal of this thesis is to design, model and simulate a new gas admission valve which utilizes the principle of digitalization. The application of the thesis is an intake valve which has been integrated gas flow edges. Through the flow edges the gas flows into the engine's cylinder. The control of the intake valve is realized by using digital hydraulics.

The second application of the thesis is digital pneumatic gas admission valve. The valve is realized by using binary coded digital flow control unit.

As the results show, digital hydraulic intake air valve with gas flow edges is a realistic construction. Both flow and simulation results indicate that the construction is functional and possible to manufacture.

This thesis has been done as a part of FIMECC EFFIMA Digihybrid research project. The target of FIMECC is to increase and deepen the cooperation between companies, universities and research institutes in R&D. The target of EFFIMA is to develop energy efficient machines and devices and the key word of the project is energy efficient. In this thesis energy efficient has been realized by using intelligent controller.

PREFACE

This thesis was done for Wärtsilä Finland R&D Research & Innovation Management under the program Intelligent Engine where the program manager is Jonatan Rösgren. I want to thank my thesis supervisor Harry Särs for giving me this opportunity to work at Wärtsilä. We both taught each other many new things. I hope that we can be friends also in the future. I want also thank Håkan Nynäs. You gave me so many new ideas and you taught me to think in a new way. Antonino Di Miceli and Lars Ola Liavåg deserve special thanks about CFD results. Jari Hyvönen and Daniel Häggblom, thank you about the initial idea of gas flow edges and conversations during the work. I would like to thank also my examiner Matti Linjama for examine the thesis.

I would like to thank my friends and my sisters Hanna and Emma. You have always helped me on good and bad times and gave me energy during the studying.

My deepest thanks belong to my parents, Tuula and Antti: Without you I could not ever been graduated to Master of Science in Engineering. I dedicate this thesis to you!

In Vaasa, 14.4.2014

_____

Jussi Peurala

CONTENTS

SYMBOLS AND ABBREVIATIONS

Variables

a	Acceleration	m/s^2
a_e	Amount of gas flow edges	-
A	Outlet of cross sectional area	m^2
A_A	A-chamber area	m^2
A_B	B-chamber area	m^2
A_m	Flow area of poppet valve	m^2
A_{gas}	Gas flow area	m^2
A_{real}	Real gas flow area	m^2
A_T	Flow area for defining discharge coefficient	m^2
A_1	Area of inner gas flow edge	m^2
A_2	Area of outer gas flow edge	m^2
b	Viscous friction coefficient	Ns/m
b_{gas}	Critical pressure ratio of gas	-
B_{eff}	Bulk modulus of oil	Pa
β	Poppet valve seat angle	°
C_d	Discharge coefficient	-
C_{ve}	Sonic conductance	$m^3/(s*Pa)$
d	Inner diameter of restriction	m
D_i	Inner seat diameter	m
D_m	Poppet valve mean seat diameter	m
D_p	Poppet valve port diameter	m
D_s	Poppet valve stem diameter	m
D_T	Diameter for defining flow area A_T	m
D_v	Poppet valve head diameter	m
ε	Relative uncertainly of step size	-
E	Energy	J
E_{cons}	Hydraulic energy consumption	J
E_{in}	Input hydraulic energy	J
E_{out}	Output hydraulic energy	J
F	Force	N
F_c	Coulomb friction force	N
$F_{damping}$	Damping force	N
F_{est}	Estimated cylinder force	N
$F_{friction}$	Friction force	N
F_s	Static friction force	N
F_{maxR}	Maximum retracting force	N
F_{min1R}	Minimum mode -1 force	N
F_{min2R}	Minimum mode -2 force	N

F_{minE}	Minimum extending force	N
F_{max1E}	Maximum mode 1 force	N
F_{max2E}	Maximum mode 2 force	N
F_{tol}	Force tolerance of controller	N
$G_p(s)$	First-order transfer function	-
$G_0(s)$	Zero-order hold transfer function	-
G(z)	Z-transformed transfer function	-
γ	Heat capacity ratio	-
h_1	Height of inner edge	m
h_2	Height of outer edge	m
I	Current	A
I_x	Inertia	m^2*kg
K	Coefficient of tanh friction equation	-
K_v	Specific flow coefficient of valve	$m^3/(s \cdot \sqrt{Pa})$
K_{vAT}	Flow coefficient of DFCU-AT	$m^3/(s \cdot \sqrt{Pa})$
K_{vBT}	Flow coefficient of DFCU-BT	$m^3/(s \cdot \sqrt{Pa})$
K_{vPA}	Flow coefficient of DFCU-PA	$m^3/(s \cdot \sqrt{Pa})$
K_{vPB}	Flow coefficient of DFCU-PB	$m^3/(s \cdot \sqrt{Pa})$
L	Length of restriction	m
L_v	Poppet valve lift	m
λ	Uniformity index	-
m	Weight	kg
$\dot{m}$	Mass flow	kg/s
$\dot{m}_{choked}$	Choked mass flow	kg/s
$\dot{m}_{ideal}$	Ideal mass flow	kg/s
$\dot{m}_{laminar}$	Laminar mass flow	kg/s
$\dot{m}_{real}$	Real mass flow	kg/s
$\dot{m}_{subcritical}$	Subcritical mass flow	kg/s
$\dot{m}_{subsonic}$	Subsonic mass flow	kg/s
N	Number of valves	-
p_c	Circuit of circle	m
p_1	Upstream pressure	Pa
p_2	Downstream pressure	Pa
p_A	A-chamber pressure	Pa
p_B	B-chamber pressure	Pa
p_{est}	Estimated chamber pressure	Pa
p_{Aest}	Estimated A-chamber pressure	Pa
p_{Best}	Estimated B-chamber pressure	Pa
p_{Aref}	A-chamber pressure reference	Pa
p_{Bref}	B-chamber pressure reference	Pa
p_p	Supply pressure	Pa

p_T	Tank pressure	Pa
p_{tr}	Transition pressure	Pa
p_{min}	Minimum pressure	Pa
p_{max}	Maximum pressure	Pa
Δp_{ref}	minimum pressure difference	Pa
Δp_{nom}	Nominal pressure difference	Pa
$\dot{p}$	Pressure change	-
P	Power	W
P_{in}	Input hydraulic power	W
P_{loss}	Hydraulic power loss	W
P_{out}	Output hydraulic power	W
Q	Flow rate (Q_{PA}, Q_{AT}, Q_{PB}, Q_{BT})	m^3/s
Q_{nom}	Nominal flow rate	m^3/s
r	Radius	m
rpm	Revolutions per minute	1/s
R	Ideal gas constant	J/(K·mol)
ρ_0	Density	kg/m^3
s_e	Length of gas flow edge	m
t	Time	s
t_p	Length of impulse	s
T	Temperature	K
T_{air}	Temperature of air	K
T_c	Time constant	s
$T_{methane}$	Temperature of methane	K
T_s	Sample time	s
T_0	Length of constant or variable frequency	s
u	Opening of valves (uPA, uAT, uPB, uBT)	-
U	Voltage	V
v	Velocity	m/s
v_{tol}	Velocity threshold of controller	m/s
v_{ref}	Reference velocity	m/s
$v_{ref\ ext}$	Reference extending velocity	m/s
$v_{ref\ ret}$	Reference retracing velocity	m/s
v_s	Velocity of minimum friction	m/s
v_{sim}	Simulated velocity	m/s
V	Volume	m^3
$\dot{V}$	Change of chamber volume	-
x_c	Circle of edge	m
x_d	Distance of curve between gas flow edges	m
w	Seat width	m
W_p	Weight of pressure differences error	-
W_{sw}	Weight of valve switching	-

Abbreviations

BBDC	Before bottom dead centre
BDC	Bottom dead centre
BMEP	Brake mean effective pressure
BTDC	Before top dead centre
CFD	Computational fluid dynamics
CNG	Compressed natural gas
CPU	Central processing unit
DF	Dual-fuel
DFCU	Digital Flow Control Unit
EFFIMA	Energy and Life Cycle Cost Efficient Machines
FIMECC	Finnish Metals and Engineering Competence Cluster
GAV	Gas admission valve
GD	Gas-Diesel
HFO	Heavy fuel oil
ICE	Internal combustion engine
IHA	Department of Intelligent Hydraulics and Automation
IVC	Intake valve closing timing
IVO	Intake valve opening timing
LFO	Light fuel oil
LNG	Liquefied natural gas
LPG	Liquefied petroleum gas
MDO	Marine diesel oil
MPI	Multi-point injection
NO_x	Nitrogen oxides
PCM	Pulse Code modulation
PFM	Pulse Frequency Modulation
PNM	Pulse Number Modulation
PWM	Pulse Width Modulation
SG	Spark-ignition
SPI	Single-point injection
TDC	Top Dead Centre
UI	Uniformity index

1 INTRODUCTION

Gas engines are widely used in different applications. Even though gas engines are more environmentally friendly as conventional diesel engines, they suffer from two massive issues: methane slip and knocking. This thesis presents new ideas how it is possible to reduce these flaws. Three different gas engine types are presented: Gas-diesel, dual-fuel and spark-ignition gas engines.

In the thesis has been looked through Miller cycle and the application of the thesis is simulated by using early Miller cycle valve timings. Because of early Miller valve timings, acceleration, velocity and forces of poppet valve are much greater than using conventional four stroke or late Miller valve timings.

Single-point and multi-point systems have been studied. Single-point injection system is usually for cheap solutions as multi-point injection is a more complex system that enables more precise fuel control.

The goal of this thesis is to find a better solution to gas admission than the solution at the moment. At the moment the main problem is that if the upstream and downstream pressure ratio is too high, the valve will not open. The wanted requirements should be fulfilled and the new solution should also be able to manufacture. The new solution is thought to be used on spark-ignited gas engine and dual-fuel engine and the simulation results are done for the spark-ignited gas engine with cylinder output power 190 kW.

The new solutions utilize digital hydraulics and pneumatics. The modern increase in computational efficiency allows the utilization of digital hydraulic technology. For example, this thesis consists of model-based controllers. Because the controllers are such complex systems they require a lot of computational time and increase the cost of calculations. However, the use of modern CPU technology offers solution to reduce the costs by parallelization, for instance.

The thesis presents two different solutions: the first one is intake valve which has gas flow edges and the valve has been controlled by digital hydraulic system. The second system is digital pneumatic valve system. The both systems are done by the principle of digitalization: one big valve is replaced by a number of smaller valves. The main benefits of smaller valves are that for example the response time, inertia and needed energy of valves are much lower than using one big valve. The simulations are done using

Matlab/Simulink. At the end of the simulation results chapter energy comparisons using different digital hydraulic systems have been done and the results have been compared to conventional proportional and mechanical valve trains. CFD results of intake valve system are done cooperation with CFD experts at Wärtsilä. Also discharge coefficient and uniformity index values have been determined.

2 GAS ENGINE

The most common gaseous fuel is natural gas. In engine applications the gas can be supplied generally in two forms, commonly known as the compressed natural gas (CNG) or liquefied natural gas (LNG). Natural gas is sulphur-free and low-carbon gas, which allows gas engines to emit less CO_2 and particular matter than marine diesel engines run by heavy fuel oil [1]. The chemical composition of the natural gas is generally simplified to methane, CH_4. An additional, third source of gaseous fuel is liquefied petroleum gas (LPG). It consists of higher molecular weight components of natural gas. LPG can be liquefied under pressure at ambient temperature. The main component of LPG is n-propane having chemical representation of C_3H_8.

Methane and natural gases are excellently suited to applications of high compression ratios. It has been generally accepted that complete and homogenous mixing with air is possible with the gaseous natural fuels. This improves flame progress rates and delays the onset of combustion irregularity while the lean mixture operational limits are extended. [2]. Because of very wide diversity of gaseous fuels commonly available, optimization and prediction of combustion behaviour in engines is more complicated compared to conventional liquid fuels.

Hydrogen has unique and excellent combustion characteristics. When hydrogen is consumed in an internal combustion engine (ICE), the only remarkable air pollutants are the nitrogen oxides (NO_x). The gaseous fuels can be used either solely or as components of different mixtures with other fuels. Due to continuously increasing environmental demands and more strict emission regulations, alternative fuels should be chosen whenever available for use to minimize the harmful emissions. Moreover, most of alternative gaseous fuels have been found to have more convenient emission characteristics. [2]. When the optimum amount of air is surrounding each gas molecule and the mixture is fully mixed, the peak temperatures are reduced resulting negligible levels of NO_x during combustion. Gas engines offer high level of reliability and this is the reason why engines are developed for use on offshore oil and gas production platforms. [3].

Despite the gas engines respectfully emit 20 – 30 % less CO_2 and particular matter than marine diesels with heavy fuel oil (HFO), they suffer two massive flaws: the first is abnormal combustion called knocking and the second is methane slip. Knocking reduces the efficiency of the engine by decreasing maximum engine torque and also it may eventually lead to premature mechanical or material failure. Methane slip means that

unburned methane escapes into exhaust port during a cylinder scavenging. However, by changing the valve timings and filling the dead volumes it is possible to reduce blowing gas in overlap period and unburned gas entering the clearance volume.

2.1 Gas engine types

There are generally three kind of engines where gas can be used; gas-diesel, dual-fuel and spark-ignition engines. Gas-diesel engines can be operated on gas mode with pilot fuel and liquid fuel mode. Dual-fuel engines can be operated in two different operating modes: in gas mode and diesel mode, whereas the spark-ignition gas engines can be operated only on gas.

Figure 2.1 maps the usual operating window of gas engine. The most favourable working area is where excess air is about 2.0 - 2.2, which also followed be highest possible brake mean effective pressure (BMEP).

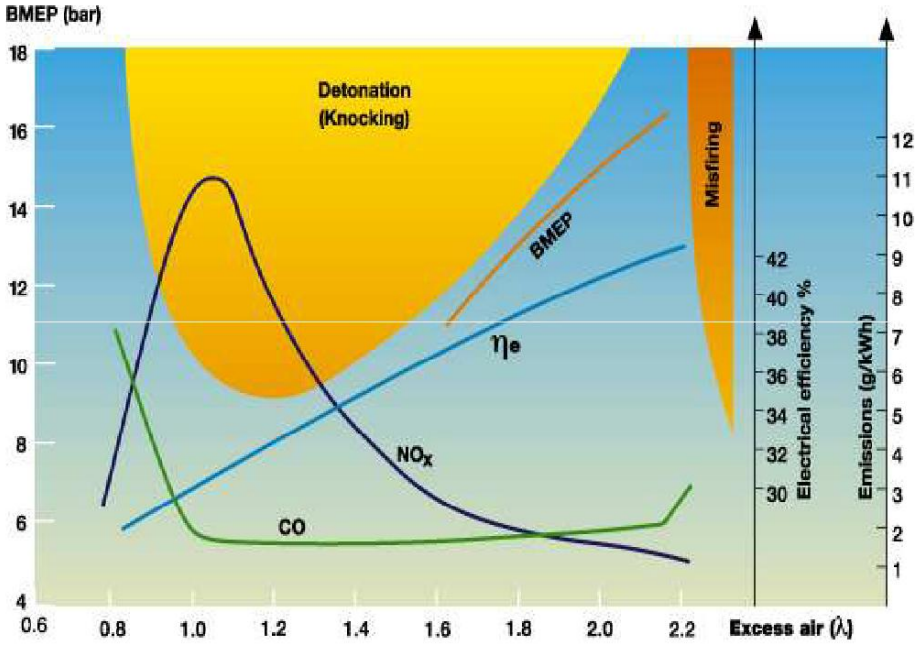

Figure 2.1. *Operating window of gas engine [4].*

Figure 2.1 shows also knocking and misfiring areas. It is clear that these areas should be avoided.

2.1.1 Gas-Diesel engine

Diesel combustion process is utilized on the gas-diesel engine where gas-diesel mixture is burnt in the engine. Gas and diesel are injected into the combustion chamber at the

end of compression stroke while the gas injection pressure is at the highest value. In a modern 4-stroke gas-diesel engine the injection pressure is rather high generally over 35 MPa [5]. Figure 2.2 illustrates the different modes of gas-diesel engine running on diesel mode.

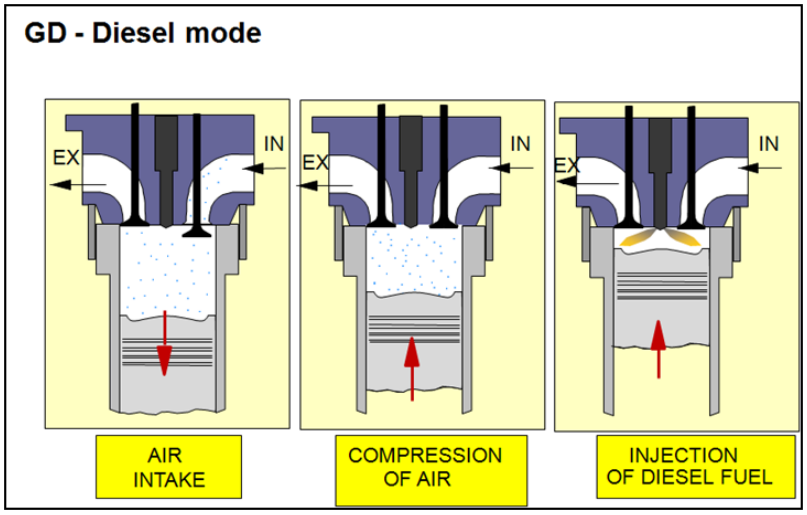

Figure 2.2. *Gas-Diesel engine, diesel mode [5].*

When the engine is running solely in the gas mode, high pressurized gas is injected into the combustion chamber and gas is ignited via pilot fuel. The amount of pilot fuel is approximately 5 % of the total fuel energy input required at full engine load. One of the advantages of a gas-diesel engine is that the process allows large variations in the gas quality. [6] A typical gas mode compression stroke is presented in figure 2.3.

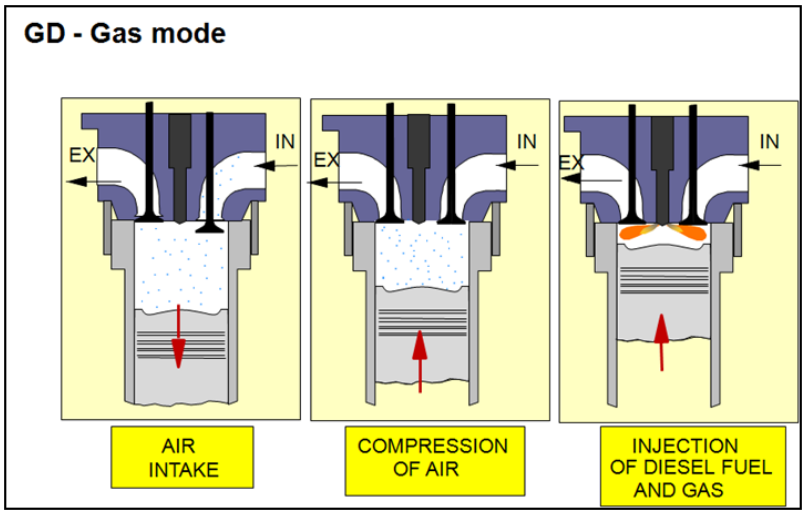

Figure 2.3. *Gas-Diesel engine, gas mode [5].*

Furthermore, it is advantageous that Gas-diesel engine can be directly without delays switched to purely liquid based operation mode. During this mode, the fuel can be either

light fuel oil, heavy fuel oil or even crude oil, which are consumed in a diesel like process. [6].

2.1.2 Dual-fuel engine

Dual-fuel engines can be operated via gas and diesel mode. In gas mode, lean-burn Otto combustion process is utilized. The gas should be fully mixed with air before entering the intake valves that admit the mixture to the combustion chamber during the intake stroke to achieve maximum efficiency. At the end of the compression stroke, a small amount of liquid pilot fuel (LFO) is injected into the combustion chamber to ignite gas-air mixture. [6]. Figure 2.4 shows the main principle of dual-fuel engine run by gas mode.

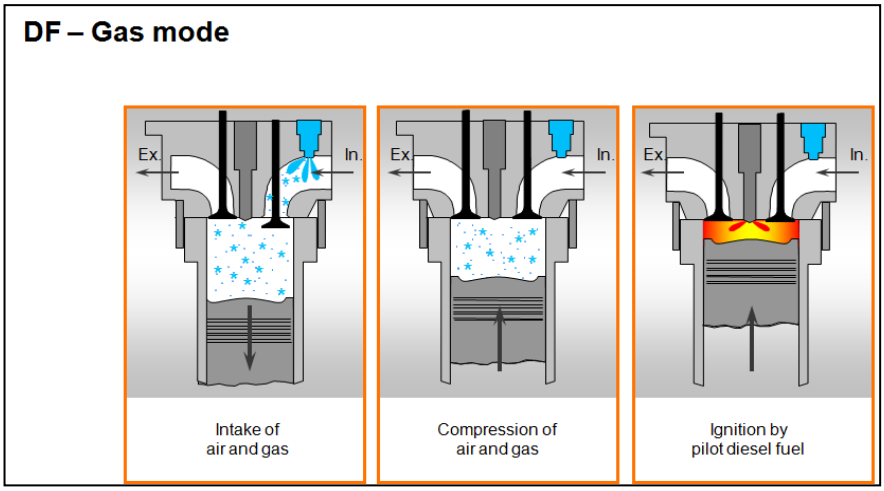

Figure 2.4. *Dual-fuel engine, gas mode [5].*

If pure diesel mode is used in the engine, the working principle of dual-fuel engine is conventional diesel process and the gas admission is ignored. Both LFO and HFO liquid fuels can be used in the process. [6]. Figure 2.5 shows the principle of dual-fuel engine run by diesel mode.

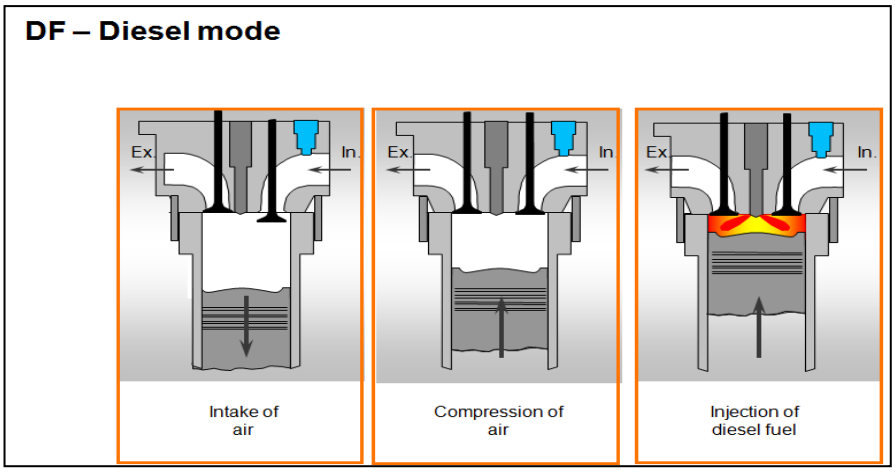

Figure 2.5. *Dual-fuel engine, diesel mode [5].*

When the engine is operated in gas mode, and supply of gas is disturbed or malfunction occurs, the engine is automatically and instantly transferred to the pure diesel mode, without loss of engine power and speed. The transition from diesel mode to gas mode can be set automatically whenever the demand is below 80 % of the load. If the HFO is being used as an additional fuel in the diesel mode, the engine will first run on MDO before transferring to gas mode. [5].

2.1.3 Spark-ignition gas engine

Spark-ignition gas engines are spark-ignited lean-burn Otto process engines. Similarly to the dual-fuel engines running in the gas mode, gas is mixed with air prior entering the inlet valves. During the intake cycle, rich gas-air mixture is injected into a small pre-chamber. At the end of the compression stroke, gas-air mixture is ignited in pre-chamber by a spark plug. The flames from the nozzle of the pre-chamber ignite gas-air mixture in the cylinder. [6]. Figure 2.6 shows principle of spark-ignition gas engine.

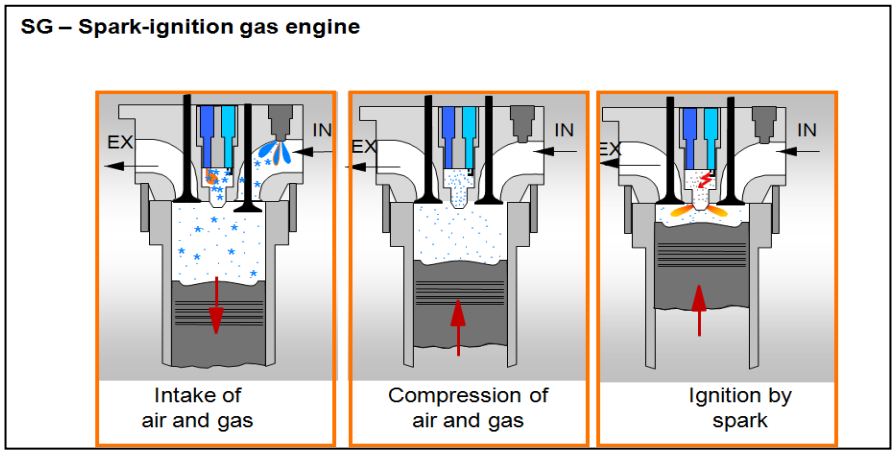

Figure 2.6. *Spark-ignition gas engine [5].*

Spark-ignition engines can run only on gas. In addition, the gas is required constantly to maintain a reasonable quality in order to ensure availability of the full engine output [5].

2.2 Miller cycle

The basic idea of the Miller cycle is to achieve lower compression than expansion ratio by valve timing. The initial idea of Miller cycle was introduced in 1947 by Ralph Miller. Originally the Miller cycle was intended to limit the peak cylinder pressure without shortening the expansion stroke while retaining decent efficiency. Commonly there are three different ways to realise the Miller cycle; Late intake valve closure, early intake valve closure and opening the exhaust valve during compression stroke [7]. All of these three methods decrease the effective compression ratio without influencing the expansion ratio.

The main principle of the late Miller cycle is that the intake valves are not closed entirely at the beginning of the compression stroke. Late Miller cycle depends greatly on turbocharger because the compression stroke is partly carried out against the back-pressure from the intake manifold. The turbocharger's overpressure prevents the air-fuel mixture flow back to the intake manifold. Consequently, without a turbocharger some of air-fuel mixture would flow back to intake manifold. To gain more efficient engine process the pressurized air from the turbocharger is run through an intercooler which lowers the boost air temperature. [8]. According to equation of ideal gas law, $pV = nRT$, when temperature T is lower, volume V or pressure p should also be lower. Due to the fact that the turbocharger is capable to produce pressure that can be considered almost constant into the intake manifold, volume should therefore be smaller because mixture of air-fuel is compressed into a more dense state. Furthermore, turbocharger increases efficiently since less energy is needed when the piston compresses air-fuel mixture against turbocharger than against cylinder walls and pumping losses remains lower than without turbocharger [8]. It has also been found that the peek temperature during the Miller's cycle are decreased which reduces probability of NO_x formation. Additional control over the reduction of NO_x formation can be achieved by higher compression ratio and slight alternations in the fuel injection timing. The peek temperature should remain below 1200 °C, where the NO_x formation is known to occur. [9]. Principle of the late Miller cycle is presented in figure 2.7.

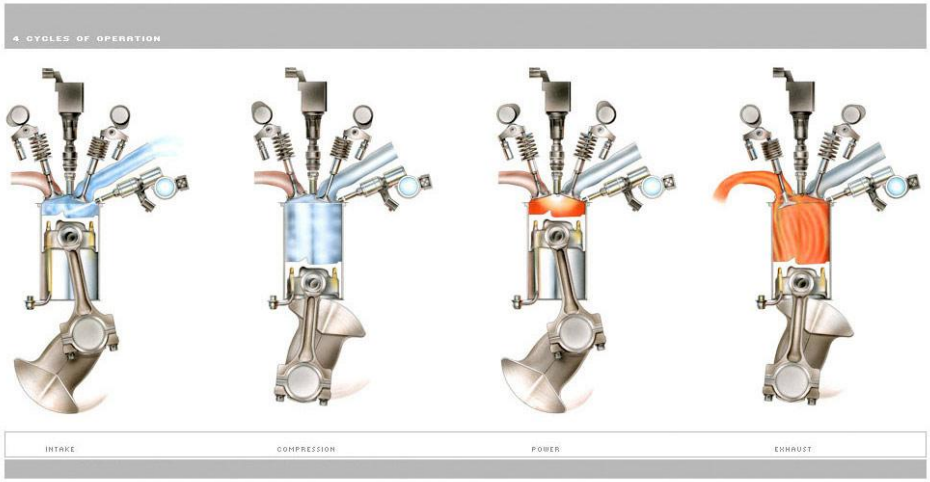

Figure 2.7. *Late intake valve Miller cycle [8].*

Figure 2.7 shows that during the compression stroke, crankshaft angle is non-zero. Piston's wrist pin, the big end of connecting rod and the main journals of the crankshaft are not vertically aligned and also the intake valve remains slightly open. The angle of crankshaft creates leverage that gives an additional momentum means that the crankshaft has a greater mechanical advantage during intake charge compression. Using late intake valve Miller cycle, crankshaft angle can be rotated nearly 70 degrees before intake valve closes [8]. It is quite different to a conventional Otto-cycle engine in which the compression stroke begins immediately when the piston reaches the bottom dead centre.

The result of shorter compression ratio of Miller cycle is increased expansion ratio. Regardless that the Miller cycle consumes energy in squeezing the intake charge for compression stroke, still the cycle results in higher torque [8]. Since higher torque is available in the engines using the Miller cycle, smaller displacement is able to facilitate the same power and torque. Miller cycle reduces the power needed to run engine by 10% to 15% [9].

The early Miller cycle is similar to the late Miller cycle. The main difference between these cycles is that whenever the early Miller cycle is utilized, the intake valves are closed before bottom dead centre of the cylinder. Using the early Miller cycle, velocity, acceleration and forces are significantly greater because there is less time to open and close the intake valves. In this work, the simulation results presented in chapter 5 are done using the principle of the early Miller cycle. Figure 2.8 presents the principle of the early closing intake valve Miller cycle.

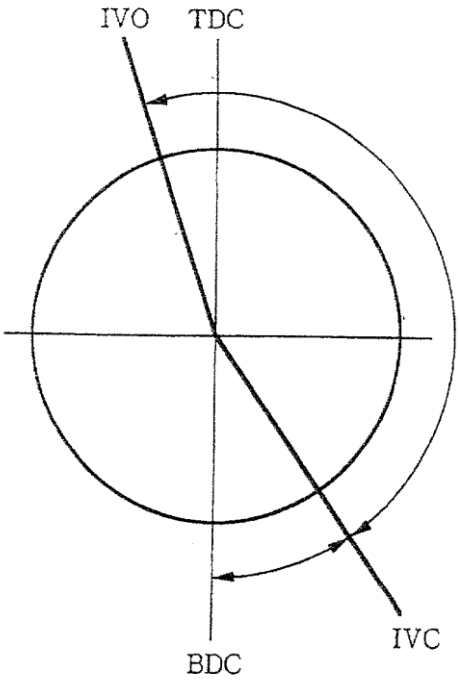

Figure 2.8. *Early closing intake valve Miller cycle [10].*

The figure 2.8 shows the intake valve timing diagram, where the intake valves are opened (IVO) before top dead centre (TDC) and the valves are closed (IVC) before bottom dead centre (BDC). In the situation shown in figure 2.8, the crack offset is zero.

2.3 Methane burning equations

The following equation shows chemical equation of methane when it is burnt.

$$CH_4[g] + 2O_2[g] \rightarrow CO_2[g] + 2H_2O[l] + 891\ kJ \quad (1)$$

As equation (1) shows, one mol of methane releases 891 kJ of energy [11]. Haataja [12] presents fuel burning process equations of hydro carbon. The following equations present burning process of carbon and hydrogen with oxygen. Equations include also molar masses.

Carbon: $C(12) + O_2(32) = CO_2(44)$ (2)

Hydrogen: $2H_2(4) + O_2(32) = 2H_2O(36)$ (3)

Methane consists of carbon and hydrogen. Equation for methane mass unit:

$$C + H = 1\ mass\ unit \quad (4)$$

When equations (2) and (3) with molar masses are multiplied with inverse of carbon (C/12) and hydrogen (H/4), the following equation is given:

$$C + H + \frac{32}{12}C + \frac{32}{4}H = \frac{44}{12}C + \frac{36}{4}H \quad (5)$$

Equation (6) shows the coefficients of carbon and hydrogen for needed amount of oxygen:

$$\frac{32}{12}C + \frac{32}{4}H = \frac{8}{3}C + 8H \quad (6)$$

When it is assumed that air consists of 23 weight percent of oxygen, the following equations show needed amount of air:

$$L_0 = \frac{8}{0.23*3}(C + 3H) \quad (7)$$

The following table 2.1 shows coefficients for C and H. Coefficients are defined by using molar mass of methane and compare the value with molar masses of carbon and hydrogen.

Table 2.1. *Carbon and hydrogen coefficients*

Methane molar mass	$4 * 1.008\frac{g}{mol} + 12.01\frac{g}{mol} = 16.042\frac{g}{mol}$
Carbon coefficient	$12.01\frac{g}{mol} \Big/ 16.042\frac{g}{mol} = 0.7487$
Hydrogen coefficient	$4 * 1.008\frac{g}{mol} \Big/ 16.042\frac{g}{mol} = 0.2513$

Equation (8) shows that theoretical amount of air is 17.4 gram when 1 gram of methane is burnt.

$$L_0 = \frac{8}{0.23*3}(0.7487 + 3 * 0.2513) = 17.4214 \quad (8)$$

As figure 2.1 shows, excess air should be about 2.1 so that knocking and misfiring would not occur and NO_x and CO emissions remain as small as possible. The amount of air can be calculated by:

$$L = \lambda * L_0 = 2.1 * 17.4214 = 36.5849 \quad (9)$$

As the equation shows, the amount of air should be about 36.6 gram when 1 gram of methane is burnt.

2.4 Gas injection systems

The gas injection system has a major contribution to the modern gas engine's environment friendliness and efficiency. In this section, two different injection systems, the single-point injection (SPI) and multi-point injection (MPI), are compared in terms of their properties related to the environment and engineering aspects. The single-point injection system is a simple and often cheap solution with only one gas injector whereas in the multi-point injection system the engine employs an injector to each cylinder that can be separately configured during the different phases of the engine cycle.

The multi-point injection system has greater advantages over the emissions because the multi-point injection reduces emissions due to more controlled environment in burning process. For example, an electronic injection system with high-speed valves can be used to change gas amount cycle by cycle. [13]. Depending on the use of the engines, it is also possible to use the combination of single-point injection and multi-point injection. The most distinctive difference between the single-point and multi-point injection system is that main gas mass flows through a single-point injection to the engine and each cylinder has own valves to control precise gas amount whereas the multi-point injection is more complex system. [14] When the flow areas of injector nozzles are constant in the single-point system, the mass flow through an injector is almost constant at constant pressure [12].

Table 2.2 presents the most crucial parameters and differences between the single-point and the multi-point injection. Originally the table has been presented by Qiang et al [13].

Table 2.2. *The comparison of single-point and multi-point injection systems [13]*

	Single-point injection	Multi-point injection
Flexible	Poor	Good
Software complexity	No	Yes
Hardware structure	Simple	Complex
Installation	Easy	Difficult
Cost	Low	High

According to the variables presented in the table 2.2, the fundamental of the construction and simplicity of the single-point injection shows many benefits. However, due to

the modern requirements in efficiency and especially in emissions, the multi-point injection allows more precise control over the engine process.

Qiang et al. [13] reported that multi-point injection reduces HC and CO emissions compared to the single-point injection because the MPI can prevent escape of the natural gas during the overlap period. Figure 2.9 shows the comparison between single-point and multi-point injection.

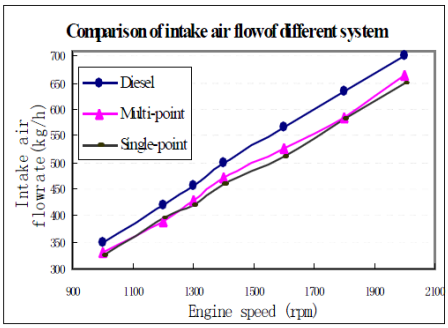

Fig.4 Comparison of intake flowerate

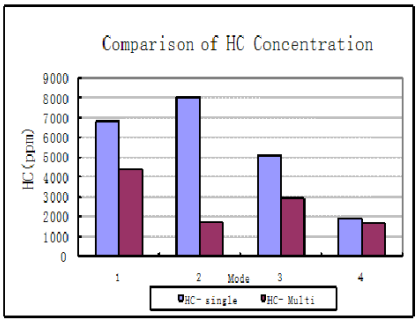

Fig.5 Comparison of exhaust HC

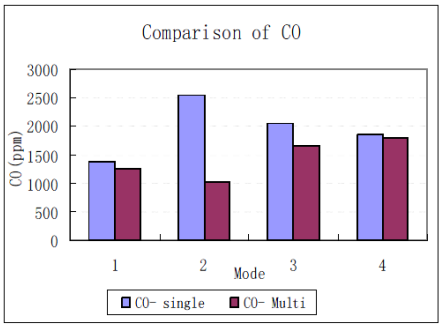

Fig.6 Comparison of exhaust CO

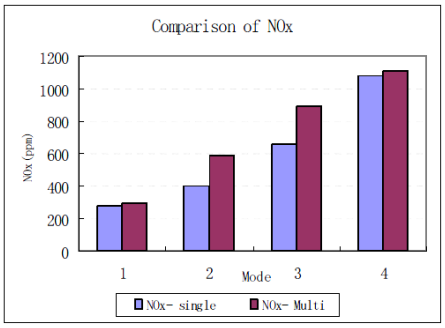

Fig.7 Comparison of exhaust NOx

Figure 2.9. *Comparison of SPI and MPI [13].*

As figure 2.9 shows, HC and CO emissions are reduced by using MPI. However, NO_x emissions will be increased.

2.4.1 Single-point injection

Single-point injection is based on only one injection valve. The injection valve feeds every cylinder on engine and the injection amount is proportional to opening of valve. Single-point injection system has only a throttle potentiometer, air-flow meter is not required. Additionally, the benefits are that the fuel supply pump is more reasonable priced, system acts on a lower supply pressure, lower vapour development and often distance between heat-stressed parts is larger. Hence, single-point injection systems are usually for low-cost systems. [14].

Figure 2.10 shows a schematic where a single-point injector is located after turbo compressor. However, the single-point injection can be also located before compressor. Then the main benefit is that the gas is not required anymore to be pressurized prior to the intake manifold since the compressor has already pressurized the gas.

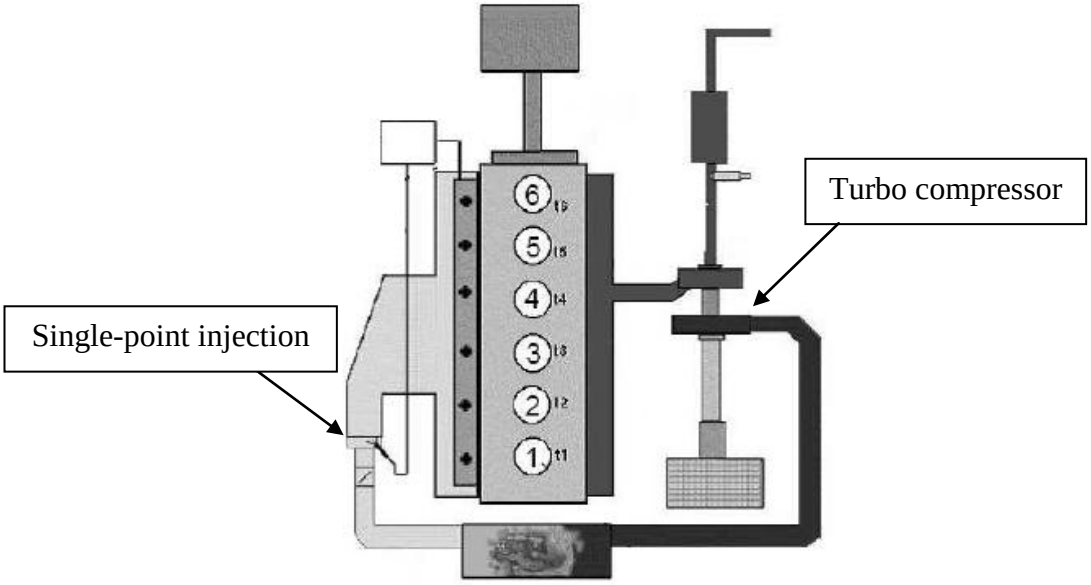

Figure 2.10. *Single-point injection after turbo compressor. Modified from original [15].*

Due to the valve overlapping period, some gas-air mixture will be escaped to the exhaust port [13]. The single-point system, however, does not allow scavenging of combustion gases without increasing emissions using mechanical valve train.

2.4.2 Multi-point injection

The multi-point injection system has own injectors to each cylinder. The advantages of the multi-point injection are the increased power and torque because of improved volumetric efficiency and more precise fuel injection. Moreover, the response of engine is more rapid when throttle position is altered, air-fuel quality control is more precise and the cylinder-to-cylinder dependence is reduced significantly [13]. The control of fuel-air equivalence is more precise during a cold-start and engine warm-up. The amount of fuel injected per cylinder depends on the operating conditions which affect to the inputs of sensors inside the engine. [16]. Figure 2.11 shows the principle of multi-point injection.

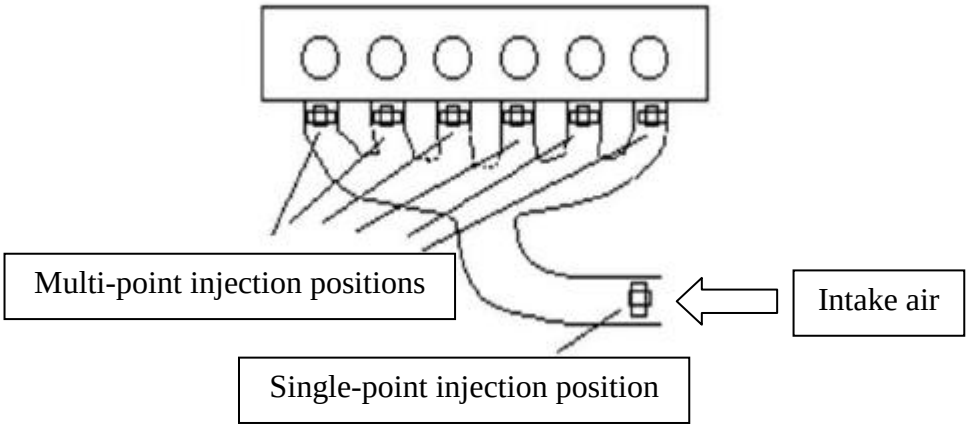

Figure 2.11. *Injection positions on engine. Modified from original [13].*

As table 2.2 shows, software structure of the multi-point injection controller is more complex than using the single-point injection. The controller of MPI requires the data from the transient speed and crankshaft position. The injection of the fuel should clearly be avoided during the overlap period to avoid excess emissions. Because different gas amount could be needed in each cylinder in each cycle, fuel quantity should be calculated. The valve injection sequence should be also verified to all injectors. In low load situations, one of the most economical ways to preserve valves and cylinders is to skip gas control. Moreover, all the cylinders are not used. [13].

2.4.3 Constructions of single- and multi-point injection systems

The above discussed single-point fuel injection system is presented in the patent (United States Patent 4257376) [17] and multi-point injection system in the patent (European patent application 1 304 477) [18]. Single-point injection system consists of fuel injector which injects a discrete, pressurized fuel pulse or charge to flow regulating device. Figure 2.12 shows the principle of single-point injection system.

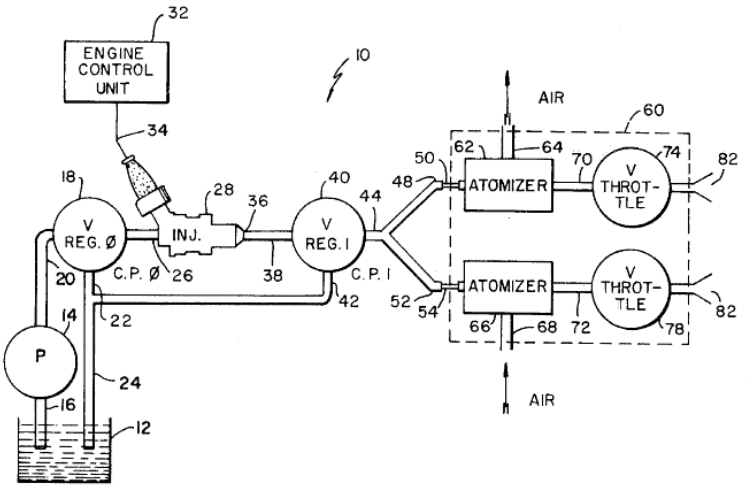

Figure 2.12. *Single injector, single point fuel injection system [17].*

The multi-point fuel injection module system consists of fuel rail and a number of injectors which delivers fuel to combustion chamber. Figure 2.13 presents the multi-point injection module. The injection module includes an electrical connector which has coupled to the fuel rail and each injector where the connector provides electrical power to each injector. The module is protected by an overmold that covers most of the fuel rail and the injectors but also electrical connectors.

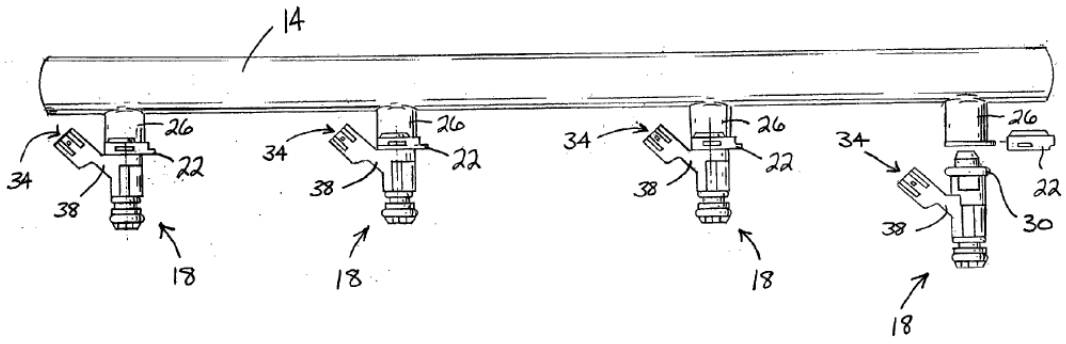

Figure 2.13. *Multi point injection module [18].*

2.5 Methane slip

The term methane slip means the unburned methane that has been escaped into the exhaust port. The sources of methane slip most often originates from the by-pass flow of the premixed gas during a valve overlap period, misfiring in a combustion chamber and flame quenching inside a boundary layer near a cylinder wall or in dead volumes around

a combustion chamber. Flame quenching inside a boundary layer consists of 50% of the total slip. Quenching distance depends strongly on the chemical properties of the pre-mixture. The reduction of the crevice volumes reduces the probability of methane slip as well. It is generally known that methane is 25 times more harmful greenhouse gas as CO_2. [1].

2.5.1 Reduction of piston topland

A volume between cylinder wall and a piston has a huge impact on the methane slip. A reduction of a piston topland has been presented by Haraldson [4]. Figure 2.14 presents the reduction of piston topland, showing the possible volume to optimization.

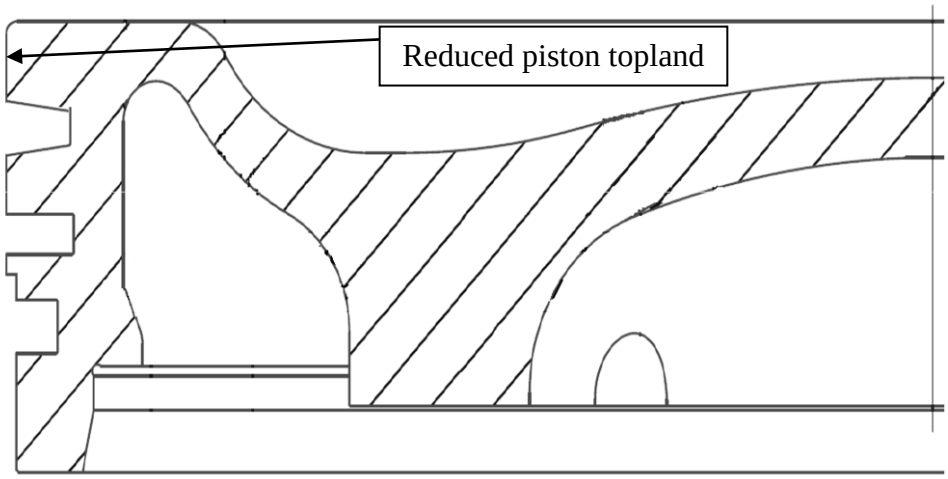

Figure 2.14. *Reduction of piston topland. Modified from original [4].*

Because of reduction of topland from 50 mm to 12 mm methane slip has reduced, for example from 8 g/kWh to 3 g/kWh by using Wärtsilä W25SG engine.

2.5.2 Quenching distance

Quenching distance is a critical diameter of a tube or critical distance between two flat plates where flame will not propagate [19]. About half of the total unburned methane is produced because of quenching distance. Most unburned methane is contained in cylinder walls because temperature of these areas is below ignition temperature of methane. [1]. Figure 2.15 presents different quenching distances with different oxygen concentrations. Longer quenching distance is produced by lower oxygen concentration because flame temperature is lower.

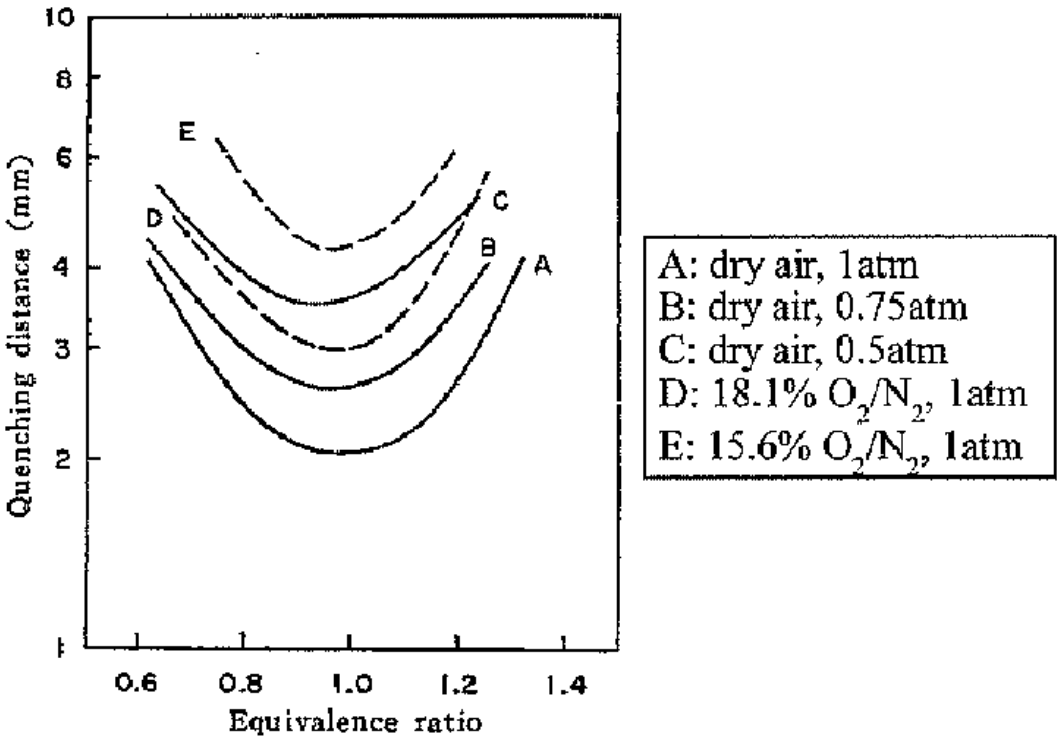

Figure 2.15. *Quenching distance with different O_2 concentration [20].*

As figure 2.15 shows, value of ambient pressure in standard atmospheres influences to the length of quenching distance. The higher is ambient pressure, the shorter is length of quenching distance.

2.5.3 Gas permeation membrane

A detailed design of gas permeation membrane has been presented by Tajima and Tsuru [1]. The main idea is to insert a membrane between a main compressor and a charge cooler. The membrane can change the composition of air and it forms unequal oxygen gradient inside a combustion chamber. Membrane separates two intake ports for oxygen enriched and nitrogen enriched air. Oxygen enriched air is pointed towards the cylinder wall which will decrease the quenching distance. Nitrogen enriched air around the cylinder centre controls the knocking tendency keeping NO_x emission at the same level. In normal conditions, O_2 concentration is 20.69 volume % and humidity 54.1 % at temperature 298 K.

Figure 2.16 presents the scheme of gas permeation membrane. The idea is to feed membrane with compressed air. When air flow through the membrane, the result is that secondary side of permeation has oxygen enriched air and primary side of permeation has nitrogen enriched air. Because oxygen is associated with faster transmission than nitrogen, oxygen enriched air flow to secondary side. [1].

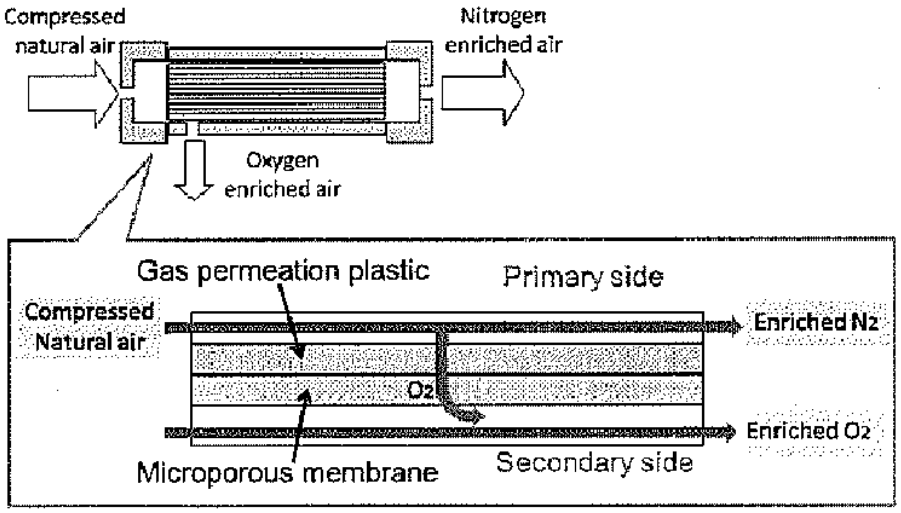

Figure 2.16. *Gas permeation membrane with primary and secondary sides [1].*

Primary side pressure affects the oxygen concentration of air. The higher is pressure in nitrogen enriched air in primary side, the lower is the oxygen concentration of air. Figure 2.17 presents a couple of oxygen concentrations in nitrogen enriched air.

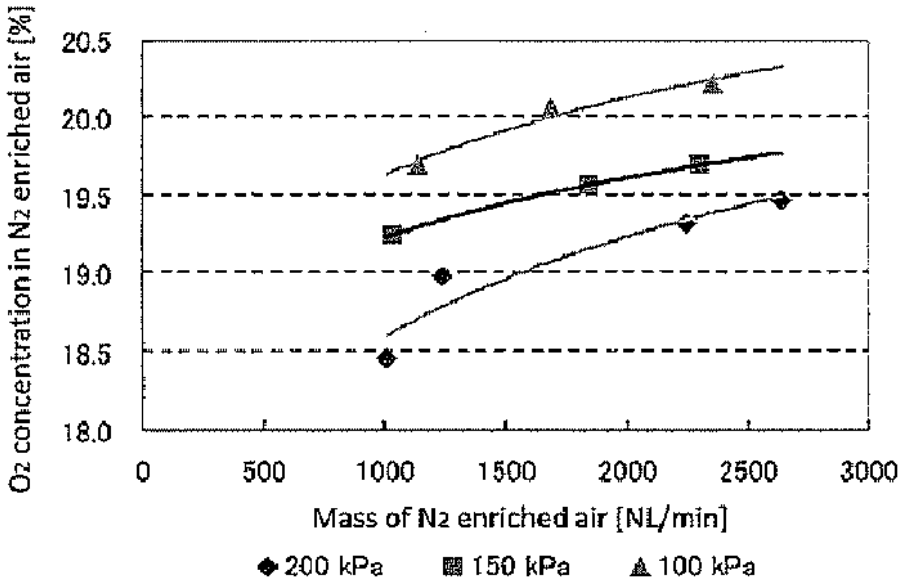

Figure 2.17. *Oxygen concentrations in nitrogen enriched air with different primary side pressures [1].*

Figure 2.18 presents the principle of feeding oxygen and nitrogen enriched air. Oxygen enriched air is injected to cylinder walls by swirl flow, nitrogen enriched air is injected directly into cylinder.

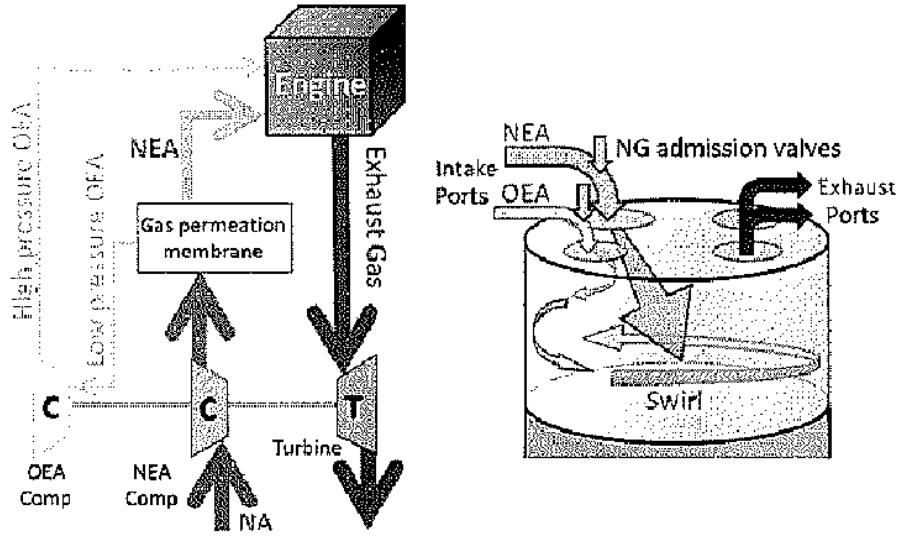

Figure 2.18. *Principle of feeding oxygen and nitrogen enriched air to engine [1].*

Table 2.3 shows different cases of methane slip, NO_x emissions and total heat release. Reduction of unburned methane increases NO_x emissions because of increased combustion temperature.

Table 2.3. *Estimated emission performance with different methane slip amounts. Modified from the original [1].*

	Methane slip [%]	Initial methane [g]	Unburned methane [g]	NO_x [mg/kg]	Total heat release [kJ]
Base	1.77	0.7559	0.0134	0.60	37.4
Case1	1.87	0.7558	0.0141	**0.49**	37.4
Case2	**1.23**	0.7558	**0.0093**	0.52	37.7
Case3	1.36	0.7559	0.0103	0.53	37.6

Figure 2.19 presents the result when air in normal conditions with 21 % oxygen is enriched to 30 %. 9 % of oxygen enrichment reduces nearly 40 % nitrogen per oxygen unit.

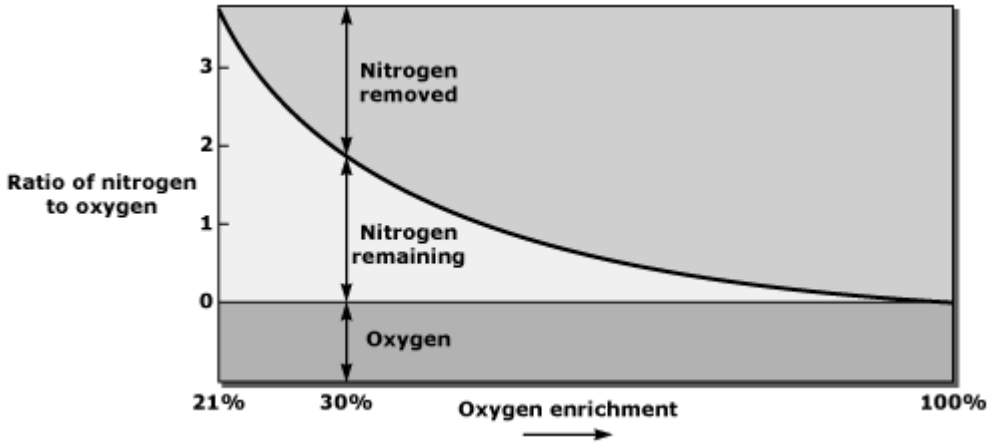

Figure 2.19. *Oxygen-enriched air from 21 % to 30 % [21].*

Oxygen enriched air near cylinder wall and nitrogen enriched air in the centre of cylinder can reduce methane slip more than 30 % [1]. Nitrogen oxides and unburned hydrocarbon emissions can be reduced efficiently with mixture formation.

2.6 Knocking on gas engine

Knocking reduces the efficiency of the engine by decreasing maximum engine torque, decreases a range of acceptable fuels but may also eventually lead to premature mechanical or material failure. Auto ignition takes the place in every cycle when the condition for borderline knock is passed. The minimum compression ratio is one of the main engine variables to induce a certain level of knock intensity. This ratio depends on a certain used fuels and operating conditions. Another indication of knocking tendency is to establish the leanest mixture that brings the onset of knocking for precise operating conditions. Also the spark timing value effects on knocking and the smallest value of spark timing can be used as indicating the tendency of fuel to knock. Increasing the compression ratio or the spark advance will increase the proportion of knocking cycles, the intensity of pressure shocks and the knocking sound. [2]. Figure 2.20 presents the knock free region limited by lean and rich operational ignition limits. Intake air and methane are unheated.

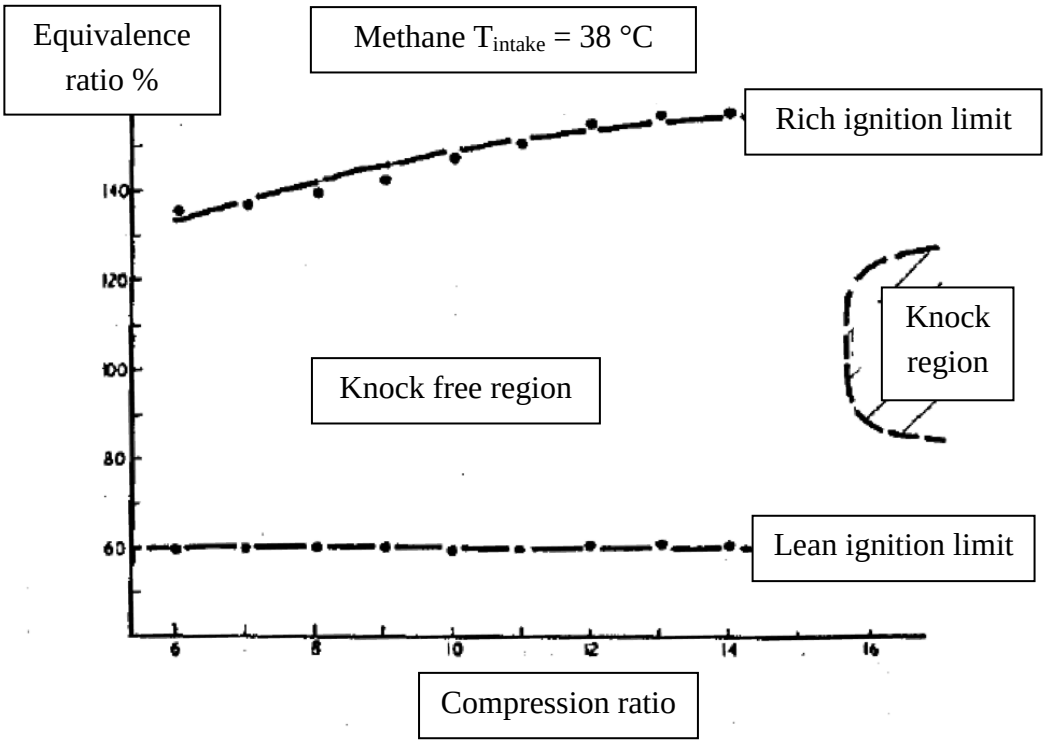

Figure 2.20. *Variation of equivalence ratio with rich and lean ignition limits at temperature 38 °C. Modified from the original [2].*

Figure 2.21 presents the knock free region when intake charge is heated. Heating the intake charge increases a lot knock region. At high compression ratios the knock free region is reduced and will reduce the available power output that can be achieved.

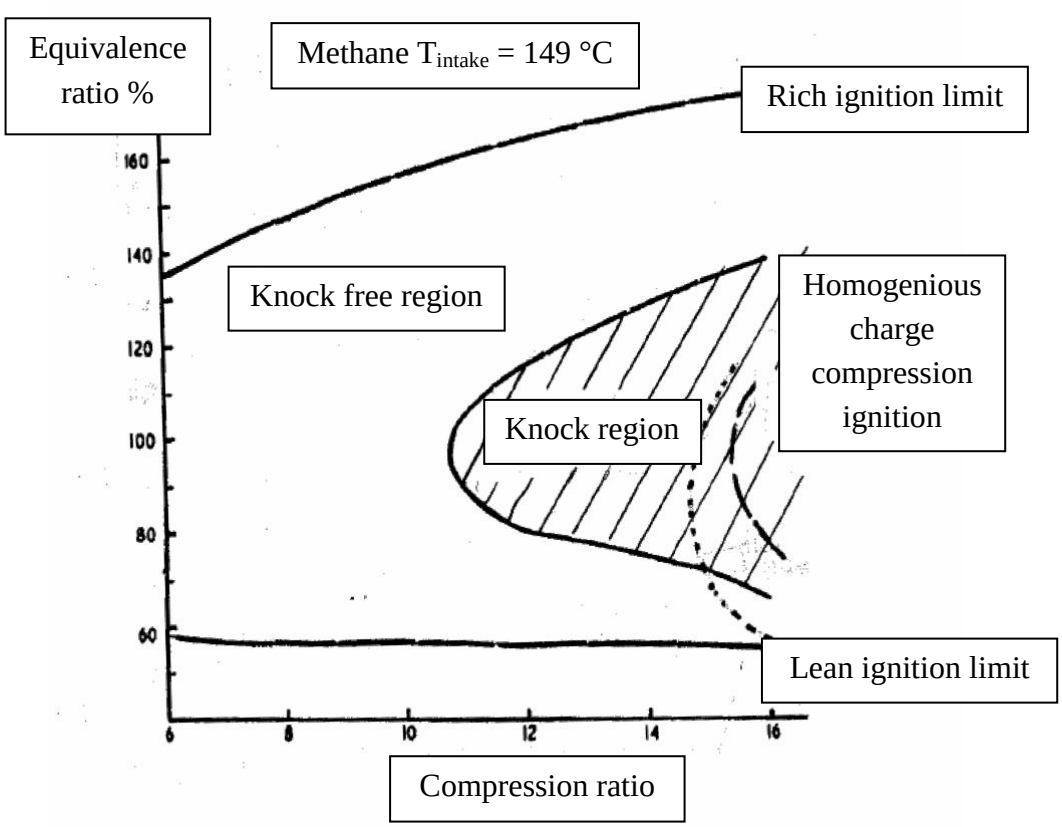

Figure 2.21. *Variation of the equivalence ratio with rich and lean ignition limits at temperature 149 °C. Modified from the original [2].*

Methane is a fuel with high resistance in tendency to knocking. Auto ignition reactions are slow and high temperature is required to auto ignition and knocking. Comparing other fuels, hydrogen as a fuel is the most prone to knocking even though it has very high flame propagation rate. This affects that very lean hydrogen mixtures can be used under knock free region and power output of engines would seriously reduced. Also gasoline is more resistant to knocking than hydrogen but significant less than methane. Dry carbon monoxide has outstanding knock resistance properties. [2].

Regardless both methane and carbon monoxide have superior resistance to knocking, mixture of methane with carbon monoxide lowers the resistance of knocking seriously. It is not reasonable to use the mixture of these gases. Figure 2.22 presents the mixture of these gases.

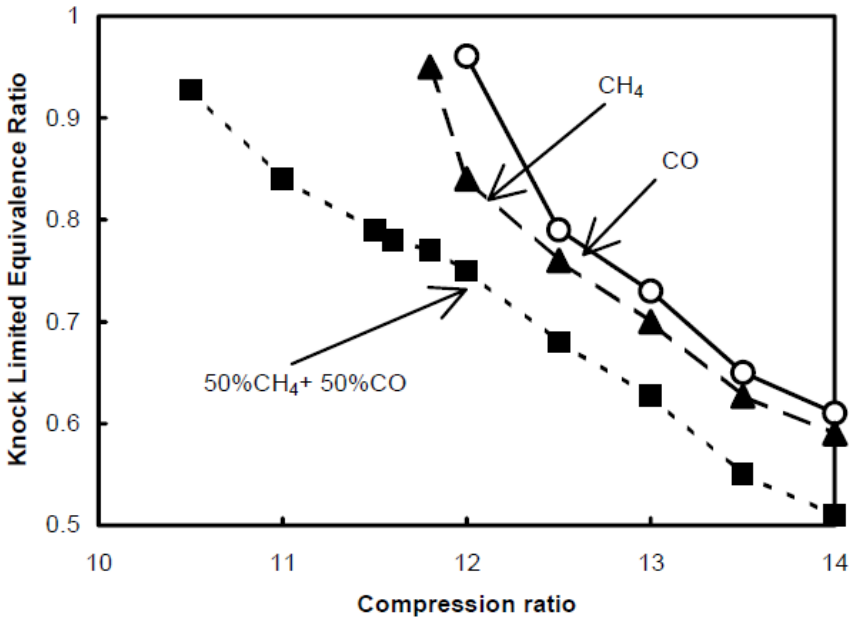

Figure 2.22. *Mixture of methane and carbon monoxide [2].*

2.7 Gas admission valve

Gas admission valve is a strategically important component on gas engine. Because LNG is very dry gas, it wears out gas admission valve plates. At the moment there are just a few commercial gas admission valve suppliers, e.g. Woodward and Hoerbiger.

2.7.1 SOGAV 250

At the moment Wärtsilä uses SOGAV 250 solenoid operated gas admission valve made by Woodward, USA. Problems with the valve are that using SOGAV, it is impossible to handle large pressure difference. If pressure difference is too high, the valve will not open. Lifetime of the valve is on the worst case really short; only 4000 hours. Opening and closing times of the valve are 2 - 4 ms and the valve leaks a bit. [22]. Figure 2.23 shows SOGAV 250.

Figure 2.23. *SOGAV 250 gas admission valve by Woodward [23].*

The valve consists of two plates. The main idea of the valve is that flow areas are large and opening movement is small. Furthermore, when the length of movement is enough small, the response time of valve can be also enough short. Figure 2.24 shows the plates of SOGAV 250.

Figure 2.24. *The plates of SOGAV 250 [22].*

2.7.2 Required features

The main goal of the thesis is to develop and design better gas admission valve than used at the moment. Table 2.4 presents demanded and optional features of the new gas admission valve. The original requirement list is presented by Heikkilä [24].

Table 2.4. *Demanded and optional features of the new gas admission valve*

Demand / Option	Requirement	Notes
Demand	Adjustable flow rate	Maximum gas flow ~500 l/min at normal conditions
Demand	Small and constant response time	< 5 ms
Demand	Ability to operate in large pressure difference	0 – 0.5 MPa
Demand	High vibration resistance	
Demand	High fault tolerance	
Demand	Working temperature 0 - 80 °C	Depends on surroundings
Demand	Gas should be mixed with air as well as possible	
Demand	Energy saving	For example differential connection using hydraulics
Demand	Operation time 18 000 hours, count of cycles 360 million.	
Demand	Early closing intake valve Miller cycle	
Option	Independence of pressure difference	
Option	ATEX (Zone 1 or Zone 2)	Depending on position of controlling electronics

The most important requirements are adjustable flow rate of gas, small and constant response time, ability to operate in large pressure difference and fault tolerance. Even though operation in large pressure difference is requirement, small pressure difference is always the wanted feature because pressurization of gas increases costs.

3 DIGITAL FLUID POWER

A digital valve system consists of discrete valued components which can be open (on) or closed (off). Figure 3.1 presents the branches of digital fluid power. This thesis is focusing on digital valves. However, other components can also be digitalized.

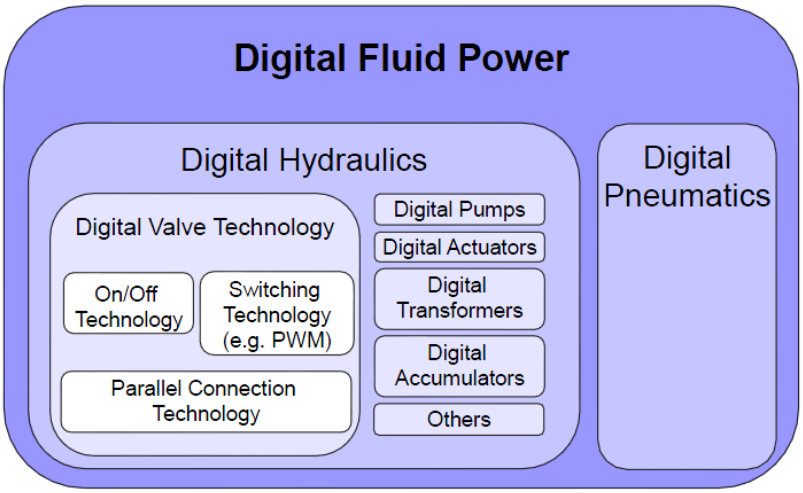

Figure 3.1. *The branches of digital fluid power [25].*

Digital valve technology consists of three different methods: on/off technology, switching technology and parallel connection technology. On/off technology is based on only one valve. There are only a few output values, usually two or three. Controllability is poor because lack of fine adjustment. Also pressure shocks are very common. [25].

Switching technology is based on one valve which is controlled using high frequency. A valve can be controlled by Pulse Width Modulation (PWM) or Pulse Frequency Modulation (PFM).

Parallel connection technology is based on using a number of different or same size valves. Output of parallel connection is a number of discrete values. Figure 3.2 maps different digital valve technologies. On the left side is presented on/off, in the middle is switching and on the right side is parallel technology.

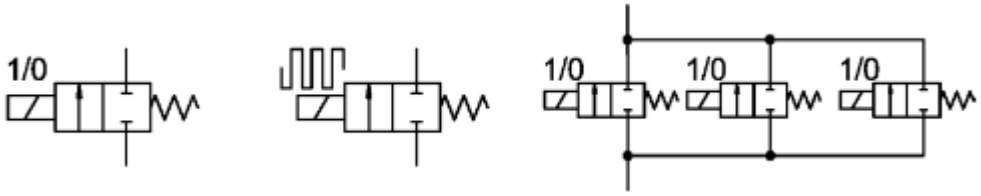

Figure 3.2. *Three different digital valve technologies [25].*

Figure 3.3 presents the idea of digital flow control unit (DFCU). It consists of a number of parallel connected on/off -valves. Right side of the figure presents the simplified hydraulic symbol of DFCU.

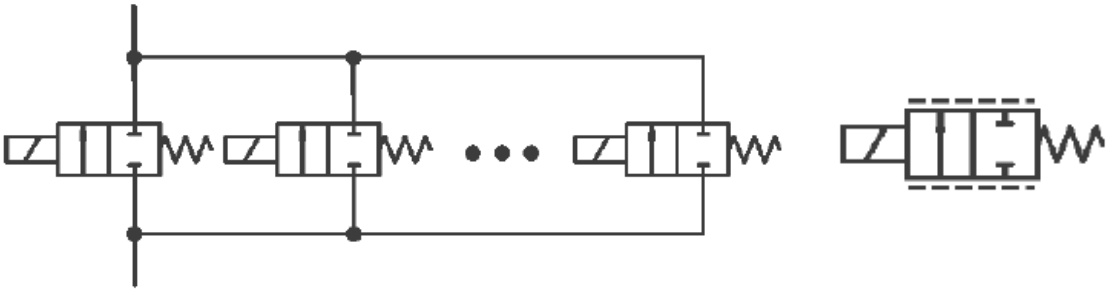

Figure 3.3. *Digital Flow Control Unit (DFCU) and simplified symbol [25].*

To achieve all possible centre positions of proportional valve, six DFCUs are needed [25]. Figure 3.4 shows the situation when six DFCUs are connected. However, bidirectional DFCUs are needed.

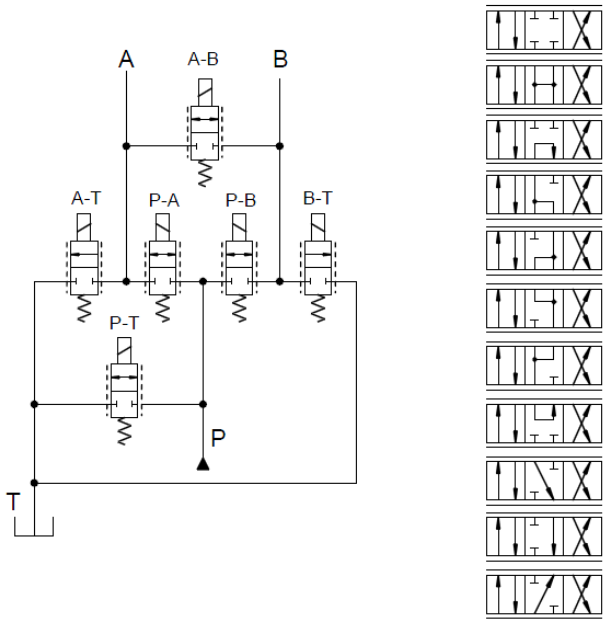

Figure 3.4. *All the flow combinations by using 6 DFCUs [25].*

As figure shows, 11 different centre position combinations are possible when 6 DFCUs are used.

3.1 Flow control techniques

Four different control techniques are presented; PWM, PFM, PCM and PNM techniques. Using PWM and PFM control methods, durability of the valve is the main problem; one valve is switched on and off via high frequency. PCM and PNM coded DFCU has a number of valves. PCM control method is based on binary coded valves. PNM control method is based on a number of same size valves.

3.1.1 PWM

The principle of PWM (Pulse Width Modulation) is that frequency of pulse is constant and width of pulse is control variable. The bigger is control pulse, the bigger is also flow rate through a valve. Using PWM control, amount of flow rate depends on how big variable impulse is compared to constant frequency. Flow rate through a valve using PWM control can be calculated via the following equation:

$$Q = Q_{nom} \frac{t_p}{T_0} \tag{10}$$

In the equation (10) Q_{nom} is nominal flow rate through the valve, t_p is length of variable impulse and T_0 is length of constant frequency. Figure 3.5 presents PWM control method and flow rate as a function of variable impulse.

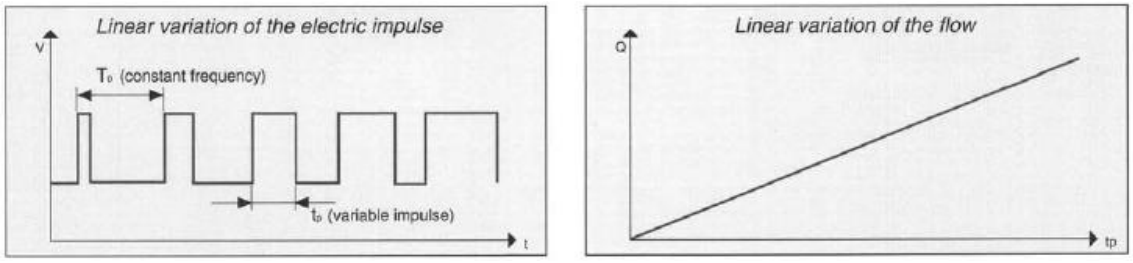

Figure 3.5. *Pulse Width Modulation, pulse length and flow rate [26].*

Duty cycle is defined as the rate between width of pulse and frequency of pulse. The rate is between [0,1]. Usable duty cycle depends on response time and switching frequency of valve. When the pulse length is shorter than response time of the valve, uncertainty of valve increases rapidly. [27].

3.1.2 PFM

PFM (Pulse Frequency Modulation) is a control method where pulse width is constant and frequency of pulse is a control variable. The shorter is variable frequency T_0, the bigger is ratio t_p/T_0 and the bigger is flow through a valve. Flow rate through a valve using PFM control can be calculated with the same equation (10) as PWM. Figure 3.6 presents PFM control method and flow rate as a function of inverse of variable frequency.

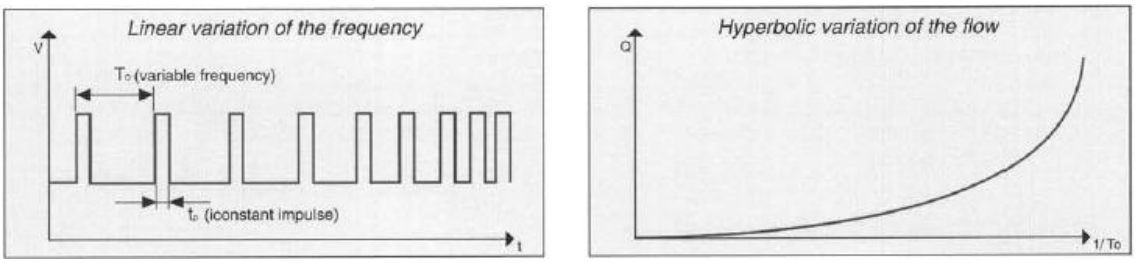

Figure 3.6. *Pulse Frequency Modulation, frequency length and flow rate [26].*

3.1.3 PCM

PCM (Pulse Code Modulation) is based on binary coding. Using PCM, DFCU has 2^N-1 different states where N is a number of valves. Using ideal binary coded DFCU, resolution is best possible: each state gives different flow rate and each step size is same. Resolution of ideal PCM –coded valve is (2^N-1):1. [25].

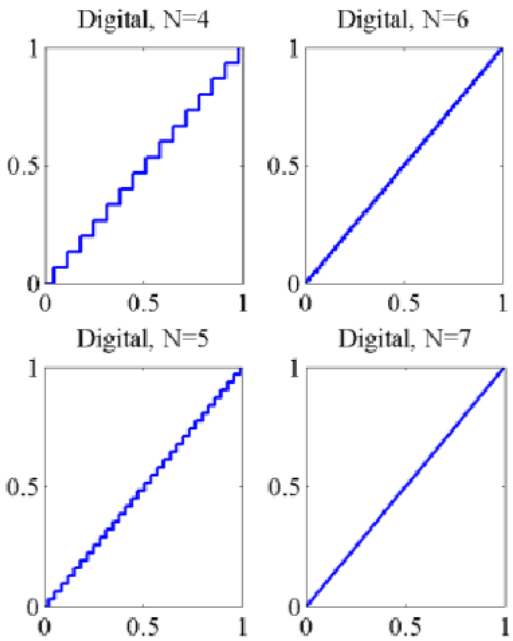

Figure 3.7. *Ideal binary coded DFCU using different number of valves [25].*

However, ideal binary coded DFCU is possible only in theory. Using the real DFCU, bad state changes are present. Bad states are unique features in digital hydraulic system. When the state is changed by the value of one, the worst bad state using PCM -coded 5-bit DFCU is when initial state is 15 and the following state is 16 or vice versa. All the valves change the states from its initial states to 0 or 1. Table 3.1 shows the situation when initial state is changed from 15 to 16.

Table 3.1. *Bad state change using 5-bit DFCU.*

State	State
15	[1 1 1 1 0]
16	[0 0 0 0 1]

When the state is changed from its initial value 15 to 16, in the worst case the transient state can be a value between 0 and 31. In appendix A is presented PCM -coding method using five valves.

3.1.4 PNM

PNM (Pulse Number Modulation) coding method is based on a number of similar components. Resolution is a number of valves, N and flow rate through each valve is same:

$$Q_i = Q_{theoretical} + \varepsilon Q_{theoretical} \tag{11}$$

In the equation (11), $Q_{theoretical}$ is theoretical flow rate through a valve and ε is relative uncertainly of step size [24]. Total flow through PNM coded valve is:

$$Q = N * Q_i \tag{12}$$

Using PNM coding, bad states are ignored because more valves are opened or closed but not both at the same time. However, using PNM coding, for example resolution 31 requires 31 valves. PCM coding requires only 5 valves. [25].

3.2 Solenoid based valve

Solenoid is a component which converts electric current to the force. A flow path of a solenoid based valve is opened or closed via solenoid force. [28]. Figure 3.8 presents the idea of direct current solenoid. Main components of solenoid are coil, core (plunger) and spring. A plunger retracts inward when a coil is energized. A spring releases a stored energy when a coil is not energized and a plunger extends outwards. [29]. Because the travel length of plunger is very short, movement time of a solenoid could be also small.

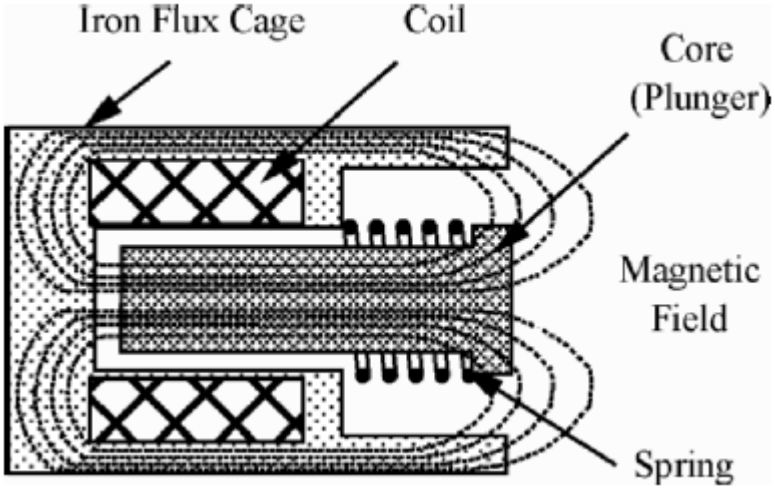

Figure 3.8. *The principle of a direct current solenoid [28].*

In digital hydraulic applications direct current solenoids are used. Alternating current solenoids needs an additional shading coil which maintains the magnetic field while the AC voltage fluctuates. Because alternating current is sinusoidal, holding force of a solenoid would drop to zero with each zero crossover. The result is that the core of a solenoid would be lifted and attracted again twice per period. [28].

3.2.1 Theory of a solenoid

Solenoid is the most common electric mechanical valve actuator. When the coil is excited, force made by solenoid is proportional to current. Solenoid is usually spring forced and it produces force only for one direction. Anyway solenoid can be either push or pull type. Solenoid needs always current when the force is generated. [25]. A direct current solenoid has one essential advantage with delayed, gentle pick-up of the armature due to the declining current rise and silent holding function. [28].

A solenoid has always an air gap between iron circuit and plunger. The smaller is air gap between iron circuit and a plunger, the greater is an available magnetic force of a coil. A coil of a solenoid would heat up greatly because electric power of a coil would be converted totally to thermal energy. Temperature of a solenoid surface would raise up to 80 - 90°C or even more. [28].

3.2.2 Boosting a solenoid

Because a solenoid is normally too slow for digital hydraulic applications, solenoid must be boosted. The idea of boosting a solenoid is to keep an over voltage over a sole-

noid. Current of a solenoid grows faster. [25]. Figure 3.9 shows on the left side different operating voltages of a solenoid. The bigger is a voltage, the bigger is a force. The right side shows the situation when a solenoid is first driven with an over voltage 36 V and after that voltage remains to constant value 12 V. As figure shows, current grows faster up with over voltage. However, current will not grow more than I_{max} because voltage value 36 V is changed to 12 V before value of current is more than I_{max}.

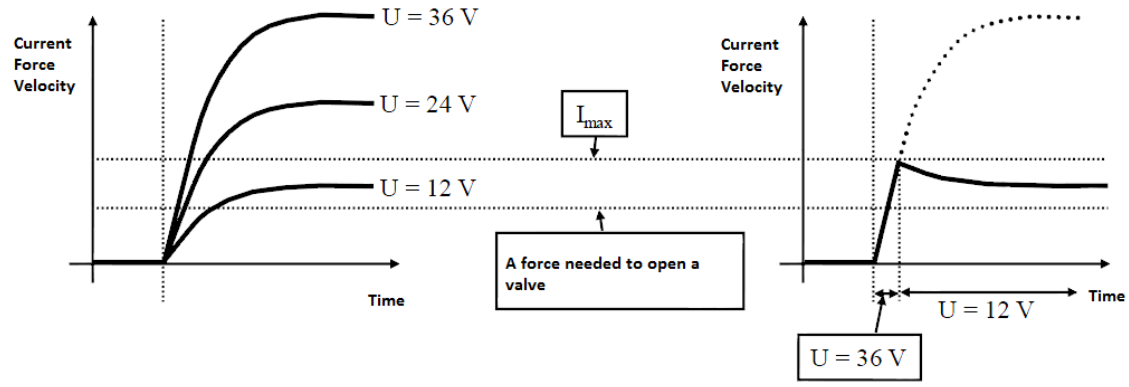

Figure 3.9. *Boosting a solenoid with over voltage. Modified from the original [25].*

If a coil is switched off, high negative voltage occurs and this could produce sparking or even destroy a power supply. This happens because the magnetic field tries to keep a coil energized. The solution to the problem for direct current systems is to use a diode across the coil. Because of a diode, current is flown only in one direction and needs only 1.5 V potential difference. [28].

Figure 3.10 shows the situation when a diode is plugged into on/off supply. When a voltage is switched on (situation 1), a diode is not used. When a voltage is switched off (situation 2), current flows through a diode and current is reduces slowly because of resistance.

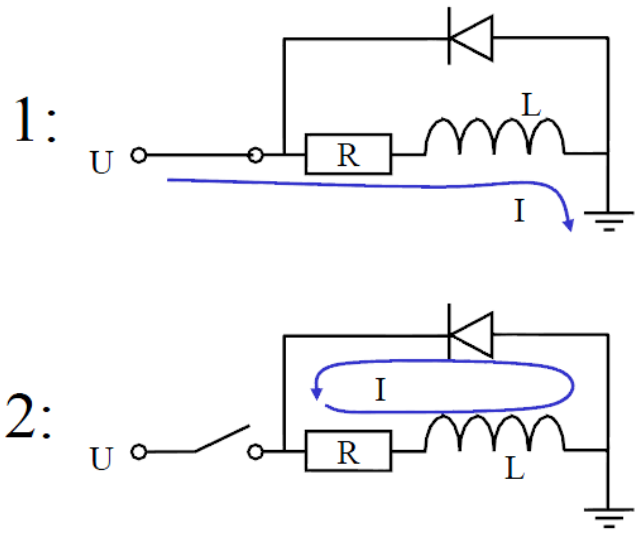

Figure 3.10. *An unloading diode circuit, voltage is switched on (1) and off (2) [25].*

Figure 3.11 shows the idea of H-bridge. When the couplings are opened negative voltage is fed to coil and force of a solenoid decreases faster. However, the coupling consumes energy. [25].

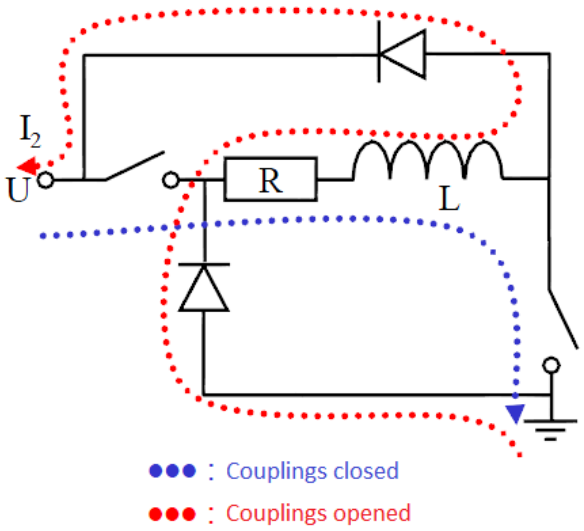

Figure 3.11. *Idea of H-bridge for decreasing solenoid force faster [25].*

A typical response time of a solenoid is 20-80 ms which is too much for digital hydraulic applications. Although, a solenoid can be sped up readily up to 70 %. [25].

3.3 Miniaturization

The principle of miniaturization is that big components are replaced by a number of smaller components. The benefits of miniaturization are that total sizes, volumes and masses of components reduce, needed control energy reduces and the components are faster because delay time reduces a lot. [25]. Furthermore, the wanted features, e.g. flow area of a valve can be same either using one big valve or a number of smaller valves.

3.3.1 Theory of miniaturization

Moment of inertia as for centre line using circular component is presented in the following equation:

$$I_x = \frac{1}{4}mr^2 = \frac{1}{4}m\left(\frac{D}{2}\right)^2 \quad (13)$$

, where m is mass of component, r is radius and D is diameter. Using a number of smaller components than just one big component moment of inertia reduces a lot. Figure 3.12 presents moment of inertia using rotation valves. The following table 3.2 shows parameters of figure 3.12.

Table 3.2. *Parameters of inertia*

Parameter	Big valve	Small size valves (3x3)
Mass	1 kg	1/3 kg
Diameter	90 mm	9 * 30 mm
Moment of inertia	$5.1*10^{-4}$ m^2*kg	$1.9*10^{-5}$ m^2*kg
Inertia ratio	27:1	
Total flow area	$6.3*10^{-3}$ m^2	$9*7.07*10^{-4}$ m^2 = $6.3*10^{-3}$ m^2

As the table 3.2 shows, inertia ratio is 27 times greater with one big valve than smaller valves. The biggest reason to decreased inertia is diameter of a valve. As the equation (13) shows, the effect of diameter to inertia is in the second power. Anyway the flow areas of valves are equal and total flow areas are calculated by using diameter of valves.

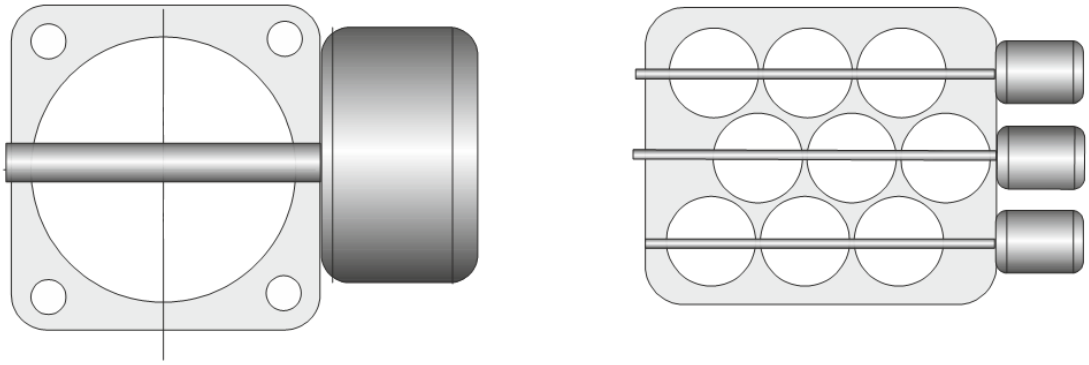

Figure 3.12. *Moment of inertia and total flow area using rotation valve [30].*

Quality factors can be calculated to valves [25]. In the following table is presented two quality factors to Sturman Industries valves. Volume of valves is assumed to proportional to spool travel and to square of spool diameter [25].

Table 3.3. *Quality factors of Sturman Industries valves. Modified from original [25].*

Name	Spool diameter d [mm]	Spool travel x [mm]	Flow area A [mm^2]	Switching time [ms]	Switching energy W [J]	$\frac{A}{W}$	$\frac{A}{d^2x}$
Pilot	3	0.16	0.75	0.19	0.011	68	0.52
SI-1000	6.4	0.38	10	0.45	0.30	33	0.64
SI-1500	9.5	0.64	23	1.0	0.70	33	0.40

As the table 3.3 shows, quality factor values support the theory of miniaturization. The bigger the quality factor, the better valve is.

The theory of miniaturization works up to orifice size 0.3 mm. When using smaller orifices than 0.3 mm flow changes from turbulent to laminar and the valve is more sensitive to contamination particles. Also viscous forces increase and packing of components will be more difficult. [25].

According to theory of miniaturization, big valves should be replaced with a number of smaller valves. The result is PNM -coded valve packages which are smaller, faster and more energy efficient than bigger valve. [25].

3.4 Commercial and non-commercial digital valves

There are a few companies on the market which have published a valve especially for the purpose of digital hydraulics and pneumatics. The main problem of the commercial

valves is response time; if response time of a valve is too long for a precise purpose, practically a valve is useless in a digital system.

3.4.1 Bucher Hydraulics Series WS22GD/OD

Bucher Hydraulics Series WS22GD/OD is designed for use in digital hydraulics. It is a direct acting solenoid operated seat valve. Maximum flow rate through the valve is 30 l/min and maximum operating pressure is 35 MPa. Figure 3.13 illustrates Bucher Hydraulics digital valve series WS22GD/OD.

Figure 3.13. *Bucher Hydraulics digital valve series WS22GD/OD [31].*

Response time of the valve is 5-15 ms and it depends on pressure difference, used oil, flow direction of the valve and amount of flow rate. Seat type valves are virtually leak-free: leak amount is maximum 5 drops per minute which is about 0.2 ml/min. Leak amount of spool type valve, WK22 by Bucher Hydraulics is 10-20 ml/min. [32].

Figure 3.14 shows hydraulic symbols of normally closed and opened versions of valves. On the left side is shown normally closed and on the right side normally opened version.

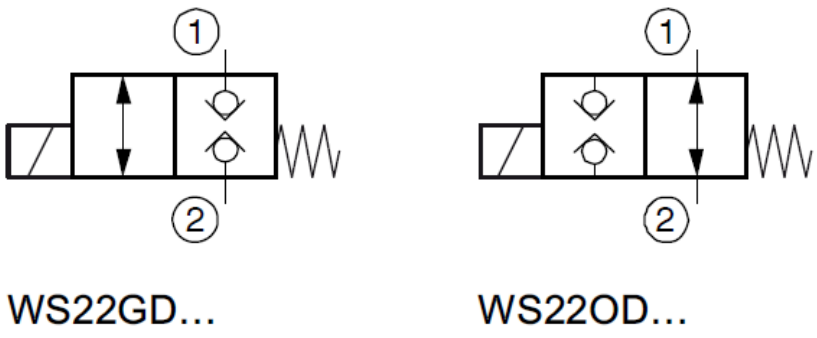

Figure 3.14. *Hydraulic symbols of normally closed (left side) and normally opened (right side) seat type valves [31].*

Figure 3.15 shows flow rate characteristic curve for normally closed valve (WS22GD).

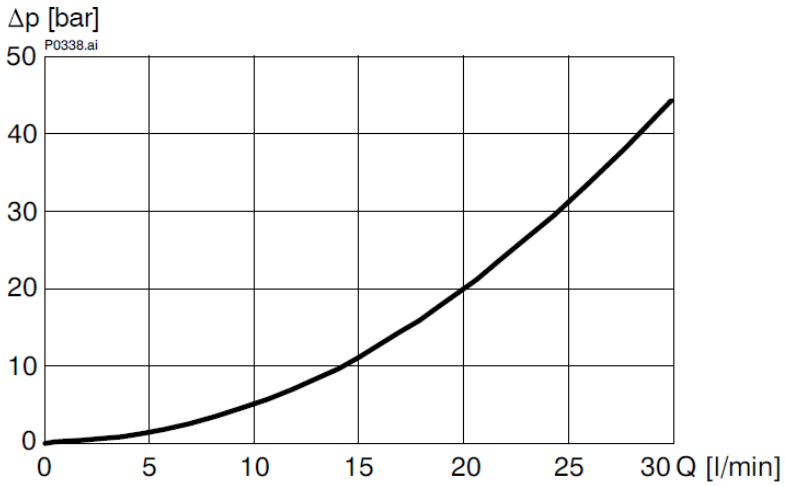

Figure 3.15. *Pressure drop – flow rate characteristic curve of Bucher Hydraulics WS22GD -valve [31].*

As the figure 3.15 shows, maximum flow rate 30 l/min is possible at pressure difference 4.4 MPa.

3.4.2 Sturman Industries SI-1000

Sturman SI-1000 valve is presented by Johnson et al. [33]. The key thing of the valve is that design is very simple. It has only one small spool which moves. Electric power is required only when the spool moves. The valve is bistable because magnetic latching force is affected in the both end of the spool. Because of latching force, power is not required to hold the spool in either end. It is also possible to use the valve as a pilot valve to control proportional main stage. Because the valve is spool type, clearances should be very small. Typical spool clearance is 5 microns and thus property filtered fluid must be used. Nominal flow is 12 litres per minute at pressure difference 0.5 MPa. Response time of the valve is only 0.45 ms. Switching energy of the valve is 0.3 J. Figure 3.16 shows the cutaway of Sturman Latching valve. Two coils in the endcaps control the motion of the spool. As figure shows, dual paths are used to provide a force balance on the spool in either position. This minimizes the latching force which is required to hold the valve in either position.

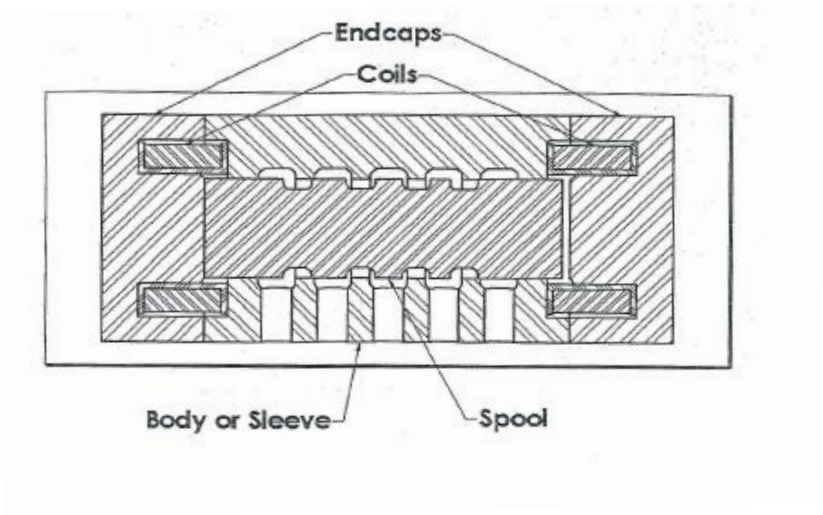

Figure 3.16. *Cutaway of Sturman Latching valve [33].*

Figure 3.17 presents Sturman SI-1000 latching valve. A spool of valve is also shown because of cut out section.

Figure 3.17. *Sturman SI-1000 latching valve and spool of valve [33].*

Axial and radial pressures and flow forces should be as small as possible. The smaller the forces are, the faster the valve can be and the smaller these forces are the more consistent whey will be. Repeatability is one of most important feature of a valve. When the goal is a very fast valve, consistent forces are very important feature. Axial forces can be minimized by using dual flow paths or negative force port geometries on the spool lands. Radial forces can be minimized by careful consideration of input and output flow paths from the valve.

Because Sturman Industries SI-1000 valve is based on two-coil design, non-excited coil can be used as a spool position sensor. Spool travel time can be determined via back-EMF waveform of non-excited coil. The ends of the spool are affected the largest loads, because ends are impacted the forces that stops the spool motion. Thus material properties and heat-treating of valves are important aspect for durability of valve and magnetic performance.

3.4.3 Bibus Matrix series 850 pneumatic valve

Bibus 850 series valves are pneumatic valves which consist of three different matrix valve versions; one-, three- and nine- outlet versions named according to number of outlets: 851, 853 and 859. Response time of the valve is a few milliseconds and with speed-up control below 1 ms response time and operating frequency of 500 Hz can be achieved. Response time is also independent from the flow rate value and operating life is more than 500 Million cycles. [26]. Figure 3.18 shows three and nine outlet versions.

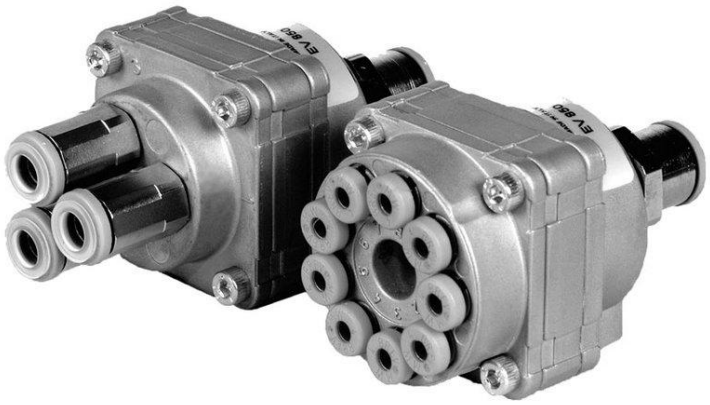

Figure 3.18. *Bibus Matrix 850 series, three and nine outlet versions [26].*

Maximum flow rates of the valves in normal conditions are: 1620 l/min (851), 520 l/min (853) and 180 l/min (859). Combinations of the control methods (PWM, PFM, PCM, PNM) can be used to achieve more linear flow rate from the valve. [26]

4 MODELLING EQUATIONS

In this chapter are presented all equations which are used on the digital hydraulic and pneumatic simulation models. The equations are divided into the specific categories depending on where the equations are used.

4.1 Proportional controller

Input values of the proportional controller are reference and simulated values, output value is output reference. The following equation presents the equation of proportional controller:

$$output_{reference} = controller_{gain} * \left(input_{reference} - input_{simulated}\right) \quad (14)$$

The controller includes proportional gain which gains the difference of inputs.

4.2 Controller equations using two DFCUs

This chapter presents all equations which are used in the controller using two DFCUs. Proportional controller has been used the upper level controller.

4.2.1 Steady-state flow rates

The following equations are used to calculate steady-state flow rate using two DFCUs.

$$Q = sign(p_1 - p_2)K_v\sqrt{|p_1 - p_2|} \quad (15)$$

$$K_v = \frac{Q_{nom}}{\sqrt{\Delta p_{nom}}} \quad (16)$$

Equation (15) calculates steady-state flow rate using turbulent flow equation and equation (16) calculates flow coefficient for valve using nominal flow rate and pressure difference values. In the equations p_1 is upstream pressure, p_2 is downstream pressure, Q_{nom} is nominal flow rate, Δp_{nom} is nominal pressure difference and K_v is specific flow coefficient for valve.

4.2.2 Cost functions

The following equation presents the cost function of short-circuit flow.

$$J_{short-circuit\ flow} = W_p \cdot \sum\left(\boldsymbol{DFCU}_{mtrx} \cdot \boldsymbol{v}_{penalty} \times \mathbf{1}\right) \quad (17)$$

The idea of the equation is to reduce short-circuit flow using specific coefficient value W_p. Depending on the sign of velocity $v_{penalty}$, valve openings of the DFCU-PA or DFCU-AT have been reduced. If velocity is positive, valve openings of DFCU-AT have been reduced and vice versa.

The following equation presents the cost function of valve switching.

$$J_{switching} = W_{sw} \cdot \sum|\boldsymbol{u}_{in}(k-1) \times \mathbf{1} - \boldsymbol{DFCU}_{mtrx}| \quad (18)$$

The idea of the function is to reduce valve switching amount using coefficient value W_{sw}. The previous state combination $\mathbf{u}_{in}$ (k - 1) of DFCUs has been used to determine cost function of valve switching. The bigger is output of cost function, the seldom the state of the valve is changed.

4.3 Controller equations using four DFCUs

This chapter presents all equations which are used in the controller using four DFCUs. The controller model has been divided into the five different sub-models: Mode selection, steady-state solver, cost function, optimal control and previous router sub-models. Proportional controller has also been used the upper level controller as using two DFCUs.

4.3.1 Mode selection

This chapter presents all equations which are used in the mode selection sub-model. The sub-model consists of load force estimator, available force range, mode selection and pressure references.

4.3.1.1 Load force estimator

Estimated load forces have been calculated using the following equation:

$$F_{est} = p_{Aest}A_A - p_{Best}A_B \quad (19)$$

, where p_{Aest} and p_{Best} are estimated A and B-chamber pressures, respectively. Using the equation (19), estimated chamber pressures have been found out using low-pass filtering.

4.3.1.2 Available force range

The following equations present available force range using retracting direction of movement. Force equation for maximum retracting force:

$$F_{maxR} = p_{max} * A_A - p_{min} * A_B \tag{20}$$

Equation for minimum mode -1 force:

$$F_{min1R} = p_{min} * A_A - (p_p - \Delta p_{ref}) * A_B \tag{21}$$

Equation for minimum mode -2 force:

$$F_{min2R} = (p_p + \Delta p_{ref}) * A_A - (p_p - \Delta p_{ref}) * A_B \tag{22}$$

For extending direction of movement, the following equations are presented. Force equation for minimum extending force:

$$F_{minE} = p_{min} * A_A - p_{max} * A_B \tag{23}$$

Equation for maximum mode 1 force:

$$F_{max1E} = -p_{min} * A_B + (p_p - \Delta p_{ref}) * A_A \tag{24}$$

Equation for maximum mode 2 force:

$$F_{max2E} = (p_p - \Delta p_{ref}) * A_A - (p_p + \Delta p_{ref}) * A_B \tag{25}$$

In the equations (20) – (25) p_p, p_{max}, p_{min} and Δp_{ref} are supply pressure of the system, maximum controller pressure, minimum controller pressure and desired pressure difference on the inflow-side whenever possible, respectively.

4.3.1.3 Mode selection

Extending mode is used when either equation (26) or (27) is realized.

$$mode_{ext} = (v_{ref\ ext}\ AND\ (F > F_{min})\ AND\ (F < F_{max1E})) \tag{26}$$

$$mode_{ext} = \left(v_{ref\ ext}\ AND\ (F > F_{min})\ AND\ (F < F_{max2E})\right) \quad (27)$$

Retracting mode is used when either equation (28) or (29) is realized.

$$mode_{ret} = -\left(v_{ref\ ret}\ AND\ (F < F_{max})\ AND\ (F > F_{min1R})\right) \quad (28)$$

$$mode_{ret} = -\left(v_{ref\ ret}\ AND\ (F < F_{max})\ AND\ (F > F_{min2R})\right) \quad (29)$$

Equation for extending reference velocity:

$$v_{ref\ ext} = \left((v_{ref} > v_{tol})OR\ (v_{ref} > 0.5 \cdot v_{tol})AND\ is\ extending\right) \quad (30)$$

Equation for retracting reference velocity:

$$v_{ref\ ret} = \left((v_{ref} > v_{tol})OR\ (v_{ref} > 0.5 \cdot v_{tol})AND\ is\ retracting\right) \quad (31)$$

In the equations (30) and (31) v_{tol} is velocity threshold of the controller.

Equations for extending force conditions:

When estimated force is greater than minimum extending force, $F_{est} > F_{minE}$:

$$(F > F_{min}) = \left((F_{est} - F_{tol}) > F_{minE}\right)$$
$$OR\ \left((F_{est} > F_{minE})\ AND\ (mode = 1)\ OR\ (mode = 2)\right) \quad (32)$$

When estimated force is smaller than maximum mode 1 force, $F_{est} < F_{max1E}$:

$$(F < F_{max1E}) = \left((F_{est} + F_{tol}) < F_{max1E}\right)$$
$$OR\ \left((F_{est} < F_{max1E})\ AND\ (mode = 1)\ OR\ (mode = 2)\right) \quad (33)$$

When estimated force is smaller than maximum mode 2 force, $F_{est} < F_{max2E}$:

$$(F < F_{max2E}) = \left((F_{est} + F_{tol}) < F_{max2E}\right)$$
$$OR\ \left((F_{est} < F_{max2E})\ AND\ (mode = 2)\right) \quad (34)$$

Equations for retracting force conditions:

When estimated force is smaller than maximum retracting force, $F_{est} < F_{maxR}$:

$$(F < F_{max}) = \left((F_{est} + F_{tol}) < F_{maxR}\right)$$
$$OR\left((F_{est} < F_{maxR})\ AND\ (mode = -1)\ OR\ (mode = -2)\right) \quad (35)$$

When estimated force is greater than minimum -1 mode force, $F_{est} > F_{min1R}$:

$$(F > F_{min1R}) = \left((F_{est} - F_{tol}) > F_{min1R}\right)$$
$$OR\left((F_{est} > F_{min1R})\ AND\ (mode = -1)\ OR\ (mode = -2)\right) \quad (36)$$

When estimated force is greater than minimum mode -2 force, $F_{est} > F_{min2R}$:

$$(F > F_{min2R}) = \left((F_{est} - F_{tol}) > F_{min2R}\right)$$
$$OR\left((F_{est} > F_{min2R})\ AND\ (mode = -2)\right) \quad (37)$$

Extending mode is used when previous mode is 1 or 2:

$$Extending = last\ mode\ (1\ OR\ 2) \quad (38)$$

Retracting mode is used when previous mode is -1 or -2:

$$Retracting = last\ mode\ (-1\ OR\ -2) \quad (39)$$

4.3.1.4 Pressure references

When the mode is extending differential, reference A-chamber pressure can be calculated using the following equation:

$$p_{Aref} = \min\left(p_A, p_p - \Delta p_{ref}\right) \quad (40)$$

A-chamber pressure:

$$p_A = \frac{1}{A_A}(F + p_{max}A_B) \quad (41)$$

Reference B-chamber pressure can be calculated using reference A-chamber pressure:

$$p_{Bref} = \frac{1}{A_B}\left(p_{Aref}A_A - F\right) \quad (42)$$

When the mode is extending inflow-outflow, reference A-chamber pressure can be calculated using the following equation:

$$p_{Aref} = \min\left(p_A, p_p - \Delta p_{ref}\right) \tag{43}$$

A-chamber pressure:

$$p_A = \frac{1}{A_A}\left(F + p_{max}A_B\right) \tag{44}$$

Reference B-chamber pressure can be calculated using reference A-chamber pressure:

$$p_{Bref} = \frac{1}{A_B}\left(p_{Aref}A_A - F\right) \tag{45}$$

When the mode is retracting inflow-outflow, reference B-chamber pressure can be calculated using the following equation:

$$p_{Bref} = \min\left(p_B, p_p - \Delta p_{ref}\right) \tag{46}$$

B-chamber pressure:

$$p_B = \frac{1}{A_B}\left(p_{max}A_A - F\right) \tag{47}$$

A-chamber pressure can be calculated using reference B-chamber pressure:

$$p_{Aref} = \frac{1}{A_A}\left(p_{Bref}A_B + F\right) \tag{48}$$

When the mode is retracting differential, reference B-chamber pressure can be calculated using the following equation:

$$p_{Bref} = \min\left(p_B, p_p - \Delta p_{ref}\right) \tag{49}$$

B-chamber pressure:

$$p_B = \frac{1}{A_B}\left(p_{max}A_A - F\right) \tag{50}$$

A-chamber pressure can be calculated using reference B-chamber pressure:

$$p_{Aref} = \frac{1}{A_A}\left(p_{Bref}A_B + F\right) \tag{51}$$

In the equations (40) and (43) reference A-chamber pressures and in the equations (46) and (49) reference B-chamber pressures have been found out using function of minimum value.

4.3.2 Steady-state solver

Chamber pressures and velocity values for different modes have been found out using the idea that Q_{PA} and Q_{AT} affect to A-chamber and Q_{PB} and Q_{BT} affect to B-chamber.

For extending differential mode, A-chamber pressure can be calculated using the following equation:

$$p_A = \frac{FA_A^2 K_{vPB}{}^2 + K_{vPB}{}^2 A_A^2 A_B p_P + p_P A_B{}^3 K_{vPA}{}^2}{A_A^3 K_{vPB}{}^2 + A_B^3 K_{vPA}{}^2} \tag{52}$$

B-chamber pressure can be calculated using calculated value of A-chamber pressure:

$$p_B = \frac{1}{A_B}(p_A A_A - F) \tag{53}$$

Velocity:

$$v = \frac{1}{A_A} K_{vPA} \sqrt{p_P - p_A} \tag{54}$$

For extending inflow-outflow mode, A-chamber pressure can be calculated using the following equation:

$$p_A = \frac{A_A^2 F K_{vBT}{}^2 + A_B^3 p_P K_{vPA}{}^2}{A_A^3 K_{vBT}{}^2 + A_B^3 K_{vPA}{}^2} \tag{55}$$

B-chamber pressure has been found out using calculated value of A-chamber pressure:

$$p_B = \frac{1}{A_B}(A_A p_A - F) \tag{56}$$

Velocity:

$$v = \frac{1}{A_A} K_{vPA} \sqrt{p_P - p_A} \tag{57}$$

For retracting inflow-outflow mode, A-chamber pressure can be calculated using the following equation:

$$p_A = \frac{(F+p_P A_B){K_{vPB}}^2 A_A^2}{A_A^3 {K_{vPB}}^2 + A_B^3 {K_{vAT}}^2} \quad (58)$$

B-chamber pressure has been found out using calculated value of A-chamber pressure:

$$p_B = \frac{1}{A_B}(A_A p_A - F) \quad (59)$$

Velocity:

$$v = -\frac{1}{A_A} K_{vAT} \sqrt{p_A} \quad (60)$$

For retracting differential mode, A-chamber pressure can be calculated using the following equation:

$$p_A = \frac{F A_A^2 {K_{vPB}}^2 + {K_{vPB}}^2 A_A^2 A_B p_P + p_P {A_B}^3 {K_{vPA}}^2}{A_A^3 {K_{vPB}}^2 + A_B^3 {K_{vPA}}^2} \quad (61)$$

B-chamber pressure has been found out using A-chamber pressure value:

$$p_B = \frac{1}{A_B}(p_A A_A - F) \quad (62)$$

Velocity:

$$v = -\frac{1}{A_A} K_{vPA} \sqrt{p_A - p_P} \quad (63)$$

4.3.3 Cost functions

Five different cost functions have been calculated using the following error functions. Velocity errors have been found out using reference and simulated velocity values:

$$velocity\ error = \left| v_{reference} - v_{simulated} \right|^2 \quad (64)$$

Chamber A and B pressure errors have been found out using coefficient value W_p.

$$Chamber\ A\ pressure\ error = W_p * \left| p_{A\ reference} - p_{A\ simulated} \right|^2 \quad (65)$$

$$Chamber\ B\ pressure\ error = W_p * \left| p_{B\ reference} - p_{B\ simulated} \right|^2 \quad (66)$$

Switching functions have been found out using previous DFCU state (**u** (k - 1)) and coefficient value W_{sw}.

$$Switching\ in = W_{sw} * (DFCU.QN \times |\boldsymbol{u_{in}}(k-1) \times \mathbf{1} - \boldsymbol{DFCU_{in\ mtrx}}|)^2 \quad (67)$$

$$Switching\ out = W_{sw} * (DFCU.QN \times |\boldsymbol{u_{out}}(k-1) \times \mathbf{1} - \boldsymbol{DFCU_{out\ mtrx}}|)^2 \quad (68)$$

4.4 Hydraulic system equations

This chapter presents all equations which are used in the hydraulic system. The equations have been used to model valves, hydraulic cylinder, load, friction and damping models and also calculate hydraulic energy consumptions.

4.4.1 Orifice

Orifice has been modelled using two different equations. Turbulent flow equation is used when absolute pressure difference $|p1 - p2|$ is higher than used transition pressure value p_{tr}.

$$Q = sign(p_1 - p_2)K_v\sqrt{|p_1 - p_2|} \quad (69)$$

When the pressure difference is lower than used transition pressure value, the following polynomial flow equation is used:

$$Q = sign(p_1 - p_2)K_v \frac{|p_1 - p_2|}{2\sqrt{|p_{tr}|}}\left(3 - \frac{|p_1 - p_2|}{p_{tr}}\right) \quad (70)$$

In the simulation models, transition pressure value 0.1 MPa has been used.

4.4.2 Hydraulic cylinder

The following equation presents pressure change in the hydraulic cylinder:

$$\dot{p} = \frac{B_{eff}}{V}\left(\Sigma Q - \dot{V}\right) \quad (71)$$

, where V is total volume of cylinder chamber and the value includes also dead volumes of the system. B_{eff} is bulk modulus of the oil.

Hydraulic cylinder force has been found out using the following force equation:

$$F = p_A A_A - p_B A_B - F_{friction} \tag{72}$$

, where $F_{friction}$ is friction force.

4.4.3 Load

Newton's second law has been used to present load equation of the system. Sum of the forces equals product of mass of the system and acceleration.

$$\Sigma F = ma \tag{73}$$

4.4.4 Hyperbolic tangent friction function

Friction force has been determined using the following friction equation.

$$F_{friction} = \tanh(\mathrm{K}\dot{\mathrm{x}}) * \left(\mathrm{F_C} + (\mathrm{F_S} - \mathrm{F_C})\mathrm{e}^{-\left(\dot{\mathrm{x}}/\mathrm{v_s}\right)^2}\right) + \mathrm{b}\dot{\mathrm{x}} \tag{74}$$

In the equation F_c is Coulomb friction force, F_s is static friction force, v_s is velocity of minimum friction, $\dot{x}$ is velocity and b is viscous friction coefficient. Parameter K is specific parameter to determine how fast friction force value changes near zero velocity.

4.4.5 Damping

The following equation shows the damping force. The force depends on velocity of the cylinder and damping force coefficient.

$$F_{damping} = |v| * b \tag{75}$$

In the equation the value b is damping coefficient, $[b] = \frac{Ns}{m}$.

4.4.6 Energy consumption

The following equation presents the hydraulic input energy from supply line:

$$P_{in} = p_p \cdot Q_p \tag{76}$$

When the input power equation is integrated, needed hydraulic input energy is found out:

$$E_{in} = \int P_{in} dt \tag{77}$$

Hydraulic system output energy has been found out using velocity, chamber pressures and areas of the hydraulic cylinder:

$$P_{out} = v \cdot (p_A A_A - p_B A_B) \tag{78}$$

When the output power equation is integrated, output energy is found out:

$$E_{out} = \int P_{out}\, dt \tag{79}$$

Power loss in the hydraulic system is presented using difference of input and output hydraulic power:

$$P_{loss} = P_{in} - P_{out} \tag{80}$$

Consumed hydraulic energy in the hydraulic system has been found out via integrating power loss equation:

$$E_{cons} = \int P_{loss}\, dt \tag{81}$$

In the hydraulic system consumed hydraulic energy is transferred into the heat.

4.5 Poppet valve

The following equations present poppet valve equations presented by Heywood [16]. Poppet valve lift is divided into the three different levels: low, medium and high valve lifts. Valve lift determines the flow area of the poppet valve.

4.5.1 Poppet valve lift and area equations

Equation for low valve lifts:

$$0 < L_v < \frac{w}{\sin\beta \cos\beta} \tag{82}$$

The minimum area using low valve lift:

$$A_m = \pi L_v cos\beta \left(D_v - 2w + \frac{L_v}{2} sin\, 2\beta\right) \tag{83}$$

Equation for the medium valve lifts:

$$\frac{w}{sin\beta cos\beta} < L_v \leq \left[\left(\frac{D_p^2 - D_s^2}{4D_m}\right)^2 - w^2\right]^{1/2} + w\ tan\beta \tag{84}$$

The minimum area using medium valve lift:

$$A_m = \pi D_m[(L_v - w\ tan\beta)^2 + w^2]^{1/2} \tag{85}$$

Equation for the high valve lifts:

$$L_v > \left[\left(\frac{D_p^2 - D_s^2}{4D_m}\right)^2 - w^2\right]^{1/2} + w\ tan\beta \tag{86}$$

The minimum area using high valve lift:

$$A_m = \frac{\pi}{4}\left(D_p^2 - D_s^2\right) \tag{87}$$

In the equations (82) - (87) the parameter w is seat width, β is seat angle, L_v is lift of the poppet valve, D_v is head diameter of the poppet valve, D_p is poppet valve port diameter, D_s is stem diameter and D_m is mean seat diameter.

4.5.2 Gas flow edge area

The following equations present gas flow area equations. The area is divided into the two different parts, outer and inner areas.

Height of outer edge:

$$h_2 = \frac{d_s}{2}\left(1 - cos\left(\frac{180° \cdot x_c}{d_s \cdot \pi}\right)\right) \tag{88}$$

,where x_c is circle of edge.

Length of the edge:

$$s_e = \sqrt{\left(\frac{d_s}{2} - \frac{h_2}{2}\right) \cdot 8h_2} \tag{89}$$

Area of outer edge:

$$A_2 = \frac{h_2}{6s_e}(3h_2^2 + 4s_e^2) \tag{90}$$

Area of inner edge:

$$A_1 = \frac{h_1}{6s_e}(3h_1^2 + 4s_e^2) \tag{91}$$

Total gas flow area per one gas flow edge is sum of areas A_1 and A_2.

4.5.3 Gas flow equations

The following equations present the flow equations of gas through poppet valve. Subcritical or critical flow equation has been used depending on critical pressure ratio of gas.

$$\dot{m}_{subcritical} = \frac{C_d A_m p_1}{\sqrt{RT}} \left(\frac{p_2}{p_1}\right)^{1/\gamma} \left\{\frac{2\gamma}{\gamma-1}\left[1 - \left(\frac{p_2}{p_1}\right)^{\gamma-1/\gamma}\right]\right\}^{1/2} \tag{92}$$

$$\dot{m}_{choked} = \frac{C_d A_m p_1}{\sqrt{RT}} \gamma^{1/2} \left(\frac{2}{\gamma+1}\right)^{(\gamma+1)/2(\gamma-1)} \tag{93}$$

In the equations (92) and (93) C_d is discharge coefficient, γ is heat capacity ratio of gas, R is ideal gas constant and T is temperature of the gas.

4.6 Pneumatic valve

The following equation presents critical pressure ratio of gas. The value can be calculated using the value of heat capacity ratio of gas.

$$b_{gas} = \left(\frac{2}{\gamma+1}\right)^{\frac{\gamma}{\gamma-1}} \tag{94}$$

The following equation presents laminar flow through the valve:

$$\dot{m}_{laminar} = k_1 p_1 \left(1 - \frac{p_2}{p_1}\right) \sqrt{\frac{T_{methane}}{T_{air}}} \tag{95}$$

In the equation (95) the gain k_1 is:

$$k_1 = 1000 C_{ve} \rho_0 \sqrt{1 - \left(\frac{0.999 - b_{gas}}{1 - b_{gas}}\right)^2} \tag{96}$$

, where C_{ve} is conic conductance and ρ_0 is density of the gas.

The following equation presents subsonic flow:

$$\dot{m}_{subsonic} = p_1 C_{ve} \rho_0 \sqrt{\frac{T_{methane}}{T_{air}}} \sqrt{1 - \left(\frac{\frac{p_2}{p_1} - b_{gas}}{1 - b_{gas}}\right)^2} \tag{97}$$

The following equation presents choked flow:

$$\dot{m}_{choked} = p_1 C_{ve} \rho_0 \sqrt{\frac{T_{methane}}{T_{air}}} \tag{98}$$

An approximation for sonic conductance has presented by Beater [28].

$$C_{ve} = 0.128 * d^2 \tag{99}$$

Using the equation, unit of sonic conductance is $dm^3/(s*bar)$.

5 SIMULATION MODELS

Three different simulation models of gas admission valves have been done: digital hydraulic system with hydraulic cylinder using two and four DFCUs and digital pneumatic valve system. All simulation models have been modelled and simulated in this thesis with Matlab/Simulink and simulation models of digital hydraulic systems are based on course exercises of IHA-2570 [25] and IHA-2580 [27]. Because some initial models consist of blocks which are part of Simulink add-ons, some parts had to code. In appendix B is presented code to vector combination and in appendix C finding minimum index -function. Matlab is based on one based indexing method because originally Matlab was written in Fortran [34]. Zero based indexing was needed because the coding method of initial digital hydraulic models. The difference between zero and one-based indexes is that using zero-based index, indexing of the matrix starts from the value zero and using one-based index, indexing of the matrix starts from the value one.

The models with hydraulic cylinder consist of models of digital valves, controller and hydraulic cylinder using three poppet valves. Hydraulic energy consumption has also been calculated. The model of hydraulic cylinder has been modelled as two chambers, chamber A and B. The model of load has been modelled as Newton's second law, $\Sigma F = ma$, where ΣF is sum of forces, m is mass and a is acceleration. The model also consists of damping model, friction model and spring with its initial force. Poppet valves have been modelled using equations which are presented by Heywood [16]. Flow area of poppet valve depends on opening of valve and flow area equations are divided into three different phases. Gas flow through a poppet valve has been modelled as two different equations, presented also by Heywood [16]: subcritical and choked flow equations. When the critical pressure ratio is greater than pressure ratio $\frac{p_2}{p_1}$, where p_2 is downstream pressure and p_1 is upstream pressure, subcritical flow is used.

Pneumatic valve model has been modelled as three different flow equations, proposed by Sanville in 1971 and it is basis for the standard ISO-6358: laminar, subsonic and choked flow equations. The model is based on two different parameters: the critical pressure ratio b_{gas} and the sonic conductance C_{ve}. The sonic conductance is the ratio between the mass flow rate through the valve and the product of upstream pressure p_1 and the mass density at standard conditions when the flow is choked. The critical pressure ratio is the ratio between the downstream pressure p_2 and the upstream pressure p_1 when air velocity achieves sonic speed. When the ratio between the downstream pressure p_2 and the upstream pressure p_1 is below the critical pressure ratio, flow is choked

and further reduction of the downstream pressure p_2 does not increase the mass flow. Typically, these parameters are determined from measurements. [28].

5.1 Model-based control design

Model-based control design is used in digital hydraulics and pneumatics. The basic principle of the model-based control is to calculate what would happen with specific valve opening combination. With cost functions it is possible to determine unwanted situations. Finally, the opening combination has been chosen, which minimizes the value of cost function. [25].

A Finnish company Metso Oyj has used model-based control design to develop controller for energy-saving digital hydraulic systems. Even though proportional hydraulic system is easy to set up with PID controller and adjust valve position, digital hydraulic system with model-based design has reduced costs and improved quality. Controller of a digital hydraulic system is more complicated and programming mistakes are common while developing a complex system. Still it enables tests and tuning a complex controller design via simulation. Also a digital hydraulic system requires less energy than proportional hydraulic system. [35].

5.2 Digital hydraulic system using two DFCUs

Simulation model consists of two DFCUs which control fluid flow to and from A-chamber. DFCU-PA controls fluid flow from supply pressure line and from B-chamber to A-chamber. DFCU-AT controls fluid from A-chamber to tank line. Supply pressure affects all the time to B-chamber. When DFCU-PA and DFCU-AT are opened simultaneously, short-circuit flow is used. This connection method increases tracking of velocity reference. However, short-circuit current increases power losses because both DFCUs are opened simultaneously. [25]. Figure 5.1 shows hydraulic circuit of digital hydraulic system using two DFCUs.

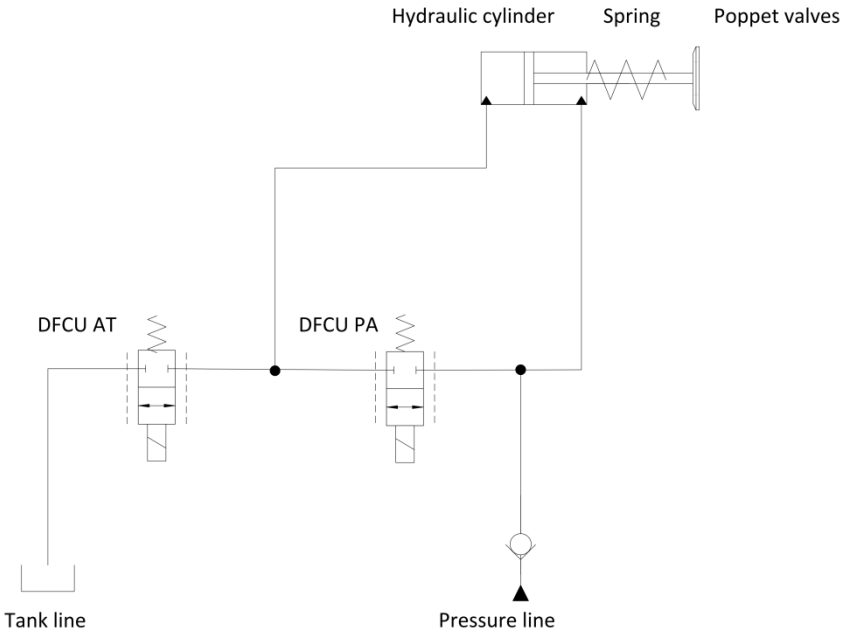

Figure 5.1. *A digital hydraulic system using two DFCUs and hydraulic cylinder actuated poppet valves.*

A spring is used in the system also as a precaution but also as a force to close the poppet valves. If the hydraulic system is totally broken, a spring is forced poppet valves to its initial, closed position. To find out flow rate and pressure of B-chamber, an orifice which is always open has been modelled to B side. Figure 5.2 shows the upper level of simulation model.

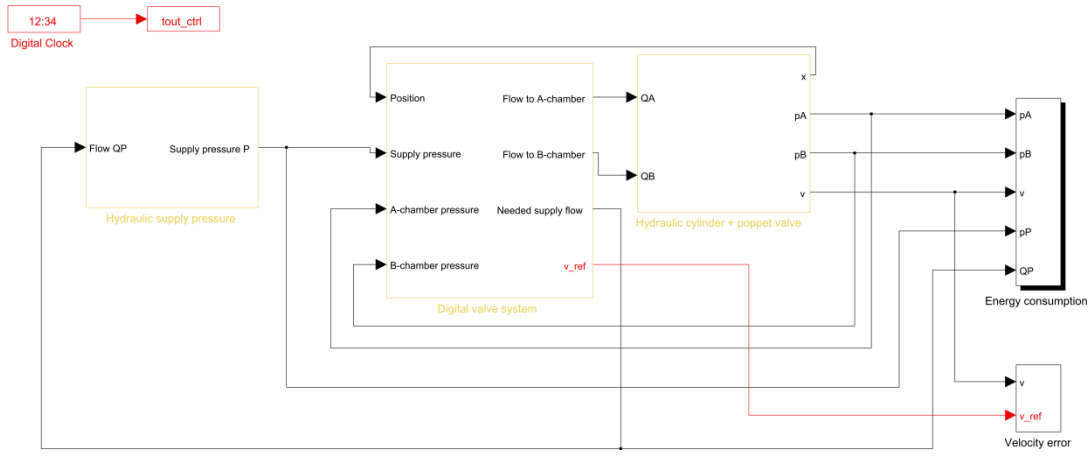

Figure 5.2. *Upper level simulation model of digital hydraulic system using two DFCUs.*

As the figure illustrates, the model consists of five main sub-models: hydraulic supply pressure, digital valve system, hydraulic cylinder and poppet valves, energy consumption and velocity error blocks. Typical feedback signals for Simulink are also shown.

5.2.1 Short-circuit flow controller

The short-circuit flow controller enables the controller to control both, DFCU-PA and DFCU-AT, simultaneously. This connection method increases tracking of velocity reference but also increases power losses because both DFCUs are opened simultaneously. Figure 5.3 shows the upper level of short-circuit flow controller. Position controller is the highest level controller.

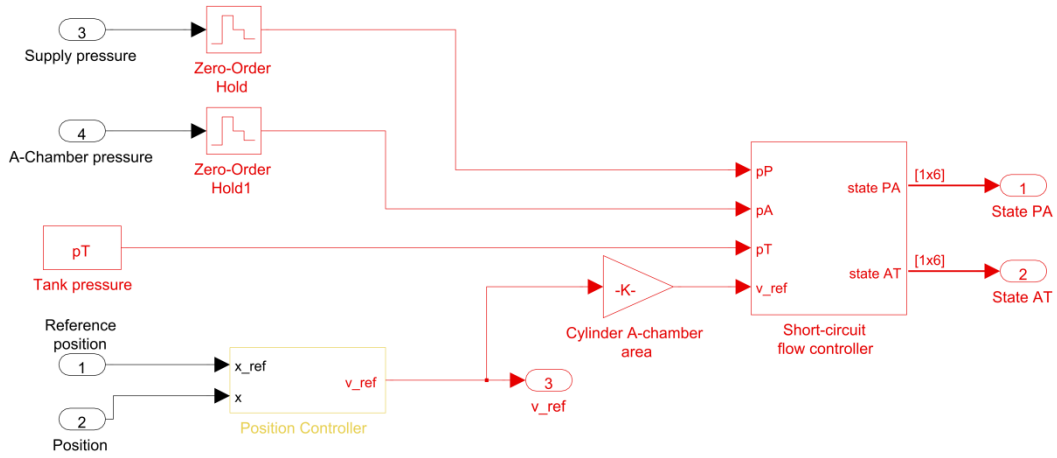

Figure 5.3. *Simulation model of short-circuit flow controller.*

The short-circuit flow controller sub-model includes pressure compensator. The idea is to calculate flow rate by using pressure differences. Steady-state flow rates are calculated with the equations (15) and (16). Because measuring of pressures have been integrated in a real digital hydraulic system and pressure compensation has been made by software, digital hydraulic system does not need extra pressure compensation valves [25].

After calculation of flow rates, output of block is multiplied with vector which consists of all opening combinations states of DFCUs. These values are compared to value of reference velocity and after that the controller chooses the smallest state which produces the wanted flow rate. Figure 5.4 shows simulation model of short-circuit flow controller.

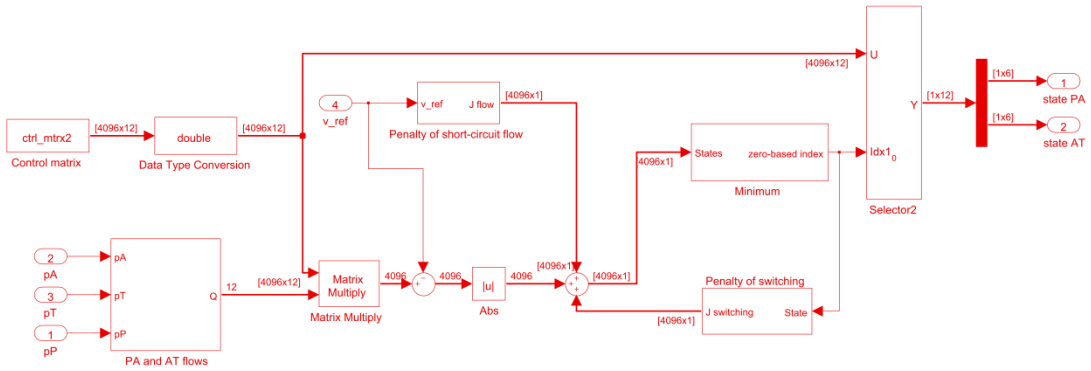

Figure 5.4. *Simulation model of short-circuit flow controller using cost functions of switching and short-circuit flow.*

Short-circuit flow controller includes also cost functions of short-circuit flow and switching the valves. Cost function of short-circuit flow reduces amount of short-circuit flow. The bigger is output of cost function, the more short-circuit flow is reduced. Equation (17) presents cost function of short-circuit flow. $v_{penalty}$ depends on value of reference velocity: if reference velocity is positive, opening of DFCU-AT is reduced.

Cost function of valve switching reduces amount of valve couplings. The bigger is output of cost function, the more couplings are reduced. Equation (18) presents cost function of valve switching.

Although, the gains of cost functions should be in a reasonable range: if cost function of short-circuit flow is too large, short-circuit flow is not used. If cost function of valve switching is too large, state of valve will be never changed.

5.2.2 Position controller

Figure 5.5 shows simulation model of the position controller. Inputs of the controller are reference and simulated positions of a hydraulic cylinder, output value is velocity reference. The controller includes discrete transfer function which softens the output value. The input value of discrete transfer function has been limited using saturation function $[v_{min}, v_{max}]$. Equation (14) presents the equation of proportional controller.

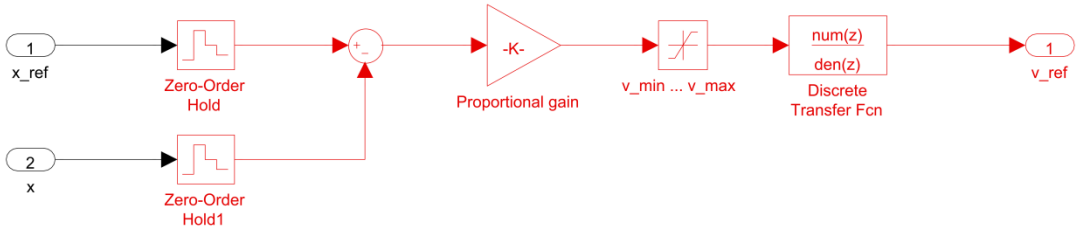

Figure 5.5. *Simulation model of position controller using velocity limiter and discrete transfer function.*

First-order transfer function has been determined using relation of input and output Laplace transformation. The following equation presents first-order transfer function:

$$G_p(s) = \frac{1}{T_c s+1} \tag{100}$$

,where s is Laplace variable and T_c is time constant.

Discrete transfer function transform has presented by Dorf and Bishop [36]. The transfer function of the zero-order hold is:

$$G_0(s) = \frac{1-e^{-sT_s}}{s} \tag{101}$$

Therefore, using time constant value $T_c = 1$, the transfer function $Y(s)/R^*(s)$ is:

$$\frac{Y(s)}{R^*(s)} = G_0(s)G_p(s) = G(s) = \frac{1-e^{-sT_s}}{s(s+1)} \tag{102}$$

From the Laplace transform to the corresponding z-transform the equation (102) is transferred into the following form:

$$G(z) = Z\{G(s)\} = (1-z^{-1})\left[\frac{(1-e^{-T_s})z}{(z-1)(z-e^{-T_s})}\right] = \frac{(1-e^{-T_s})}{(z-e^{-T_s})} \tag{103}$$

When sample time $T_s = 1$, discrete transfer function is obtained:

$$G(z) = \frac{0.6321}{z-0.3679} \tag{104}$$

The following table shows transfer function and discrete transfer function using time constant and sample time values. Using Matlab, discrete transfer function has been found out using the function ‘tf’ and continuous-time dynamic system has been converted into the discrete time system using the function ‘c2d’.

Table 5.1. *Transfer functions of the position controller*

Sample time T_s	Time constant T_c	Transfer function	Discrete transfer function
1 ms	1 ms	$G(s) = \frac{1}{T_c s + 1}$	$G(z) = \frac{0.6321}{z - 0.3679}$

As the table shows, discrete transfer function is same than the equation (104) shows.

5.3 Digital hydraulic system using four DFCUs

Simulation model consists of four DFCUs, hydraulic cylinder and poppet valves with spring. With four DFCUs fault tolerant control is possible and controllability improves about amount of 2 bits. However by using four DFCUs more calculation time is needed and the system is more sensitive to changing of load forces. Also the system with four DFCUs increases power losses a bit. [25]. Figure 5.6 shows the hydraulic circuit of digital hydraulic system using four DFCUs.

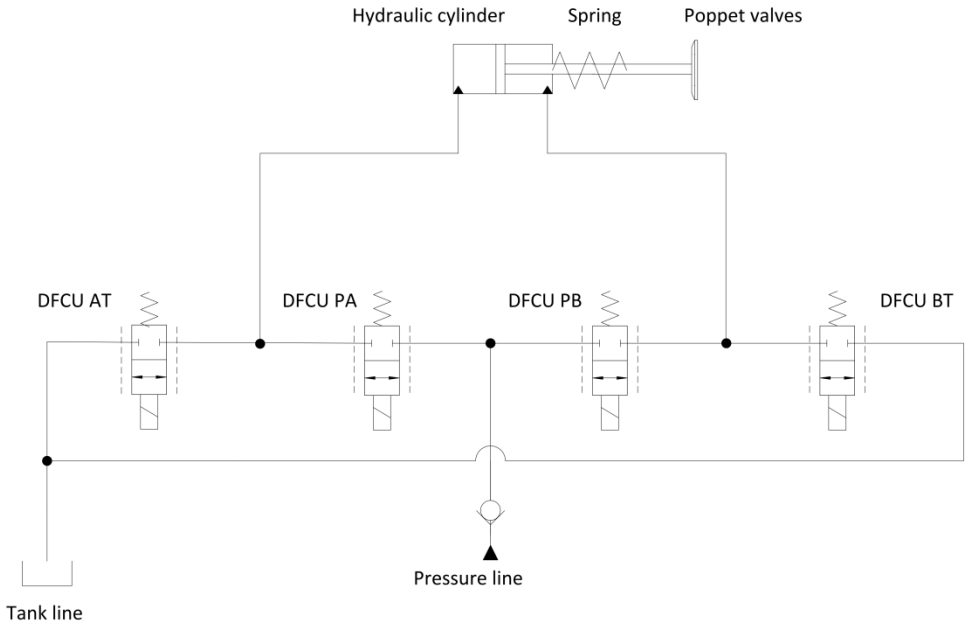

Figure 5.6. *Digital hydraulic system using four DFCUs and hydraulic cylinder actuated poppet valves.*

Because pressurized tank line is not used, it is not possible to utilize fluid flow from the tank line. Thus, fluid flow to tank line is always energy loss.

5.3.1 Model-based valve controller

In this chapter is presented model-based controller using four DFCUs. The upper level model is similar to the model presented in the figure 5.2 using two DFCUs but two extra DFCUs are included into the system.

Figure 5.7 shows the upper level of controller and model of digital valves. The controller consists of two different sub-models: position and model-based controller.

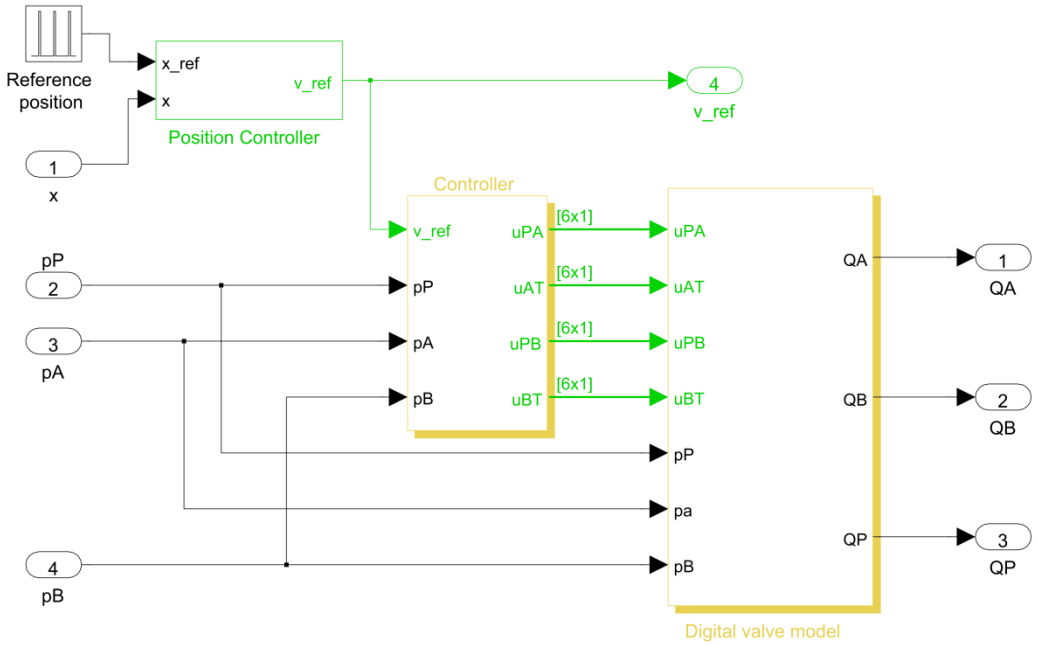

Figure 5.7. *Simulation model of upper level controller and digital valve model.*

Figure 5.8 illustrates the upper level of model-based controller. The inputs of the model are velocity reference from position controller sub-model and simulated supply and chamber pressures. The idea of model-based controller is to calculate and select the mode which uses as less energy as possible and enables as well as possible the required velocity and pressure references.

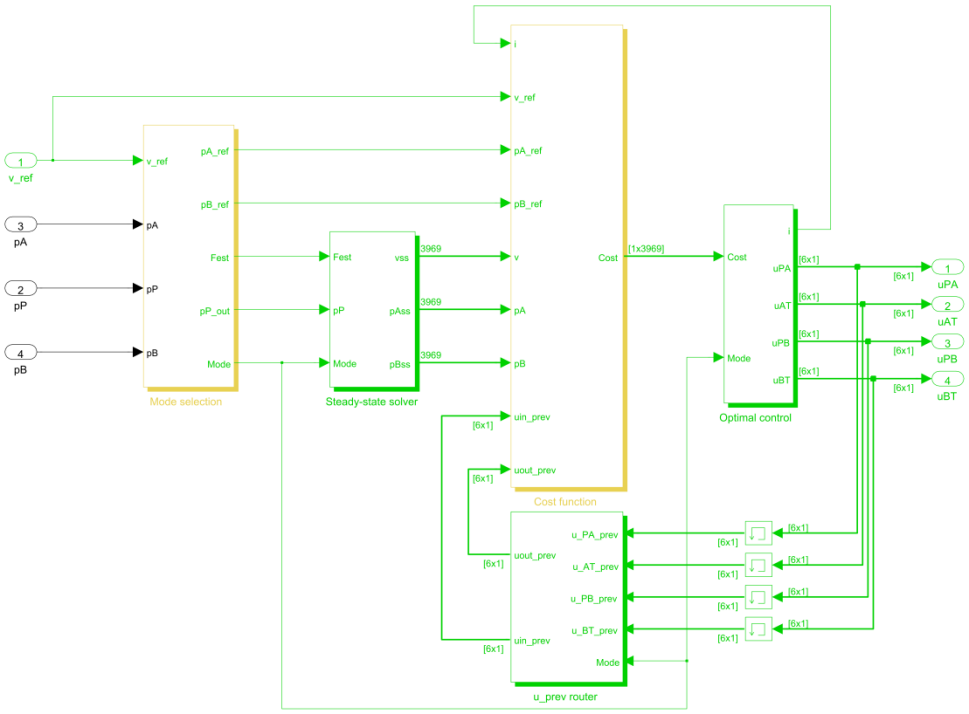

Figure 5.8. *The upper level of controller for four DFCUs.*

The controller consists of five different sub-models: Mode selection, steady-state solver, cost function, previous value and optimal control blocks. The following chapters present working principles of the most important sub-models of controller.

5.3.2 Mode selection

The sub-model mode selection selects the most optimal mode according to load and movement states. Table 5.2 shows all the possible modes which are possible using four DFCUs. Differential modes save always energy. Using extending differential connection mode, oil flows from the B-chamber to the A-chamber. In connection mode retracting differential oil flows from the A-chamber to the B-chamber. Using differential modes, velocity of hydraulic cylinder is greater but available force from the cylinder is reduced.

Table 5.2. *Available modes using four DFCUs*

Mode	Name	Available DFCUs
+2	Extending differential connection	PA, PB
+1	Extending inflow-outflow	PA, BT
0	Stop	None
-1	Retracting inflow-outflow	PB, AT
-2	Retracting differential connection	PB, PA

Choosing the most optimal mode the available forces should be calculated in the model available force range. The equations (20) - (25) present available force range.

Using calculated hydraulic cylinder chamber pressures, estimated cylinder force is calculated in the model load force estimator using equation (19). Using the estimated cylinder force and available force ranges, the mode is calculated using the equations (26) - (39). After that, the pressure references are calculated. Using load force estimator model, the simulated chamber pressures are filtered because the control should not react to too fast pressure differences. In the model chamber pressures are changed to discrete values. After that the values are low-pass filtered and changed back to discrete values using length of controller's sample time. Figure 5.9 shows the simulation model of load force estimator.

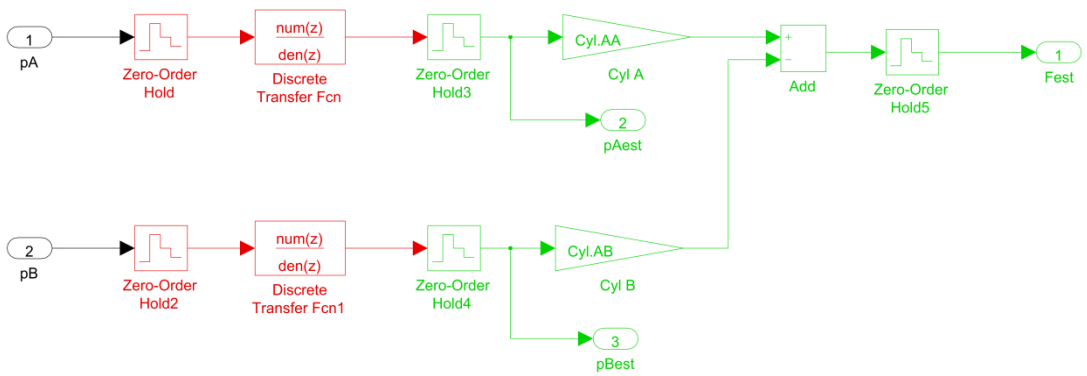

Figure 5.9. *Simulation model of load force estimator using discrete transfer function.*

Table 5.3 shows transfer function and discrete transfer function of load force estimator.

Table 5.3. *Discrete transfer function of load force estimator*

Sample time	Time constant	Transfer function	Discrete transfer function
0.1 ms	1 ms	$G(s) = \frac{1}{0.001s + 1}$	$G(z) = \frac{0.0952}{z - 0.9048}$

Figure 5.10 shows hydraulic cylinder A-chamber pressures before and after discrete transfer function. As the figure shows, the discrete transfer function softens the chamber pressure curve.

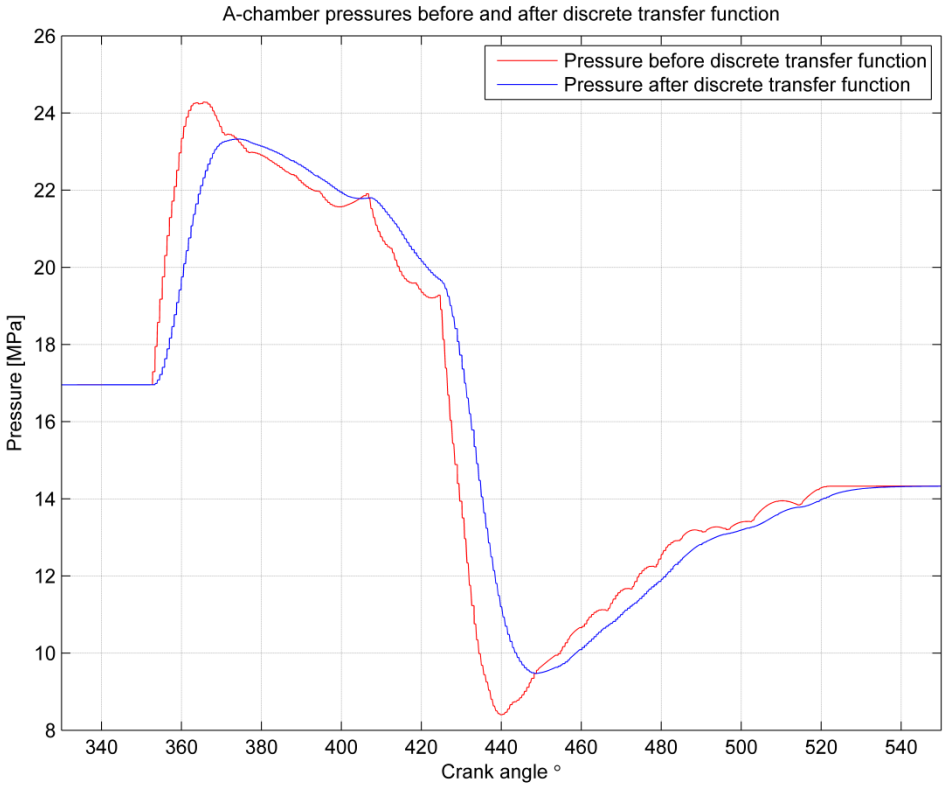

Figure 5.10. *Calculated A-chamber pressures before and after discrete transfer function.*

The model pressure references calculates the reference chamber pressures of cylinder that primary side DFCU has always when possible minimum pressure difference Δp_{ref} and chamber pressure of delivery side will not exceed the largest allowed chamber pressure p_{max}. Equations (40) – (51) have been used in the sub-model pressure references.

5.3.3 Steady-state solver

The sub-model steady-state solver calculates all possible chamber pressures and velocities of cylinder in equilibrium states. The equilibrium states are come true after a short transient time when the state has changed. The chamber pressures and velocity of cylinder are calculated with the equations (52) – (63). Figure 5.11 and equations (105) – (107) show the idea of the steady-state solver.

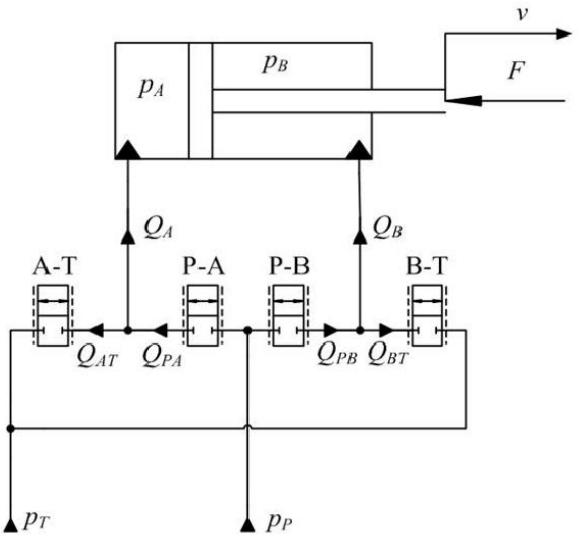

Figure 5.11. *The idea of steady-state solver for calculate chamber pressures and velocity of cylinder using digital valve system. [27].*

$$Q_{PA}(u_{PA}, p_P, p_A) - Q_{AT}(u_{AT}, p_A, p_T) = A_A v \tag{105}$$

$$Q_{PB}(u_{PB}, p_P, p_B) - Q_{BT}(u_{BT}, p_B, p_T) = -A_B v \tag{106}$$

$$F = p_A A_A - p_B A_B \tag{107}$$

The steady-state solver enables proactive control of valves because the sub-model calculates what happens with each state at the following time value.

5.3.4 Cost function and optimal control

The sub-model cost function calculates the quality of DFCU states. The quality of state has been estimated using velocity error, chamber pressure errors and needed coupling amounts of state of change. Steady-state velocity and chamber pressures have already been resolved at the model steady-state solver. Error values which have caused by different factors are gained with suitable values and the values are added up. Velocity error equation (64) has been used between reference velocity and simulated velocity. Equations (65) and (66) show square error of pressure differences using coefficient value W_p. Equations (67) and (68) show square error of valve switching using coefficient value W_{sw}.

When the quality has been calculated to all state of changes, the sub-model optimal control chooses the best state.

5.4 Hydraulic system model

Modelled hydraulic systems consist of five different sub-models: hydraulic supply pressure, digital valve system, hydraulic cylinder and poppet valves, energy consumption and velocity error. Because all models have been modelled using Matlab/Simulink, the signals between the blocks are only one way. Furthermore, the blocks are linked with each other using feedback signals. This modelling method is typical for Simulink: for example simulation programs which uses Modelica language, equations have no predefined causality [37].

5.4.1 Supply pressure model

Supply pressure model consists of three different methods how to determine pressure. Supply pressure can be constant, variable or non-ideal. If constant supply pressure model is used, a value of supply pressure remains always constant. Using variable supply pressure, for example sine wave supply pressure can be used but the system will not affect to the value of supply pressure. Non-ideal model consists of disturbance compensator which integrates the disturbance. The model has drop and integrator gains. Drop gain affects how big flow drop could be and integrator gain affects to the compensation of disturbance. First-order transfer function has been used to break algebra loop of the ideal supply pressure. Using non-ideal supply pressure model, the system affects to the value of supply pressure. The following table shows transfer function of the non-ideal supply pressure.

Table 5.4. *Transfer function of non-ideal supply pressure*

Time constant	Transfer function
1 ms	$G(s) = \frac{1}{0.001s + 1}$

Figure 5.12 shows the simulation model of hydraulic supply pressure.

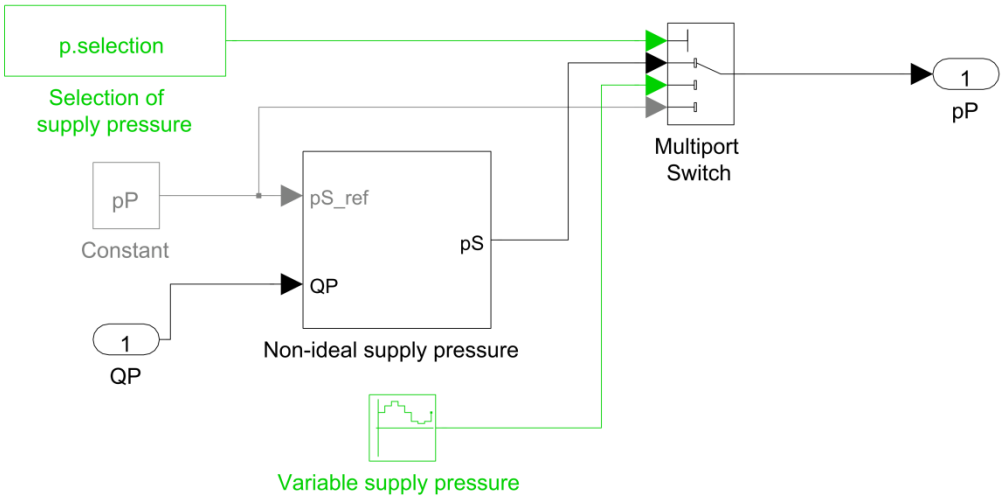

Figure 5.12. *Simulation model for choosing correct hydraulic supply pressure.*

Inputs of the simulation model are constant of selection correct supply pressure, constant supply pressure and variable supply pressure but also needed flow rate from pressure line. Output of the model is supply pressure used in the system.

5.4.2 Model of valve dynamics

Using 2/2 solenoid-based valves, the control signal of the valve is a discrete, zero or one. When the control signal is zero, the valve remains in its initial position, which can be either open or closed. When control signal is one, basic valve dynamics model consists of delay and constant speed values. Delay time is a time value between a given control signal and armature movement. Movement time is a time which describes armature motion from the start to fully open or closed position. Response time is sum of delay and movement time. Figure 5.13 shows the idea of delay and movement time parameters.

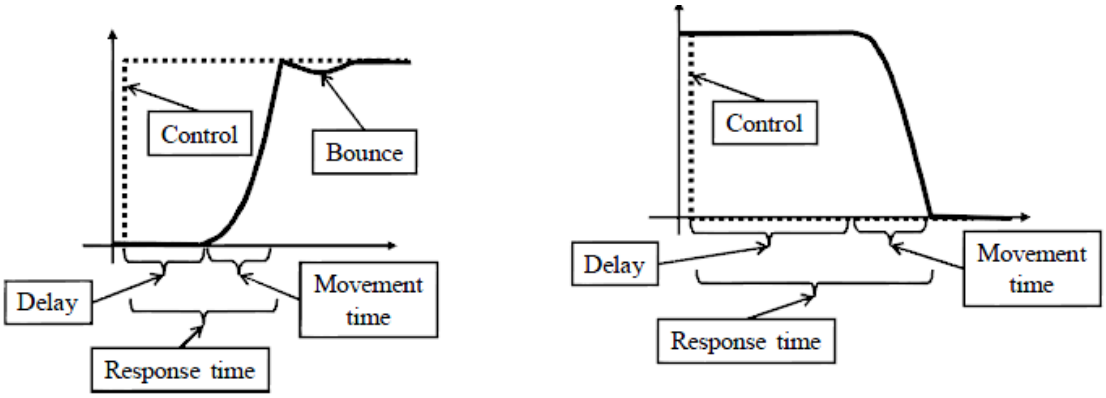

Figure 5.13. *Principle of valve dynamics with opening and closing the valve [27].*

Figure 5.14 shows the simulation model of valve dynamics using delay and movement time values. Opening delay is used when input of the switch block is greater than 0.5, otherwise closing delay is used. Rate limiter limits the movement time of a valve with opening and closing time values.

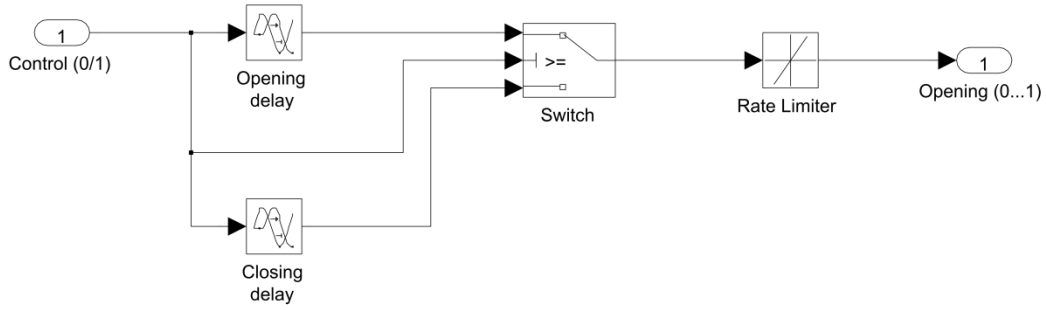

Figure 5.14. *Valve main dynamics model using delay and movement time values [25].*

A better model of valve dynamics has presented by Schepers et al. [38]. The idea of model is based on virtual range concept where the range is from -1 to 2 and real opening from 0 to 1. Figure 5.15 shows the concept of virtual range. It consists of three different phases; opening and closing delay phases, movement phases and sticking phases. During opening and closing delay phases only virtual opening is changed. As figure shows, in opening delay phase, a value of virtual opening is first -1 and at the end it is changed to value 0. Vice versa in closing delay phase a value of virtual opening phase is 2 and at the end it is 1. During movement phases virtual and real opening phases are equal in the range [0, 1]. Sticking phases are thought to be phases when a value of virtual opening phase increases to its value 2 from value 1 and closing phase decreases from its value 0 to value -1. Sticking time determines how fast the armature gets stuck into the end position [27].

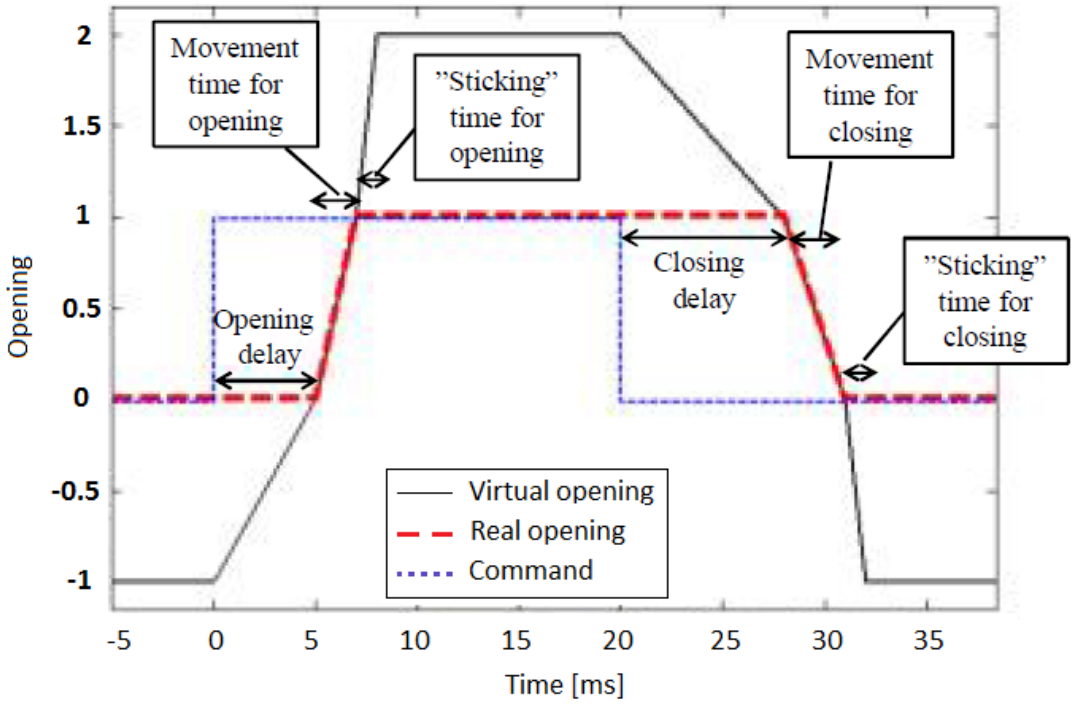

Figure 5.15. *Concept of virtual range using three different phases. Modified from original [27].*

Figure 5.16 presents the simulation model of valve dynamics using concept of virtual range. Integrator block limits its output values from -1 to 2 and initial input value of block is -1. Output value of integrator block is compared to constants and depending on an output value of integrator, output of opening or closing range block is chosen. Finally saturation block limits output value of model from 0 to 1. Delay value of a valve is usually significantly longer than movement time. Although, sticking time is difficult to know. [27].

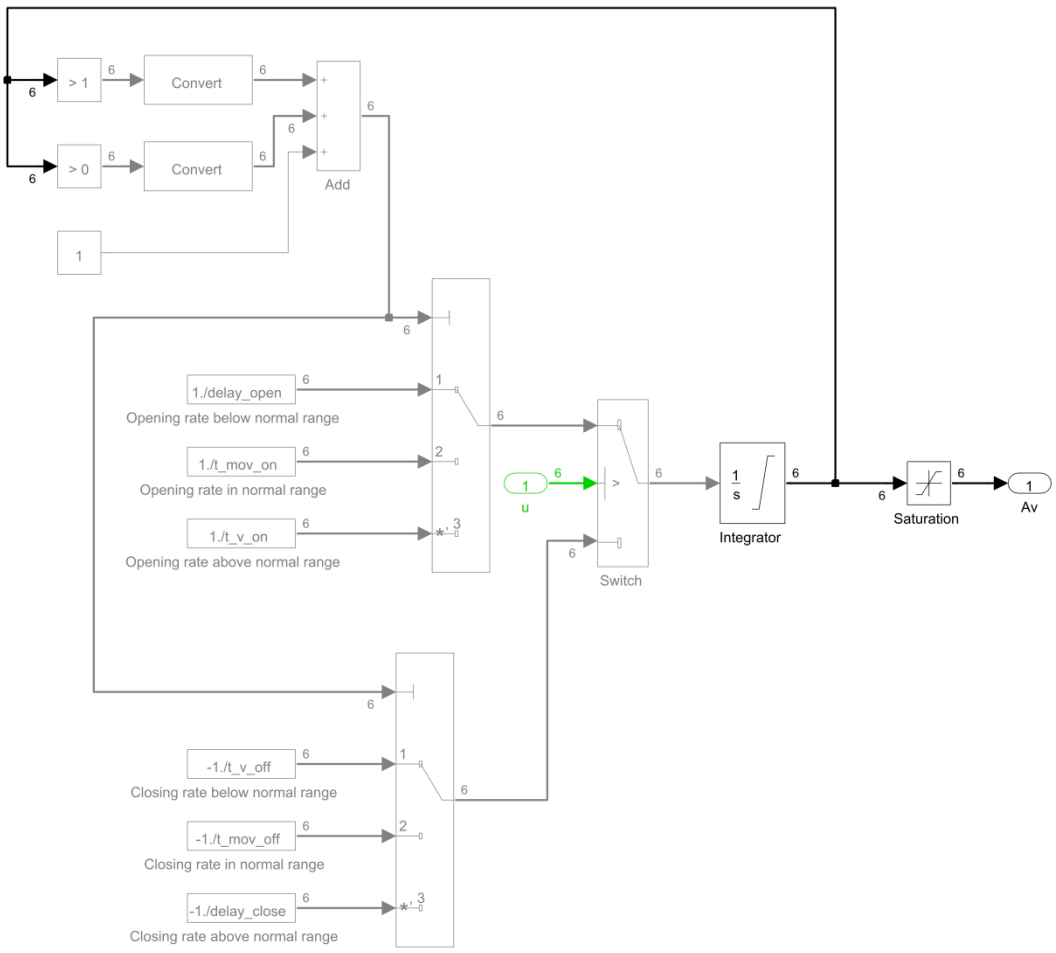

Figure 5.16. *Concept of virtual range, Simulink model.*

In the real world parameters are different for opening and closing a valve and parameters depend on e.g. oil viscosity and pressure conditions but also control electronics, voltage and cabling [25].

5.4.3 Orifice

The equations of hydraulic valve flow are presented by Ellman and Piche [39]. When flow is turbulent, equation (69) is used. When pressure difference is smaller than used transition pressure value p_{tr}, the polynomial flow equation (70) is used.

5.4.4 Hydraulic cylinder model

The equation (71) presents the state equation of hydraulic cylinder volume. In the equation $\dot{p}$ is difference of pressure, B_{eff} is bulk modulus of oil, V is volume of cylinder chamber, ΣQ is sum of flow rates and $\dot{V}$ is difference of chamber volume. The equation

shows that changing of pressure is affected by sum of flow rates and difference of volume. Figure 5.17 presents the simulation model of hydraulic cylinder. Hydraulic cylinder has been modelled as two different chambers, A and B. Friction model with hyperbolic tangent function has been included to cylinder model. Equation (72) shows the force equation of the hydraulic cylinder.

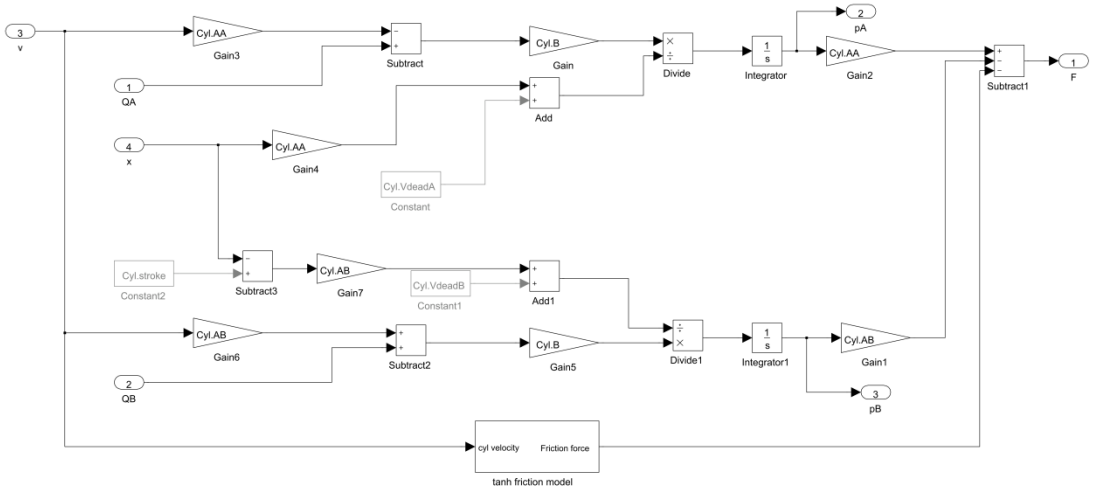

Figure 5.17. *Simulation model of hydraulic cylinder.*

Inputs of the model are velocity and position of cylinder and chamber A and B flow rates. Also dead volumes of chambers have been taken into account. Outputs of the model are chamber pressure A and B and hydraulic cylinder force.

5.4.5 Cylinder friction model

Friction model of hydraulic cylinder has been modeled as tanh friction model. The idea of model is to replace sign -function with hyperbolic tangent function and soften the change of friction force around zero velocity. The equation (74) shows tanh friction force. The equation includes the parameter K which determines how fast friction force value changes near zero velocity. A suitable value range of K is 2000 - 20000 [40].

5.4.6 Load model

System load has been modelled as Newton's second law, shown in the equation (73). Figure 5.18 shows the simulation model of system load. Input forces are cylinder force and pre-load of spring. Outputs are acceleration, velocity and position of cylinder.

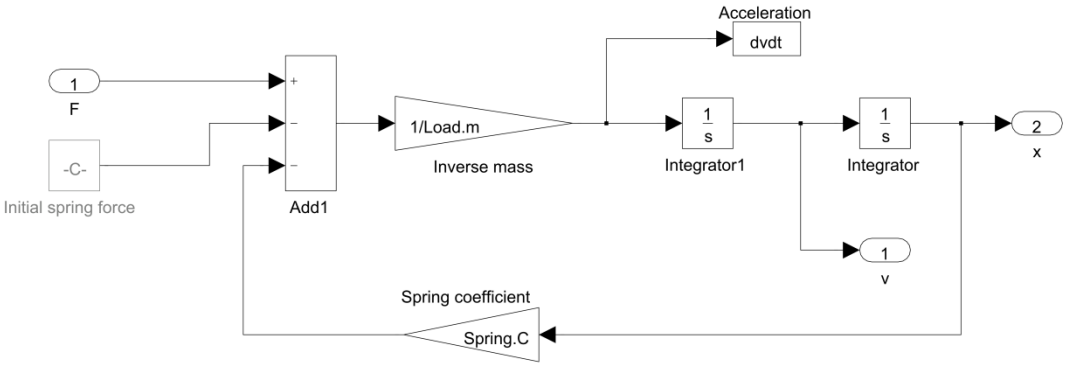

Figure 5.18. *Simulation model of load.*

Using a spring with a big pre-load force it is possible to use spring as safety mechanism for poppet valves. It ensures safety valve closing to its initial, closed position. Big spring force also accelerates poppet valves during the closing phase.

5.4.7 Damping model

Idea of damper is to decrease velocity of poppet valves before it is in the closed position. Before the poppet valves are totally closed velocity should be less than 0.5 m/s according to the principle of Wärtsilä [41]. Figure 5.19 presents the simulation model of damper. Damping threshold determines the position when damping force occurs. Damper works only when velocity of poppet valves is negative.

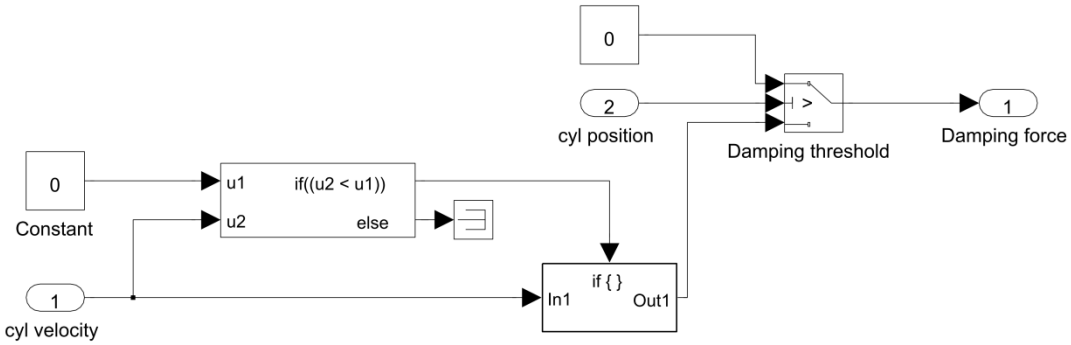

Figure 5.19. *Simulation model of damper. The model works only with negative velocity values.*

Damping force is linear to velocity of poppet valve. The equation (75) presents damping force.

5.5 Poppet valve

Figure 5.20 illustrates the design of spring forced intake air valve with gas flow edges. When the intake valve is opened, gas and air mixture flows through the poppet valve into the cylinder. Amount of gas and air depends strongly on opening of valve, shape of gas flow edges and dimensions of poppet valve but also pressure difference before and after the poppet valve.

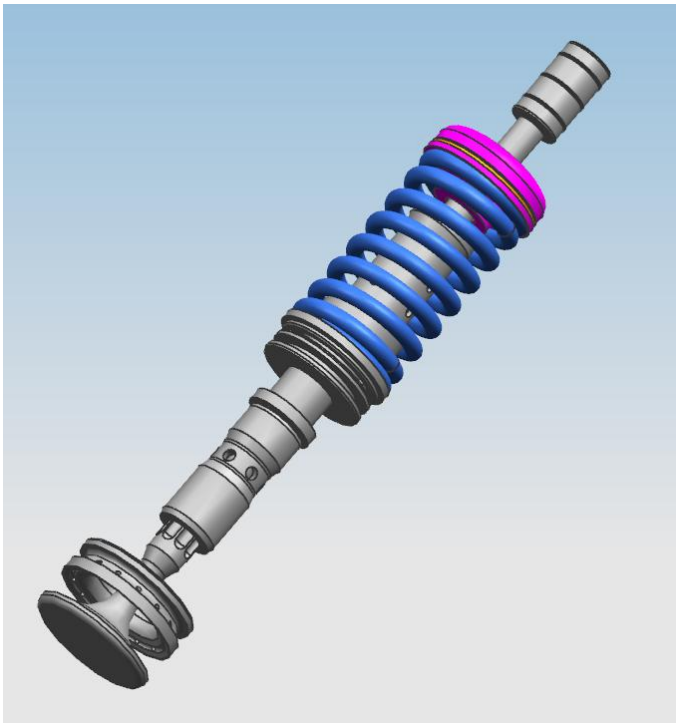

Figure 5.20. *Spring forced intake air valve with gas flow edges [42].*

The intake valve movement is controlled by hydraulic cylinder. In appendix D are presented force balance equations which determine initial chamber pressures of hydraulic cylinder.

5.5.1 Poppet valve geometry

Figure 5.21 shows design parameters of the poppet valve geometry. The main components are a poppet valve head, a valve shaft and a seat of the valve. The poppet valve lift should be at least 25 % of the valve head. This provides the annular valve opening area equal to the port throat area. If the poppet valve lift is less than 25 %, the volumetric efficiency of the engine will be decreased. [43].

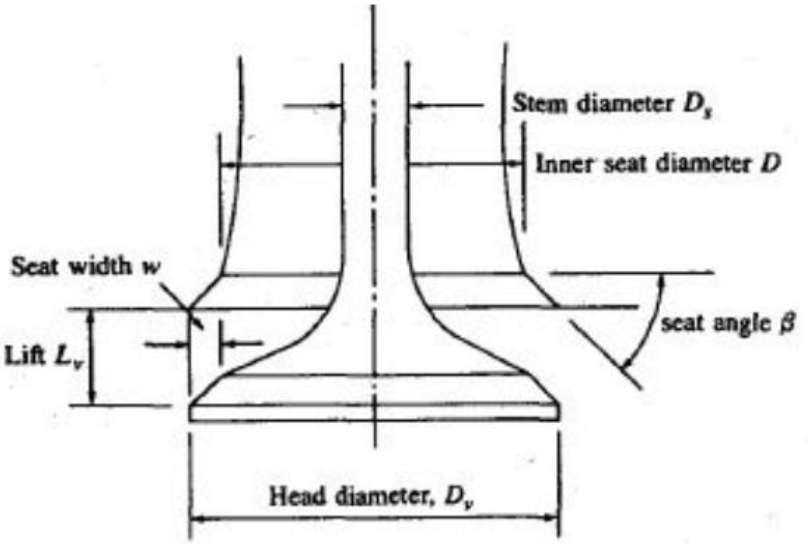

Figure 5.21. *Poppet valve geometry parameters [16].*

The equations (82) – (87) present poppet valve lift and area. Flow area of a poppet valve depends on opening of valve and flow area is divided to the three different areas. In the equations the parameter w is seat width, β is seat angle, L_v is lift of the poppet valve, D_v is head diameter of the poppet valve, D_p is poppet valve port diameter, D_s is stem diameter and D_m is mean seat diameter. Figure 5.22 shows the value ranges to determine correct values of intake valve and valve port. Used parameters are listed in appendix E.

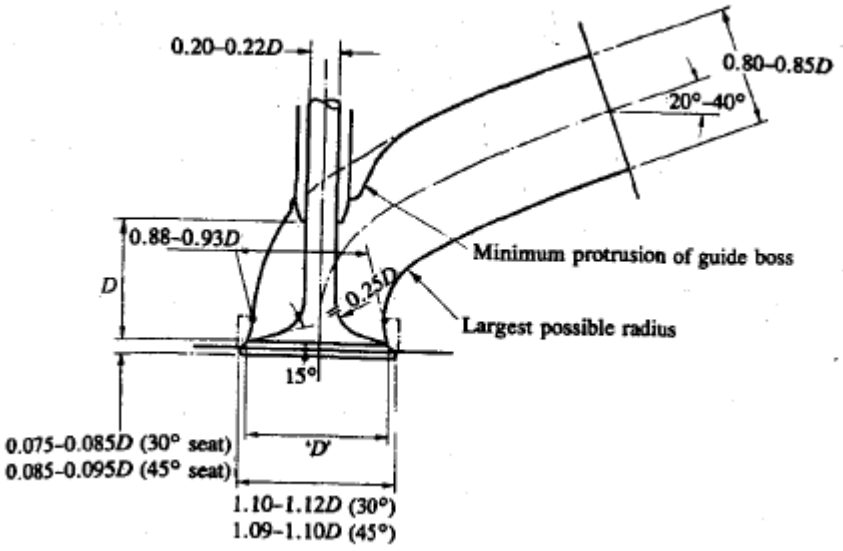

Figure 5.22. *Intake valve port design values [16].*

5.5.2 Gas flow equations

Gas flow through a restriction has been modelled with two different equations (92) and (93). When the critical pressure ratio is greater than pressure ratio $\frac{p_2}{p_1}$, where p_2 is downstream an p_1 is upstream pressure, subcritical flow is used. When the pressure ratio is less or equal to the critical pressure ratio, choked flow is used. In the equations (92) and (93) the parameter C_d is value of discharge coefficient, A_m is flow area, R is ideal gas constant, T is temperature of the gas and γ is heat capacity ratio of the gas. Figure 5.23 shows various orifice shapes and discharge coefficient values.

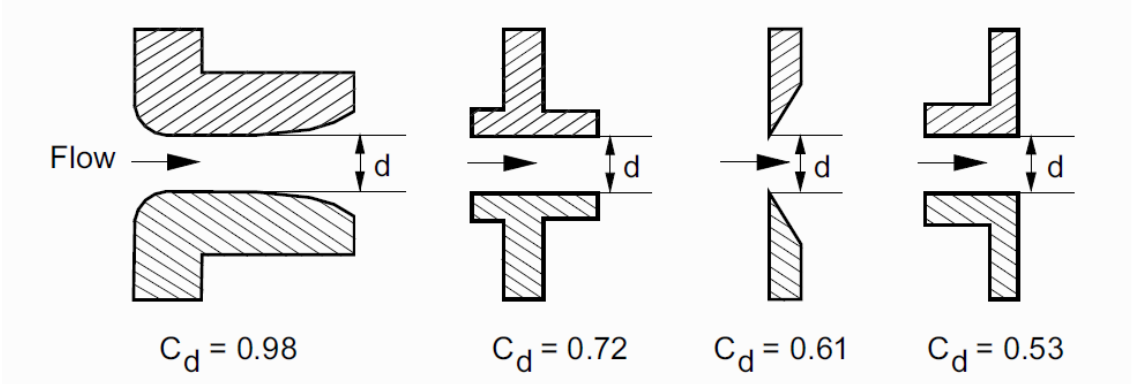

Figure 5.23. *Various orifices and discharge coefficients [28].*

5.5.3 Area of gas flow edges

Shape of gas flow edges and opening of valve affect to the gas flow area. Figures 5.24 and 5.25 present parameters which have been used to determine gas flow areas.

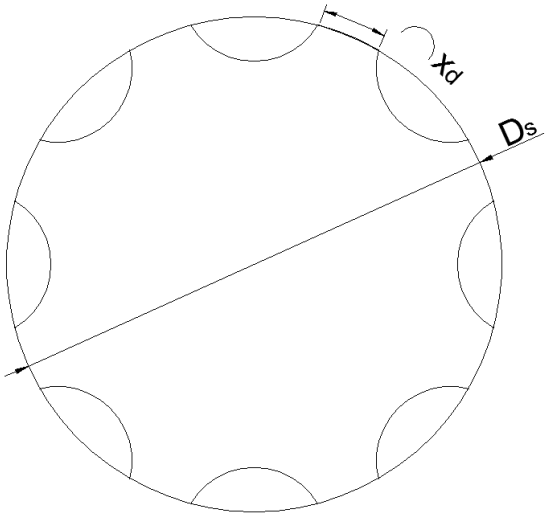

Figure 5.24. *Gas flow edges on poppet valve's shaft.*

Equations (88) - (91) present flow area equations and flow calculations are presented in appendix E. Flow area is divided to two different areas, A_1 and A_2. These areas are based on two different segments, shown in figure 5.25. A_2 is outer area and A_1 is inner area.

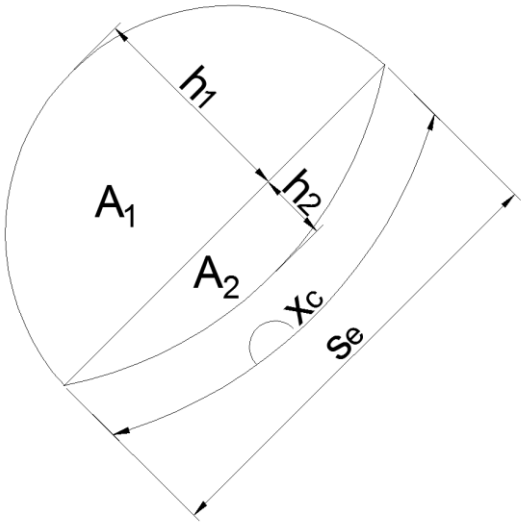

Figure 5.25. *Detailed view of gas flow edge.*

Figure 5.26 presents some different shapes of gas flow edges. Edges have a big impact on gas flow amount. The shape of edge with opening of valve determines the real flow area of a gas edge.

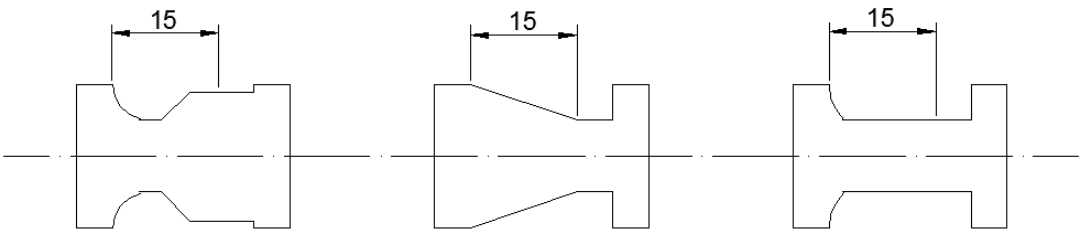

Figure 5.26. *Different shapes of gas edges.*

In the simulation results shown in the chapter 6, shape of gas edge shown in the figure 5.26 on the right side has been used.

5.5.4 Simulation model of poppet valve

Figure 5.27 shows the simulation model of a poppet valve. The model consists of a poppet valve area, gas feeding edges, and air and gas mass flow equations. The inputs of

the model are poppet valve lift, and air, gas and initial cylinder pressures. The outputs are fed air and gas masses and the flow rates.

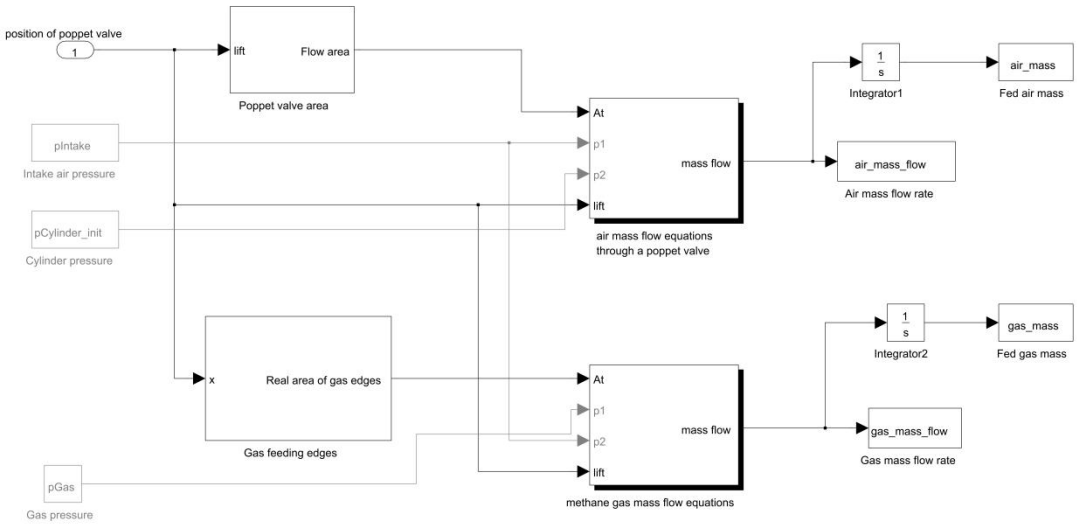

Figure 5.27. *Simulation model of poppet valve including poppet valve and gas feeding edge areas and mass flow models.*

Figure 5.28 shows the simulation model of gas feeding edges. Shape of gas edge is modelled with one dimension lookup table. Position of cylinder has been divided by maximum stroke of a cylinder. Input of lookup table is between [0,1] because area of gas edges are proportional to position of cylinder. Saturation block makes sure that output of lookup table is between [0,1]. Output of saturation block is multiplied by total area of gas edges and amount of poppet valves. Output of model is real gas flow area.

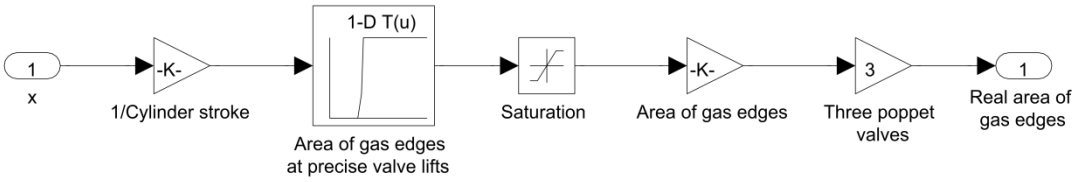

Figure 5.28. *Simulation model of gas feeding edge area using look-up table to determine shape of gas flow edges.*

Figure 5.29 shows simulation model of gas mass flow. Air mass flow model is similar to gas mass flow model: the model consists of subcritical and choked flow blocks which are used when input of critical pressure ratio is realized. Differences between air and gas mass flow models are just heat capacity, temperature of the gases and critical pressure ratios of the gases. The same discharge coefficients values for both gases have been used.

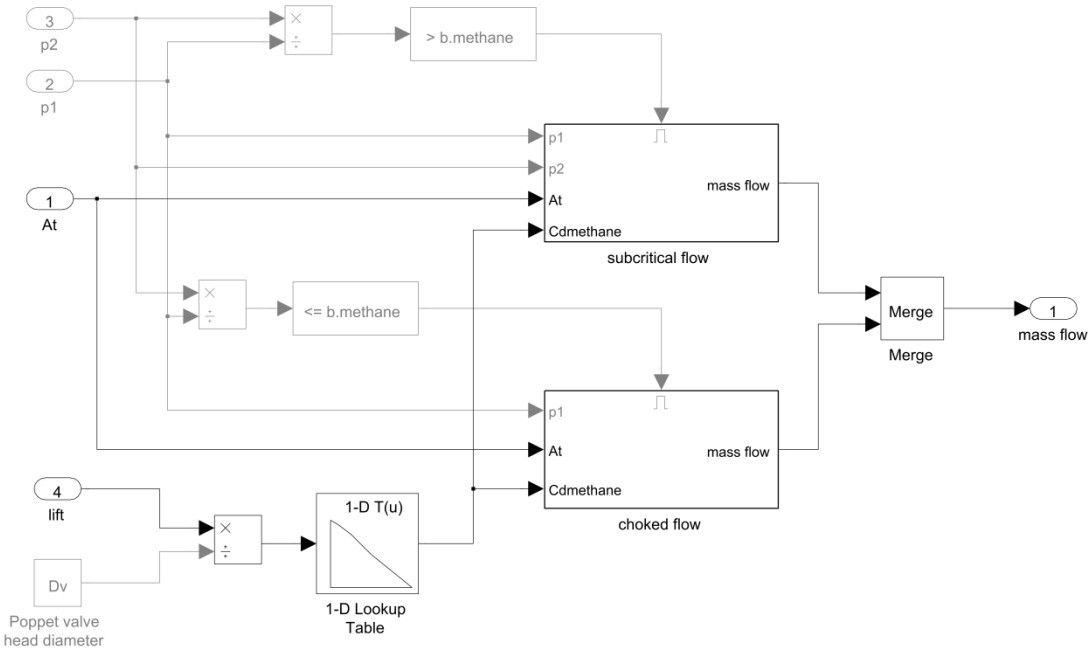

Figure 5.29. *Simulation model of gas mass flow using subcritical and choked flow blocks.*

5.6 Solenoid based gas admission valve

The third system is based on digital pneumatic valve driven by solenoid. The main difference between pneumatic valve system and poppet valve system is that pneumatic valve controls only amount of gas mass.

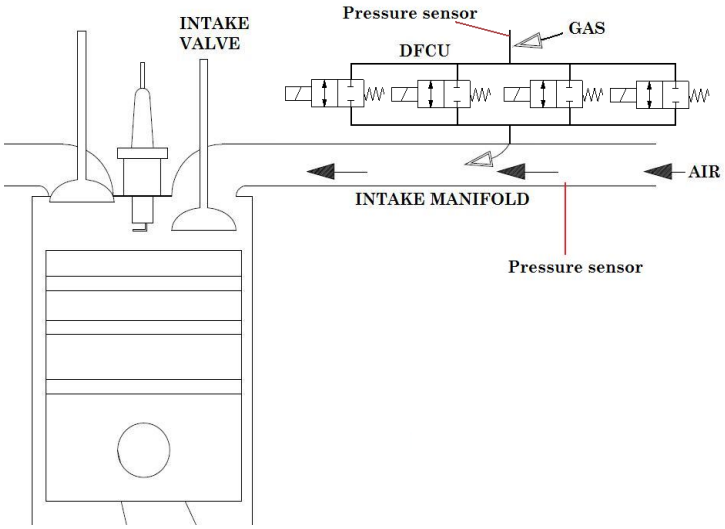

Figure 5.30. *Gas admission valve located next to intake manifold [24].*

The position of digital pneumatic valve is similar to the SOGAV valve which is used at the moment: the valve is located next to intake manifold before intake valves.

5.6.1 Modelling of solenoid based gas admission valve

Figure 5.31 shows the upper level of pneumatic valve model. The model consists basically two different blocks: controller and digital valve system.

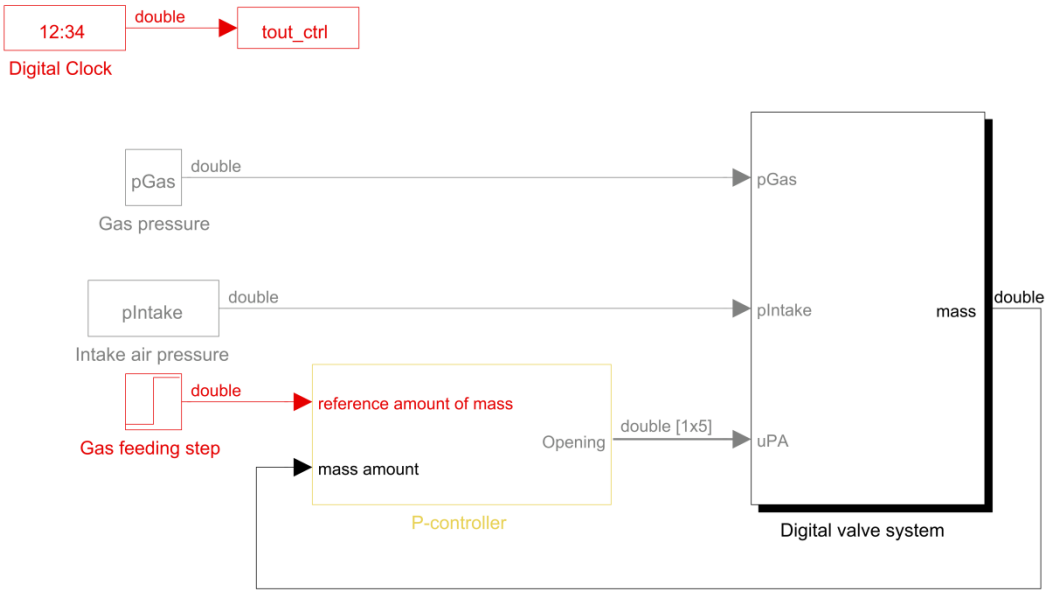

Figure 5.31. *Simulation model of digital pneumatic valve.*

Figure 5.32 shows the simulation model of pneumatic DFCU.

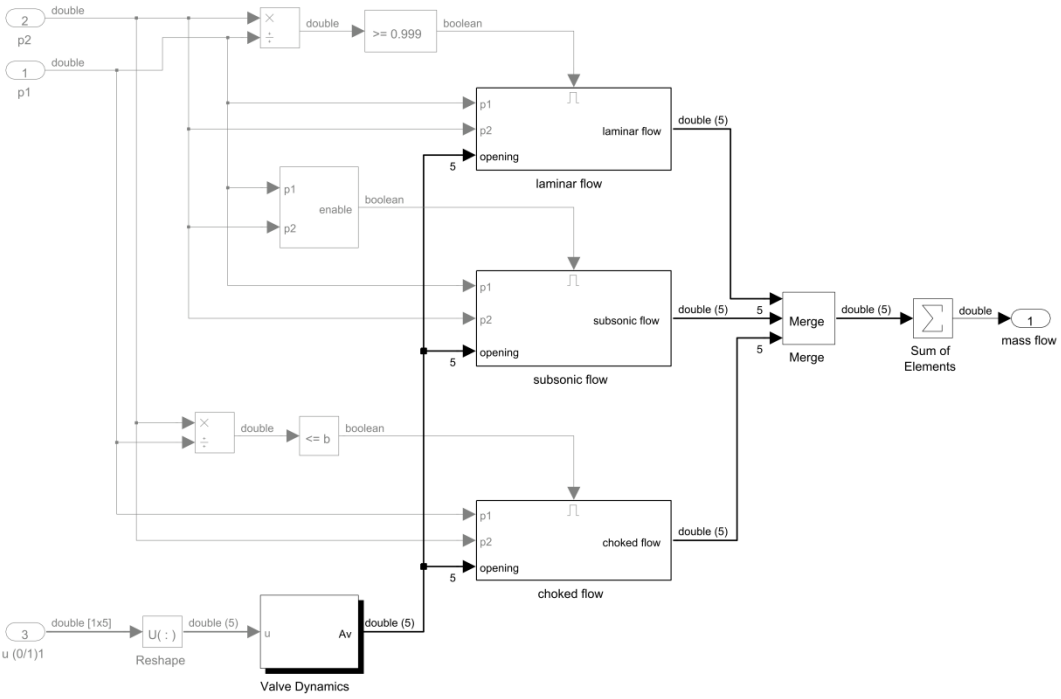

Figure 5.32. *Simulation model of pneumatic DFCU, valve dynamics and flow models.*

The model has been divided into the three different flow models: laminar, subsonic and choked flow. Depending on upstream and downstream pressures, the correct model has been chosen. The virtual range valve dynamics model has been used.

5.6.2 Simulation model, PCM –coded

Controller of PCM -coded solenoid based gas admission valve is basic proportional controller. Inputs are reference amount and fed amount of gas masses and the difference has been gained in the controller. The equation (14) presents proportional controller.

5.6.3 Modelling of pneumatic equations

ISO-6358 standard [44] presents pneumatic fluid power equations which consist of two parameters: the critical pressure ratio b_{gas} and the sonic conductance C_{ve} [28]. With these parameters the flow rate can be presented. Equation (94) shows pressure ratio b_{gas}. In the equation γ is heat capacity ratio for specific gas.

Beater [28] has presented pressure ratio $\frac{p_2}{p_1} > 0.999$ for laminar flow. The ratio is arbitrarily done and more physical oriented way would be to use Reynolds number to determine flow through a valve. However, laminar flow is typically active only in the

steady state simulations and another choice of the pressure ratio limit will not change the result. Equations (95) - (98) shows laminar, subsonic and choked flow equations. In the equations ρ_0 is density of methane.

Beater [28] presents an approximation for restrictions. Originally the equation was presented by Gidlund (1977). When the ratio of length L to diameter d is less than 10, the equation (99) can be used to define the sonic conductance. In the equation (99) d is inner diameter of restriction in millimetres. Using the equation, unit of sonic conductance is $dm^3/(s * bar)$. Figure 5.33 presents the schematic view of restriction.

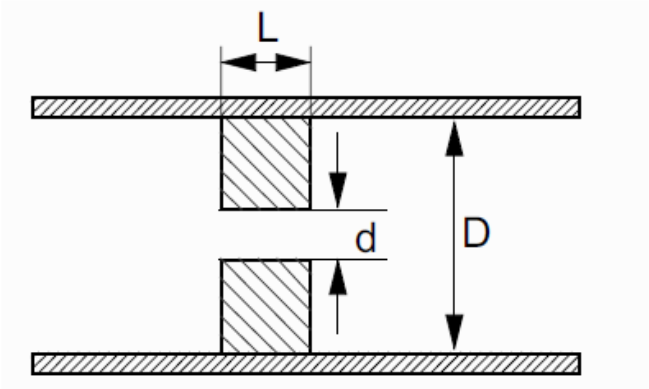

Figure 5.33. *Schematic view of restriction [28].*

6 SIMULATION RESULTS OF THE SYSTEMS

Simulation results using digital hydraulic systems with two and four DFCUs and results using digital pneumatic valve system are shown in this chapter. Needed gas amount is calculated using parameters shown in appendix F. The both systems using hydraulic cylinder include three poppet valves and poppet valve parameters are presented in appendix E. Final velocity before poppet valves are totally closed should be lower than 0.5 m/s according to principle of Wärtsilä [41]. The digital pneumatic valve system includes five PCM coded valves. The simulation results shown in this chapter are for the engine specification shown in table 6.1 and all common simulation parameters are shown in appendix G.

Table 6.1. *Engine specification, needed cylinder power 190 kW*

Parameter	Value
Needed power per cylinder	190 kW, 1000 rpm
Cylinder bore diameter	180 mm
Inlet valve head diameter	40 mm
Amount of inlet valves	3
Needed total gas amount	1.32 g / cycle
Needed total air amount	48 g / cycle
Methane gas pressure	0.58 MPa
Intake air pressure	0.5 MPa
Initial cylinder pressure	0.332 MPa

All simulation results are done using Matlab/Simulink. Usually, for sufficient accuracy of simulation results, experimental results are needed to calibrate simulation parameters and results. It was noticed that the simulation results used an open-source Modelica-based simulation program OpenModelica (version 1.8.1) behaved at times similar than results from Simulink model but at times totally different [45]. The parameters and models were similar. As the example shows, there can be also differences between programs because code errors always exist.

6.1 Digital hydraulic system using two DFCUs

Two different simulation results are done using two DFCUs. The both systems using supply pressure 30 and 25 MPa are simulated without end damping model. The wanted final velocity below 0.5 m/s is more difficult to achieve without end damping model.

However, acceleration of the poppet valve is significantly lower. As the results show, in the both cases the final velocity is below 0.5 m/s. Chapter 5.2.1 shows short-circuit flow controller which has been used in the simulation results.

6.1.1 Simulation results using supply pressure 30 MPa

Simulation parameters which are specific for the system using two DFCUs and supply pressure 30 MPa have been listed in appendix H. Figure 6.1 shows the hydraulic cylinder position, and chamber A and B and supply pressures. Maximum lift is 14.7 mm and poppet valve is totally closed at crank angle 499°. The poppet valve is in the position of 1 % of cylinder bore diameter at crank angle 484°. Thus, Miller timing is 56° BBDC.

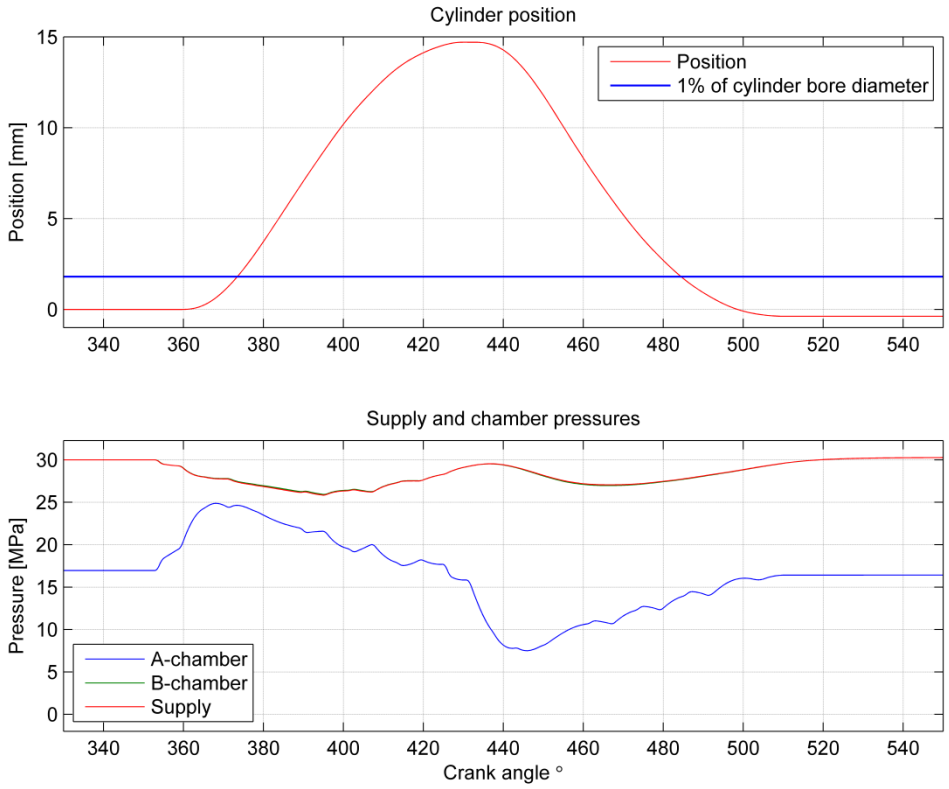

Figure 6.1. *Hydraulic cylinder position and system pressures.*

Because supply pressure affects all the time to the B-chamber, pressure values of B-chamber and supply pressure are almost the same. An orifice has been modelled next to B-chamber with the flow rate value 60 l/min at pressure difference 0.5 MPa to find out pressure and flow rate of the chamber. Because of high flow rate through the orifice with small pressure difference the orifice affect just a very little to the chamber pressure.

Figure 6.2 shows air and mass flow rates through the poppet valve and fed mass amounts. Fed amount of air is 50.2 g and gas amount is 1.34 g.

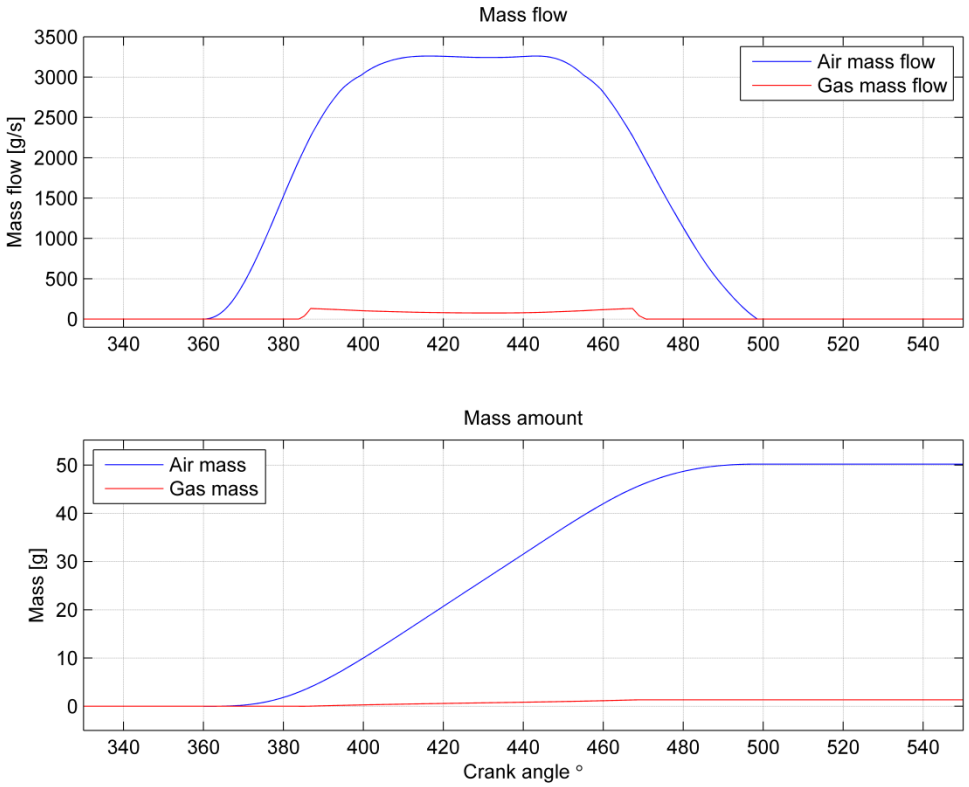

Figure 6.2. *Air and gas mass flow rates and fed amount of gases.*

The poppet valve should be opened more than 5 mm before gas flow through the poppet valve is possible. This is done by determining the shape of the gas flow edges.

Figure 6.3 illustrates simulated and reference velocities of hydraulic cylinder and cylinder force. Simulated velocity curve tracks the reference velocity curve but also overruns are exists at maximum velocities. The final velocity before poppet valve is totally closed is 0.41 m/s. The maximum cylinder force is 5.2 kN.

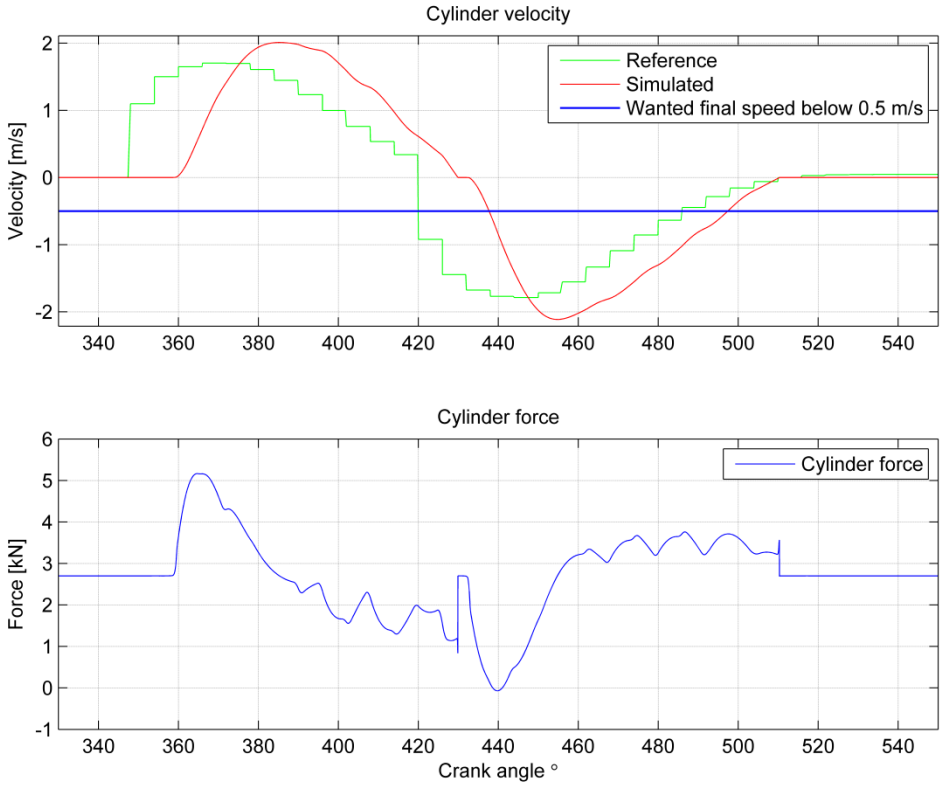

Figure 6.3. *Reference and simulated cylinder velocities and force.*

As the reference velocity curve shows, discrete transfer function lowers the slope of reference velocity. Especially the effects are seen at the beginning, after crank angle 340° and when the reference velocity value has been changed from positive to negative around crank angle 420°.

Figure 6.4 presents DFCU-PA and AT states and flow rates to and from the cylinder chambers and flow rate to tank line and from the supply line. Total switch count of DFCU-PA is 13 and DFCU-AT is 15.

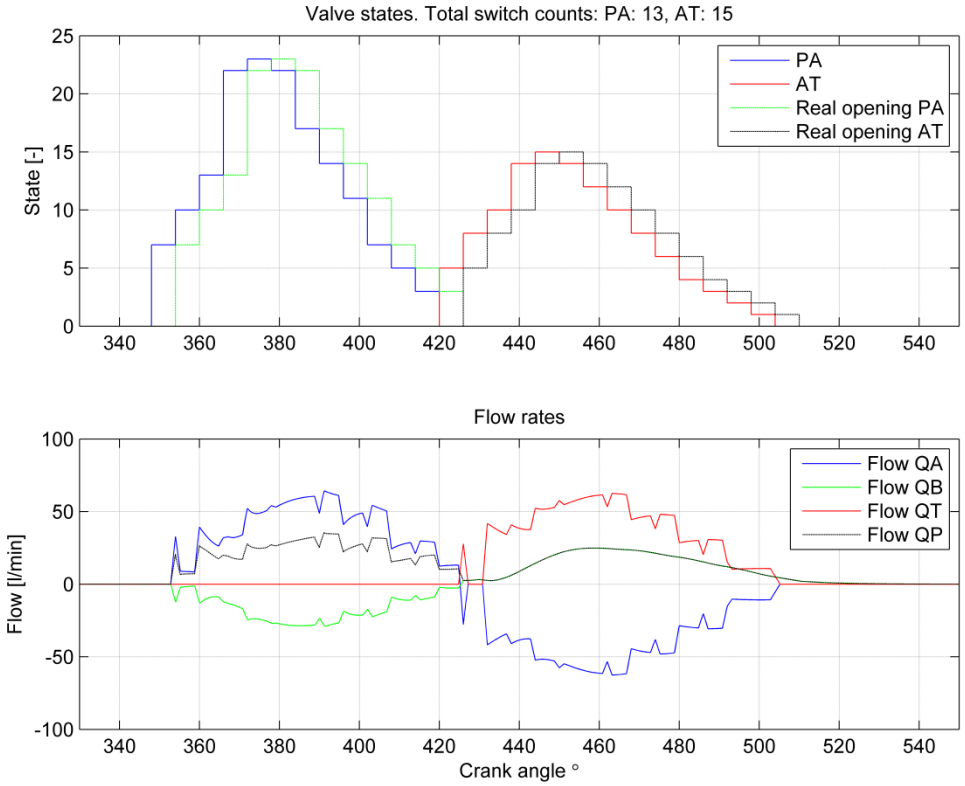

Figure 6.4. *DFCU-PA and AT states, switching counts and system flow rates.*

Figure 6.4 shows the given signals and real openings of DFCUs. Between given signals and real openings there is 1 ms difference which is amount of response time of valves. Flow rate curves illustrate that during opening the poppet valve differential connection is used and during closing the poppet valve inflow-outflow minus connection is used. The curves show that during opening the poppet valve needed flow to chamber A is absolute sum value of flow from supply line and B-chamber. During closing the poppet valve flow rate to B-chamber is as large as flow rate from supply pressure line. Because oil fluid from A-chamber to tank line, these flow rates are equal but opposite in sign.

Figure 6.5 shows hydraulic cylinder acceleration and hydraulic energy consumptions. The peak acceleration is 821 m/s^2 and peak deceleration is 924 m/s^2.

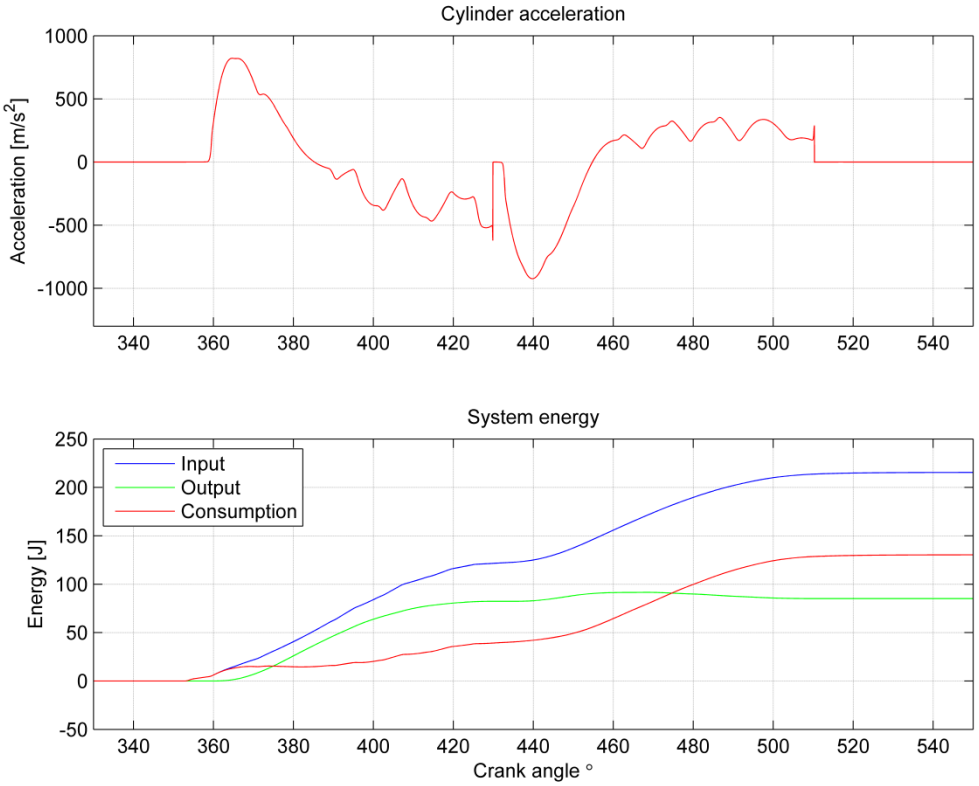

Figure 6.5. *Hydraulic cylinder acceleration and system energies.*

Hydraulic input energy of the system is 215 J, output energy is 85 J and energy consumption of the system is 130 J.

6.1.2 Simulation results using supply pressure 25 MPa

The next simulated system is similar to the system which results have been shown in the chapter 6.1.1 but supply pressure is 25 MPa. Specific simulation parameters have been listed in appendix I.

Figure 6.6 shows the hydraulic cylinder position, and chambers and supply pressures. The maximum lift is 13.3 mm. The poppet valve is totally closed at crank angle 516°. The poppet valve position at 1 % of cylinder bore diameter is crank angle 478°. Thus, the Miller timing is 62 BBDC.

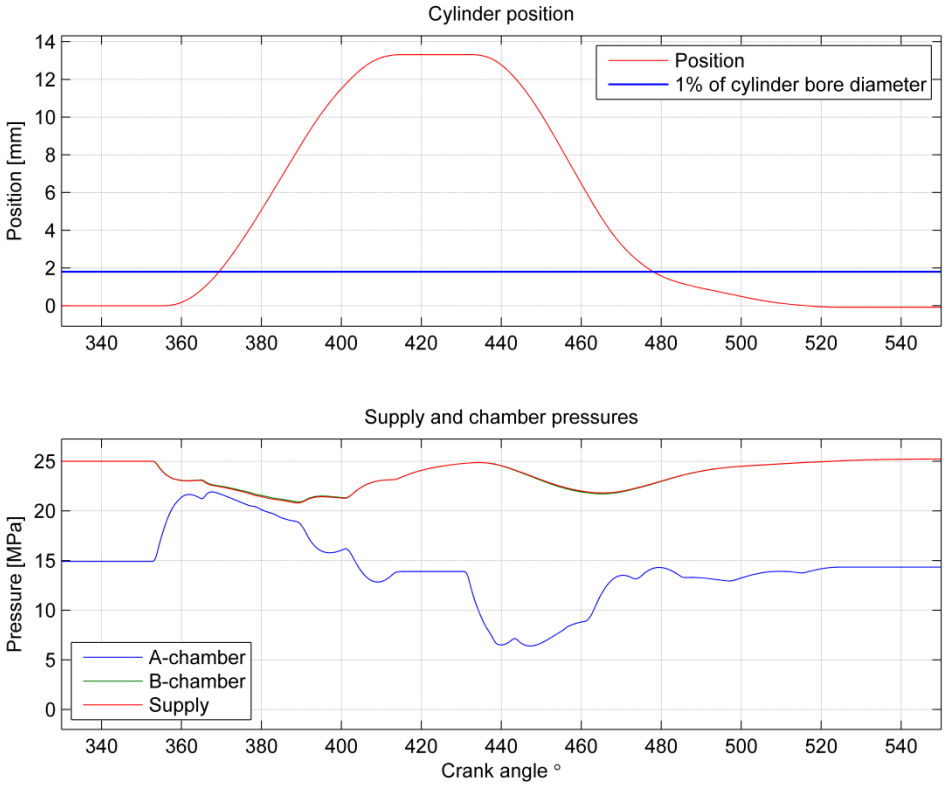

Figure 6.6. *Hydraulic cylinder position and system pressures.*

As the system which has been modelled with supply pressure 30 MPa, also in this system next to the B-chamber has been modelled an orifice to find out chamber pressure and flow rate.

Figure 6.7 shows air and gas mass flows and fed amounts. Fed gas amount is 1.33 g and air amount is 50.2 g.

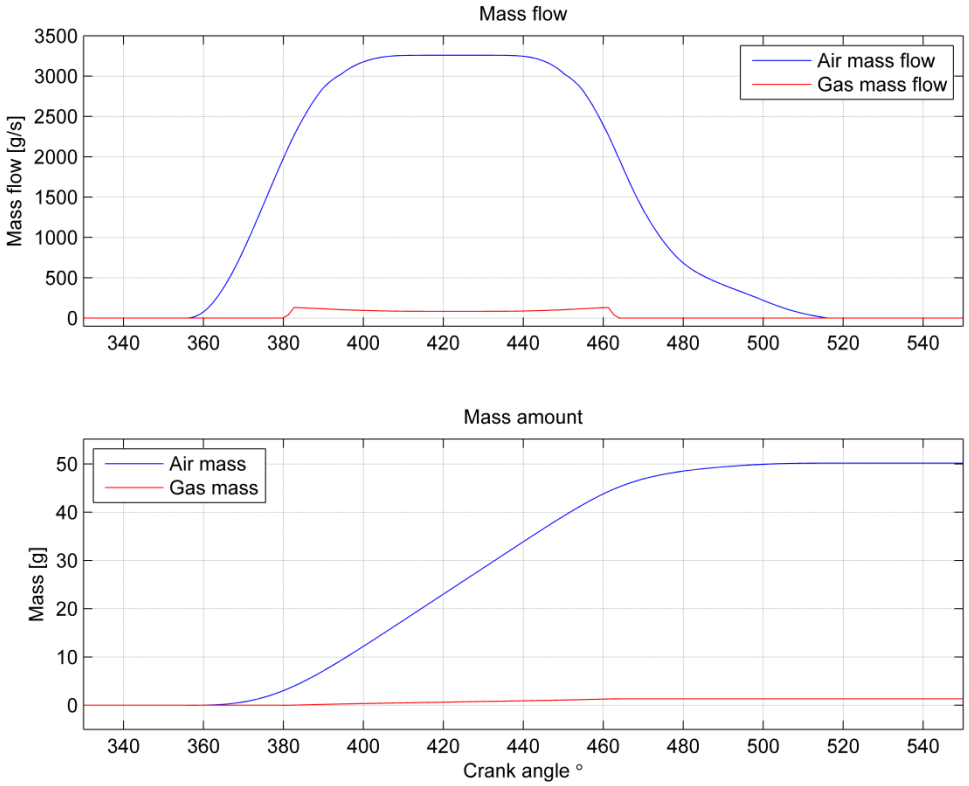

Figure 6.7. *Air and gas mass flow and fed mass amounts.*

At crank angle 464° all gas has been fed and after that lift of the poppet valve is below 5 mm.

Figure 6.8 shows simulated and reference velocities and force of hydraulic cylinder. The final velocity of poppet valve is 0.1 m/s before it is totally closed. The maximum cylinder force is 5.1 kN.

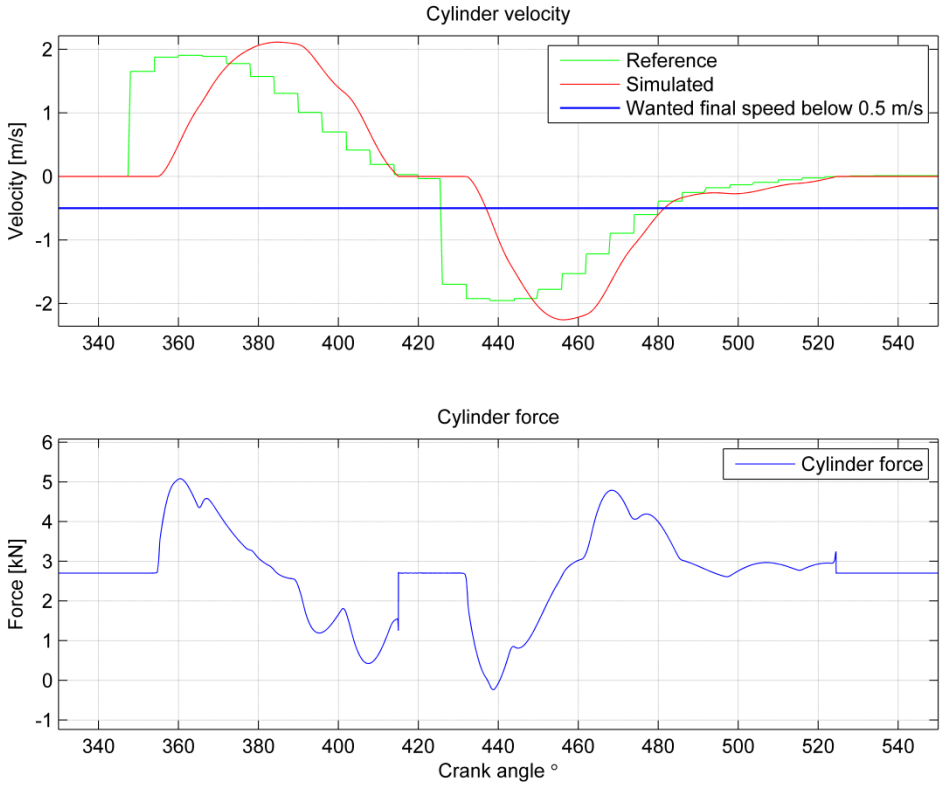

Figure 6.8. *Reference and simulated cylinder velocities and cylinder force.*

As the figure 6.8 shows, between reference and simulated velocities differences exist and maximum simulated velocity values are higher than reference velocity values.

Figure 6.9 shows the switching amounts of DFCU-PA and AT. Total switch counts of DFCU-PA is 12 and DFCU-AT is 11. The figure shows also flow rates to and from A and B-chambers, and to tank line and from the supply line. As the flow rates figure shows, during the opening phase of the poppet valve differential connection is used because flow rate to the tank line is zero. During the closing phase inflow-outflow method is used and fluid flows from the A-chamber straight to the tank line.

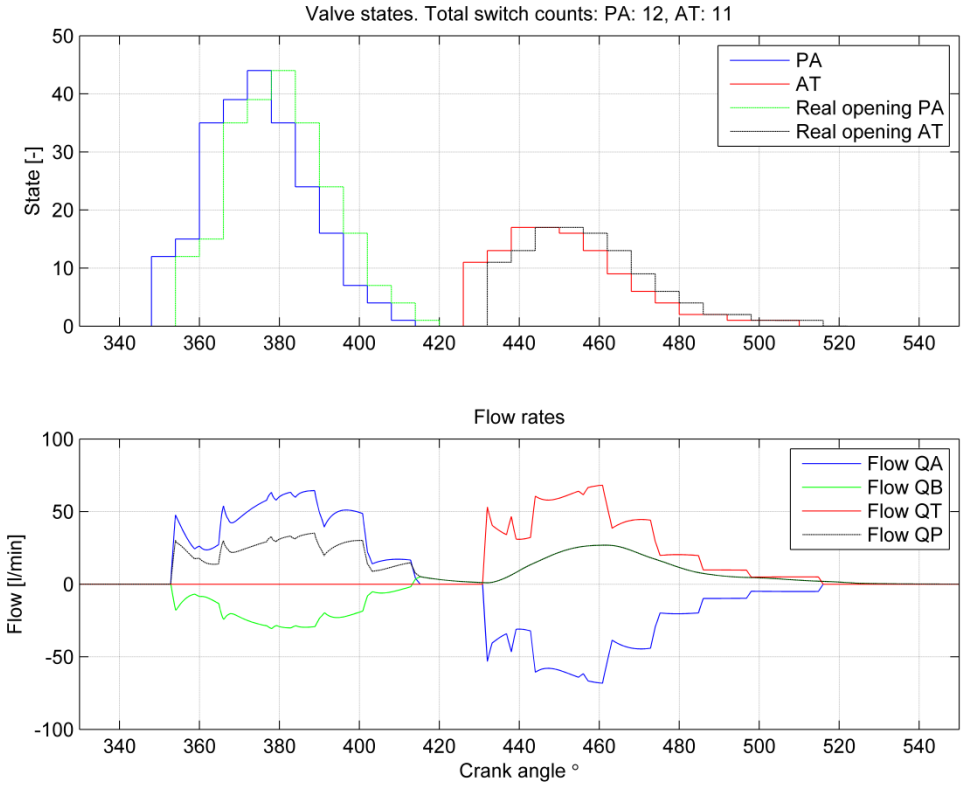

Figure 6.9. *DFCU states, switching counts and flow rates.*

Figure 6.10 shows acceleration of hydraulic cylinder and hydraulic energy consumptions. Maximum acceleration value is 794 m/s^2 and deceleration is 980 m/s^2. Total hydraulic input energy amount is 157 J and total output energy is 66 J. The system consumes 91 J of hydraulic energy.

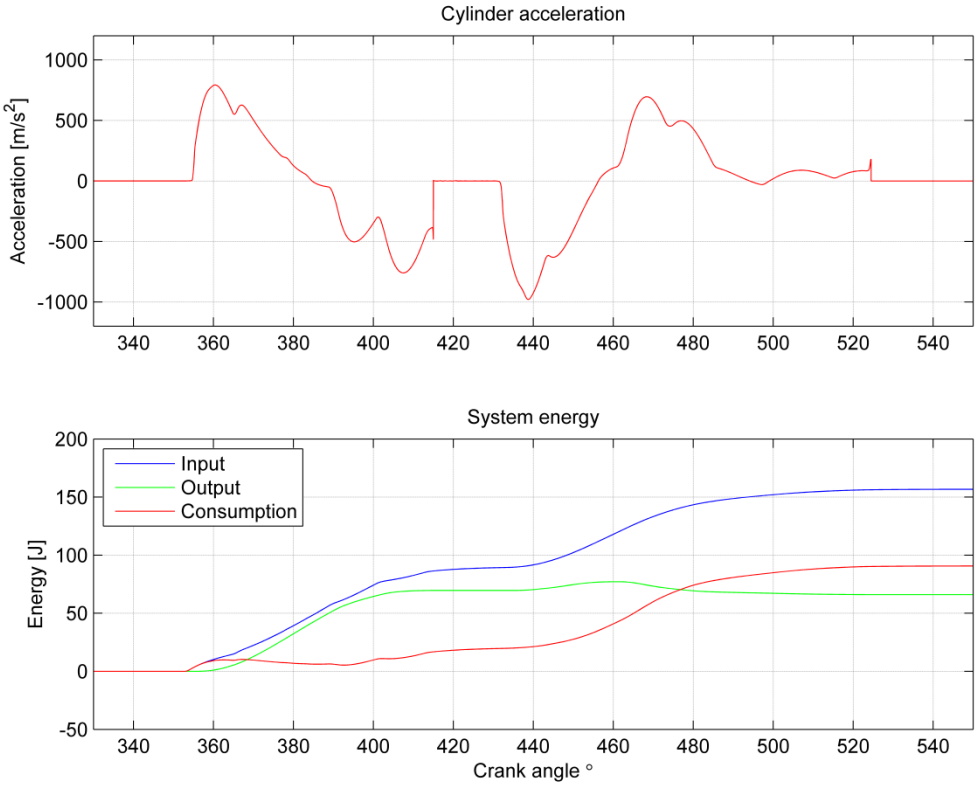

Figure 6.10. *Hydraulic cylinder acceleration and hydraulic energy consumption.*

Figure 6.11 shows acceleration of hydraulic cylinder when end damping model is used. The peak acceleration is over 2500 m/s^2 and the value is over two times greater than the maximum peak deceleration without end damper.

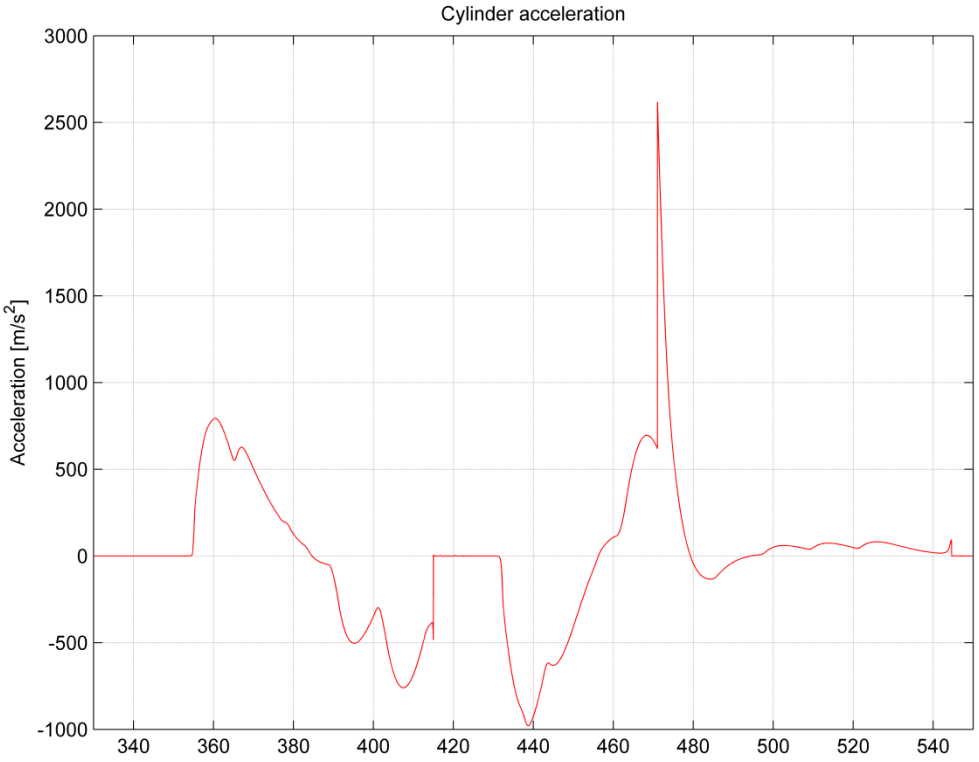

Figure 6.11. *The hydraulic cylinder acceleration using end damping model.*

As the figure 6.11 illustrates, acceleration of hydraulic cylinder using end damping model is similar before the damping model is used. When the damping model is used, the peak acceleration value is obvious. Using end damping model the final velocity of poppet valve is easier to limit below 0.5 m/s. Without the model, parameters of the controller determine how well wanted final velocity value is achieved.

6.2 Digital hydraulic system using four DFCUs

The system with four DFCUs has been simulated using two different supply pressures, 25 and 30 MPa. Chapter 5.3 shows the controller which has been used in the systems.

6.2.1 Simulation results using supply pressure 30 MPa

Specific simulation parameters for system using supply pressure 30 MPa have been listed in appendix J. Figure 6.12 shows hydraulic cylinder position and system chamber and supply pressures. The maximum lift is 13.7 mm and poppet valve is totally closed at crank angle 520°. At crank angle 486° poppet valve is still opened 1% of cylinder bore diameter. Thus, Miller timing is 54 BBDC.

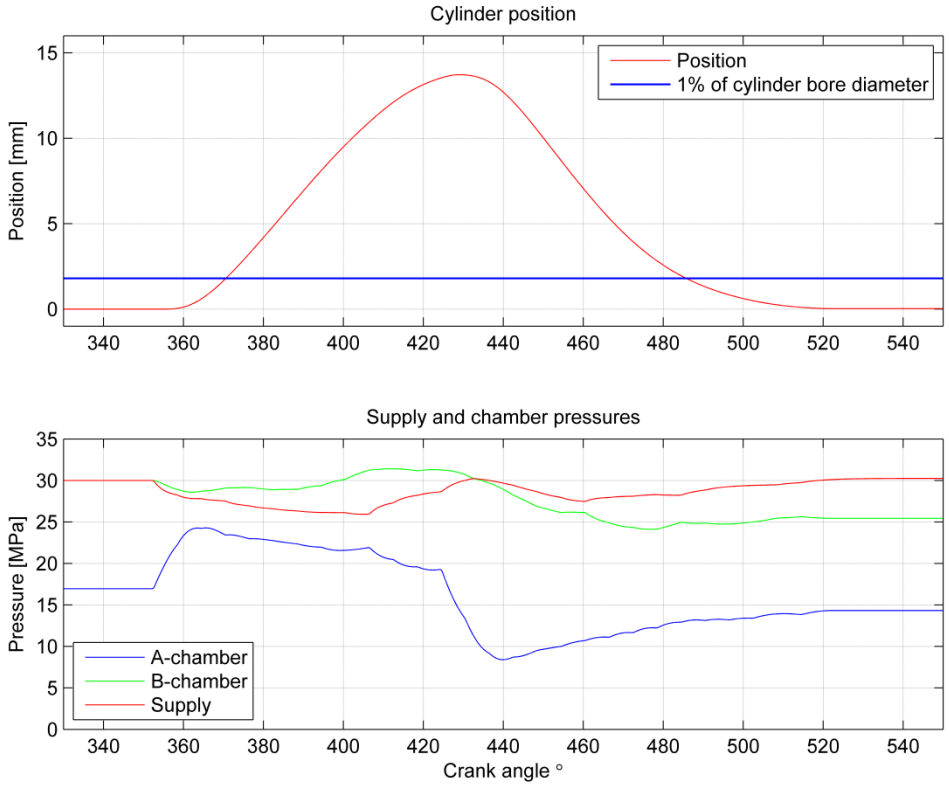

Figure 6.12. *Hydraulic cylinder position and system pressures.*

As the pressure figure illustrates, the final chamber pressures are lower than initial pressure values. The controller parameter velocity tolerance enables this difference. In the results, velocity tolerance value 200 mm/s has been used.

Figure 6.13 presents air and gas mass flow rates and fed mass amounts. Fed amount of air is 50.9 g and gas is 1.32 g.

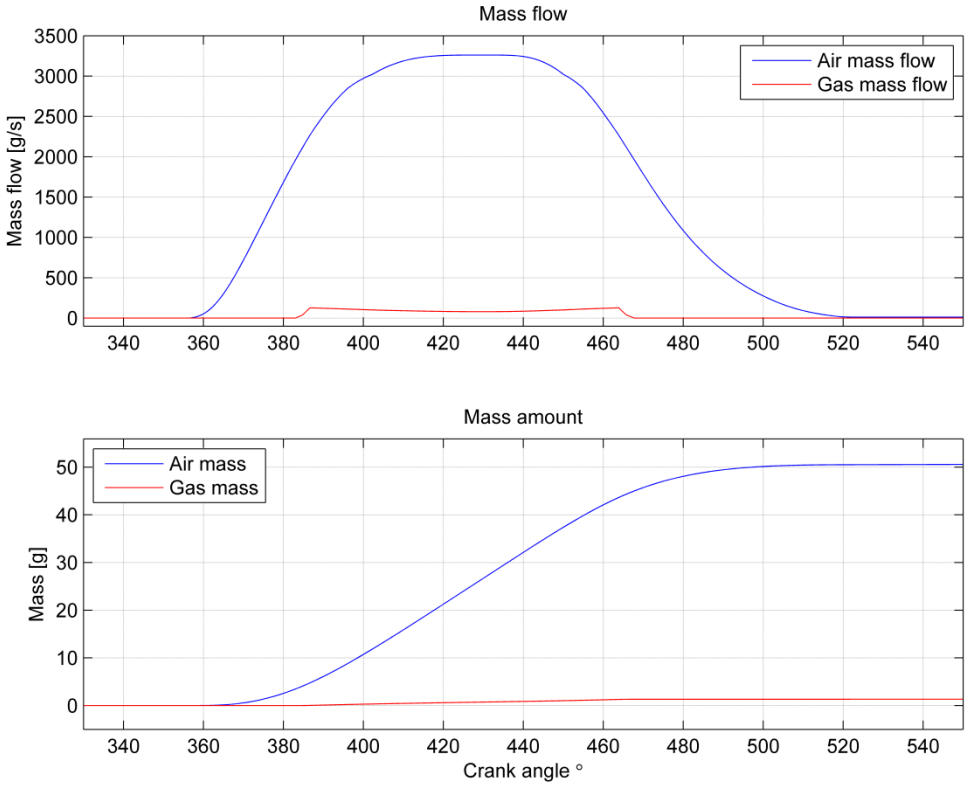

Figure 6.13. *Air and gas mass flow rates and fed mass amounts.*

Figure 6.14 shows simulated and reference velocities of hydraulic cylinder and cylinder force. According to results, the final velocity of the poppet valve is 0.04 m/s before it is totally closed.

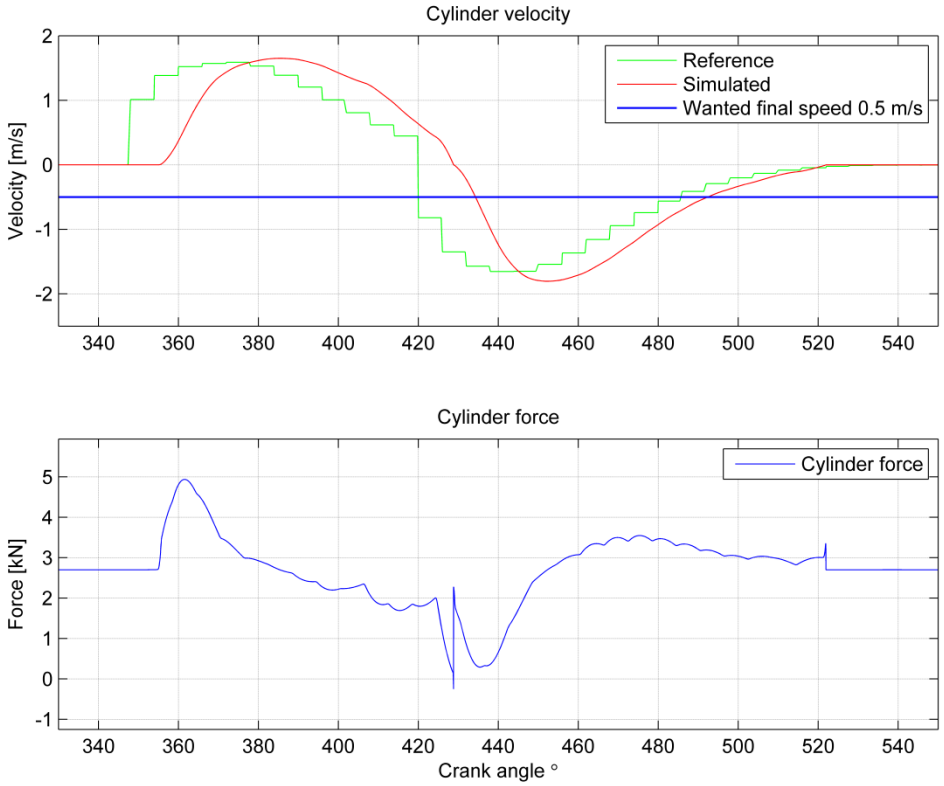

Figure 6.14. *Hydraulic cylinder velocity and force.*

As the figure 6.14 shows, the simulated velocity curve is more alike reference velocity curve than in comparison to the figure 6.3 where are presented velocity curves using two DFCUs using the same supply pressure value.

Figure 6.15 shows DFCU states and total switch counts. As figure shows, DFCU-BT is not opened at all and the system behaves as the system with three DFCUs (DFCU-PA, AT and PB). Total switch counts of DFCU-PA is 11, AT is 15 and DFCU-PB is 24.

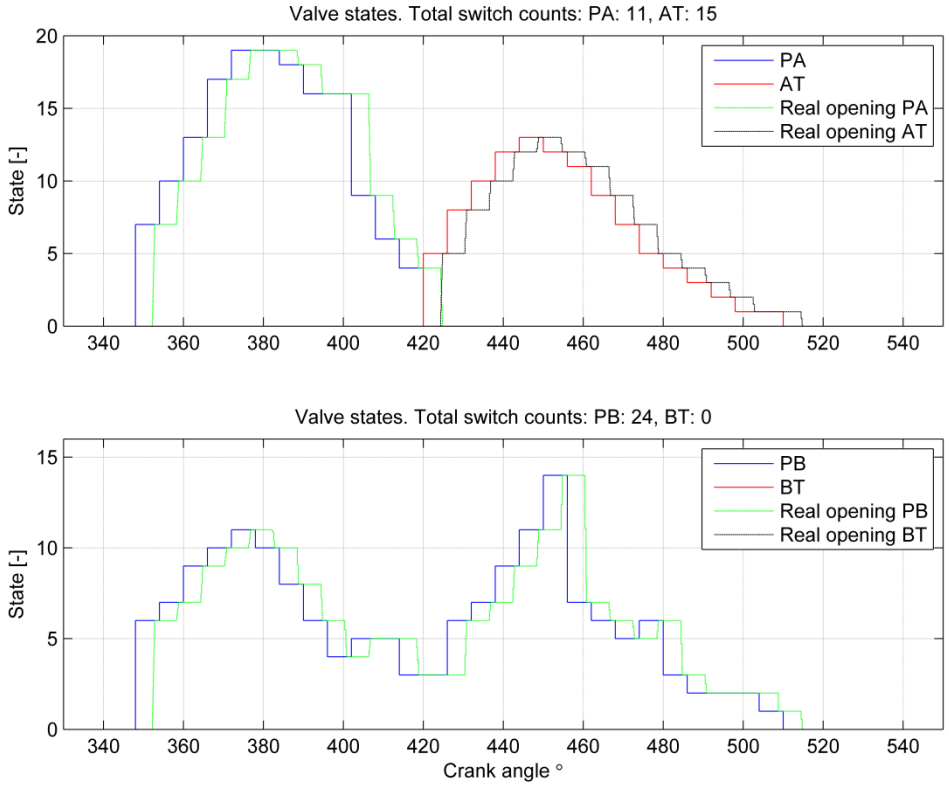

Figure 6.15. *DFCU states and total switch counts.*

Because DFCU-BT is not used, DFCU-PB controls the flow rate to and from the B-chamber. DFCU-PB is always used when the cylinder moves.

Figure 6.16 shows the system modes and flow rates to and from the cylinder chambers and flow rate to tank line and from the supply line. Because DFCU-BT is not used, the mode 1 is not possible.

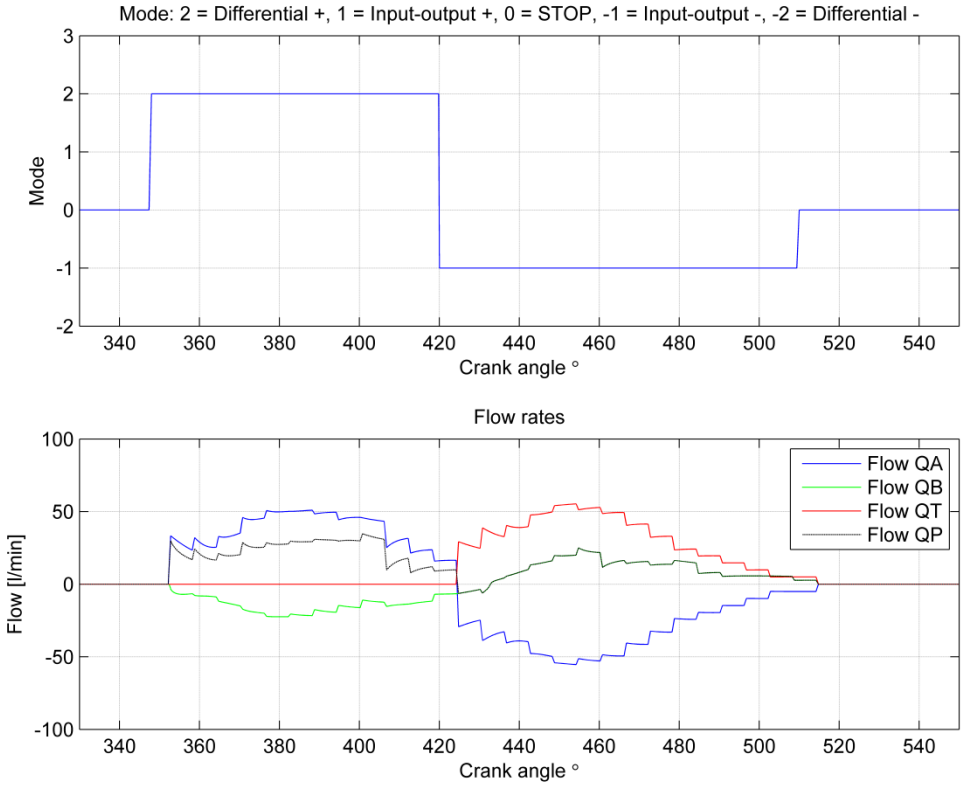

Figure 6.16. *System mode and flow rates.*

Figure 6.17 presents acceleration of hydraulic cylinder and hydraulic energies of the system. The peak acceleration value is 745 m/s^2 and deceleration is 983 m/s^2.

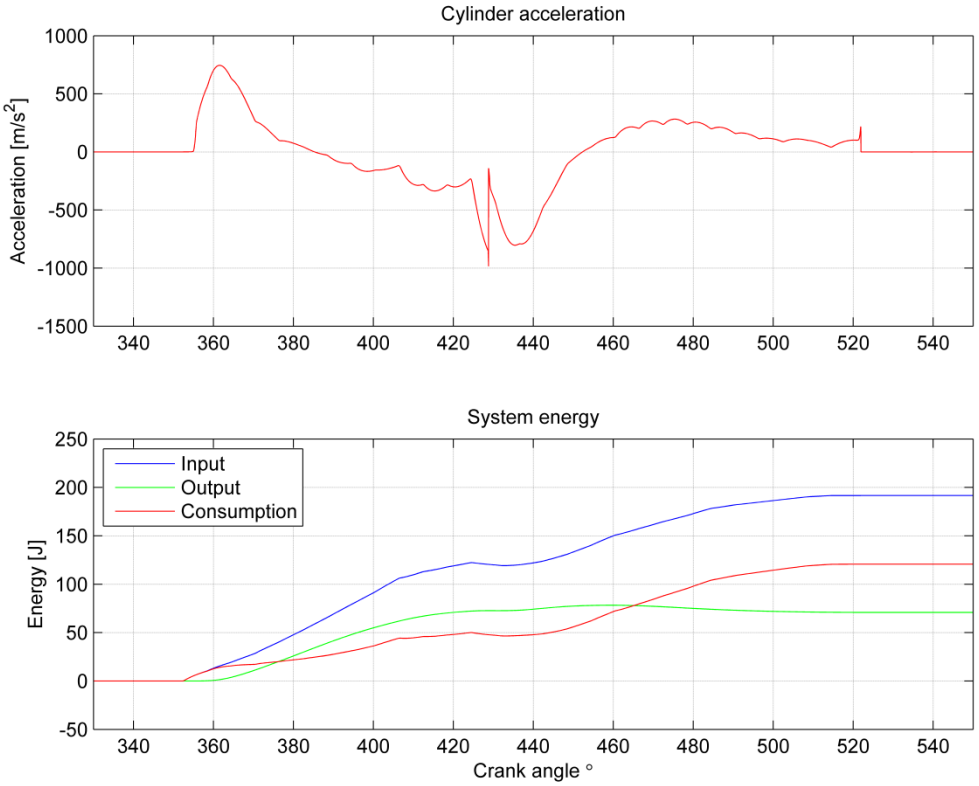

Figure 6.17. *Hydraulic cylinder acceleration and system energies.*

As the figure 6.17 shows, total input hydraulic energy is 192 J, output energy is 71 J and system consumption is 121 J.

6.2.2 Simulation results with supply pressure 25 MPa

Specific simulation parameters for system using supply pressure 25 MPa have been listed in appendix K. Figure 6.18 presents hydraulic cylinder position and system pressures. The maximum poppet valve lift is 13.2 mm.

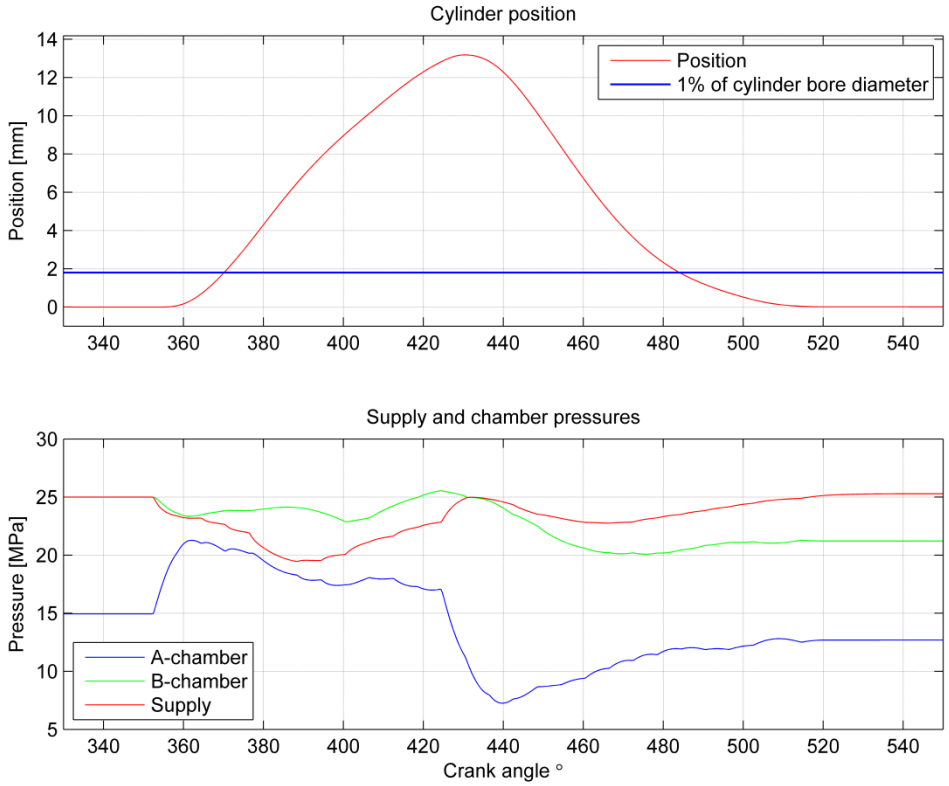

Figure 6.18. *Hydraulic cylinder position and system pressures.*

Poppet valve is totally closed at crank shaft angle 510° and at 484° poppet valve is at the position of 1% of cylinder bore diameter. Thus, Miller timing is 56° BBDC.

Figure 6.19 presents air and gas mass flow and fed amounts of gases. Fed gas mass is 1.34 g and air mass is 49.0 g.

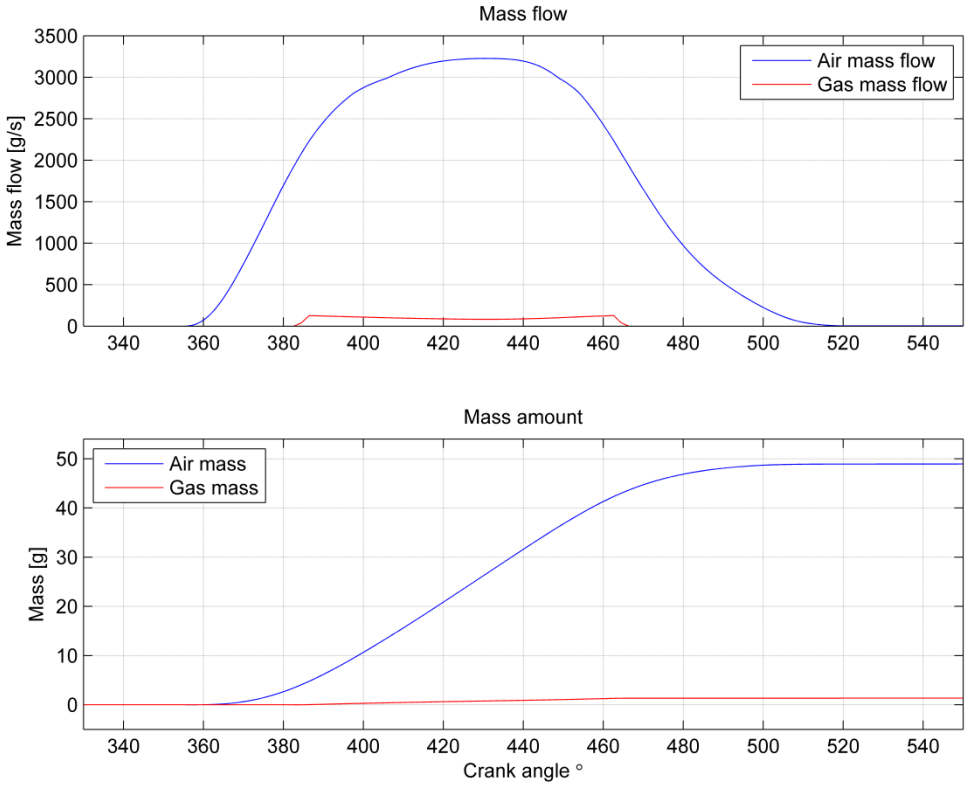

Figure 6.19. *Air and mass flow and fed amount.*

At crank angle 466° all gas has been fed and after that lift of the poppet valve is below 5 mm.

Figure 6.20 presents simulated and reference velocities of cylinder and cylinder force. The shape of simulated cylinder velocity is similar to the curve presented in the figure 6.14 using supply pressure 30 MPa. However, crossing the reference velocity is observable at minus velocity. The final velocity of the poppet valve before it is totally closed is 0.1 m/s. The maximum cylinder force value is 4.9 kN.

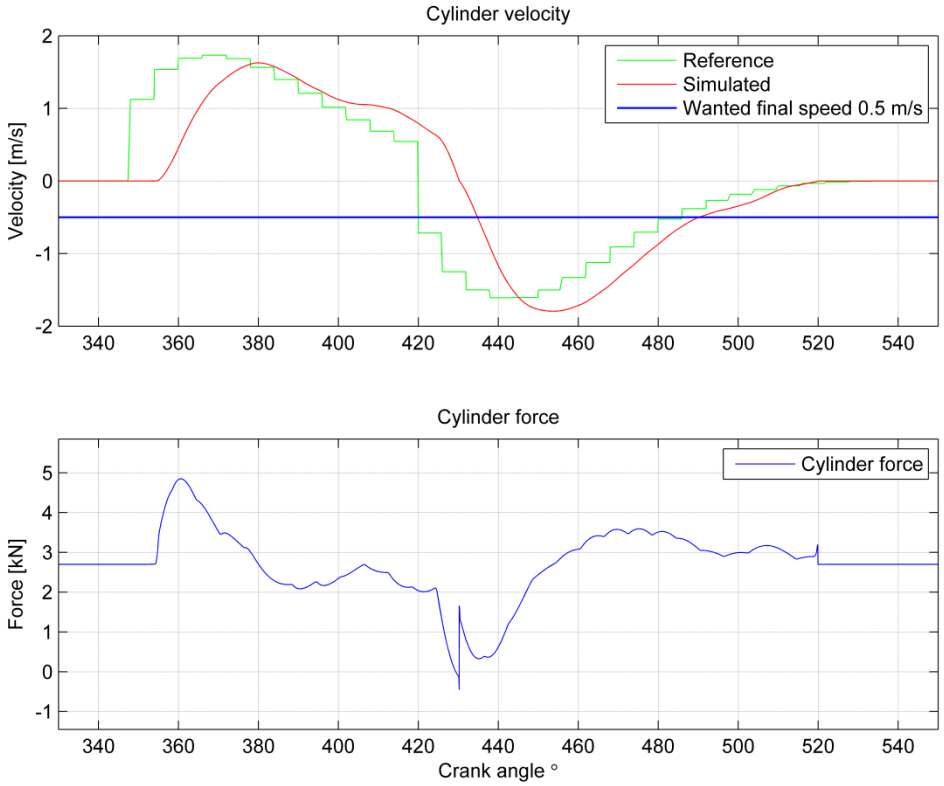

Figure 6.20. *Hydraulic cylinder velocity and force.*

Because controllability of the system is improved when four DFCUs are used, also velocity tracking is better.

Figure 6.21 presents DFCU states. In comparison to the results using supply pressure 30 MPa, also DFCU-BT is opened. Total DFCU-PA switch count is 12 and AT is 15. DFCU-AT switch count is 21 DFCU-PB switch count is 2.

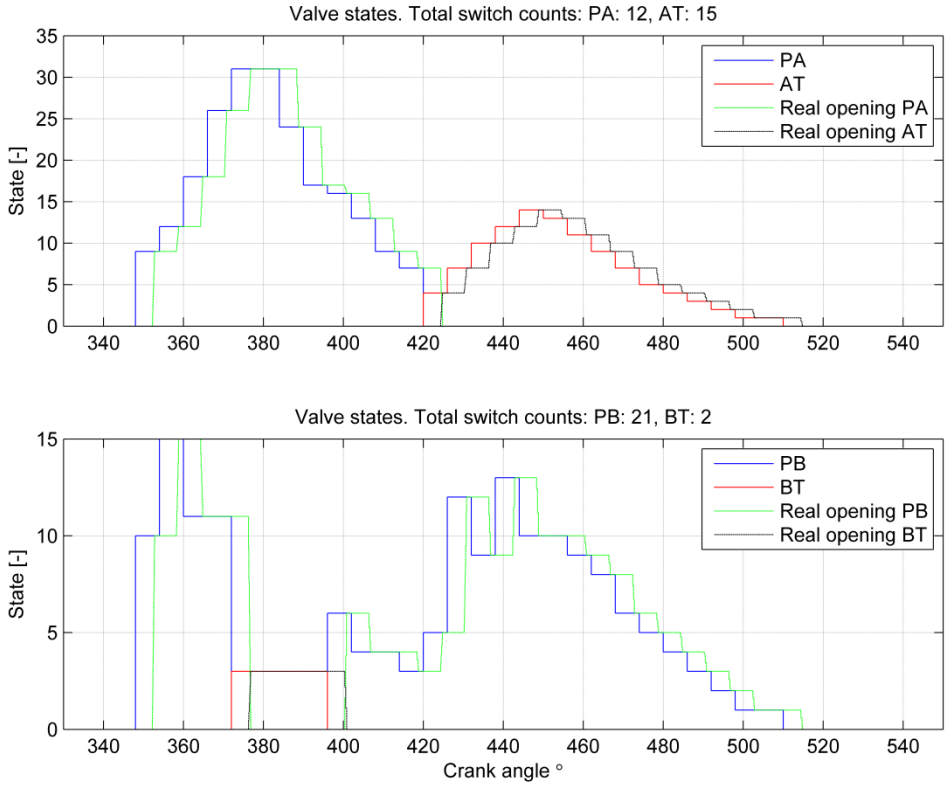

Figure 6.21. *DFCU states and switch counts.*

Figure 6.22 presents the system modes and flow rates. In comparison to the modes using supply pressure 30 MPa, also input-output plus mode is used.

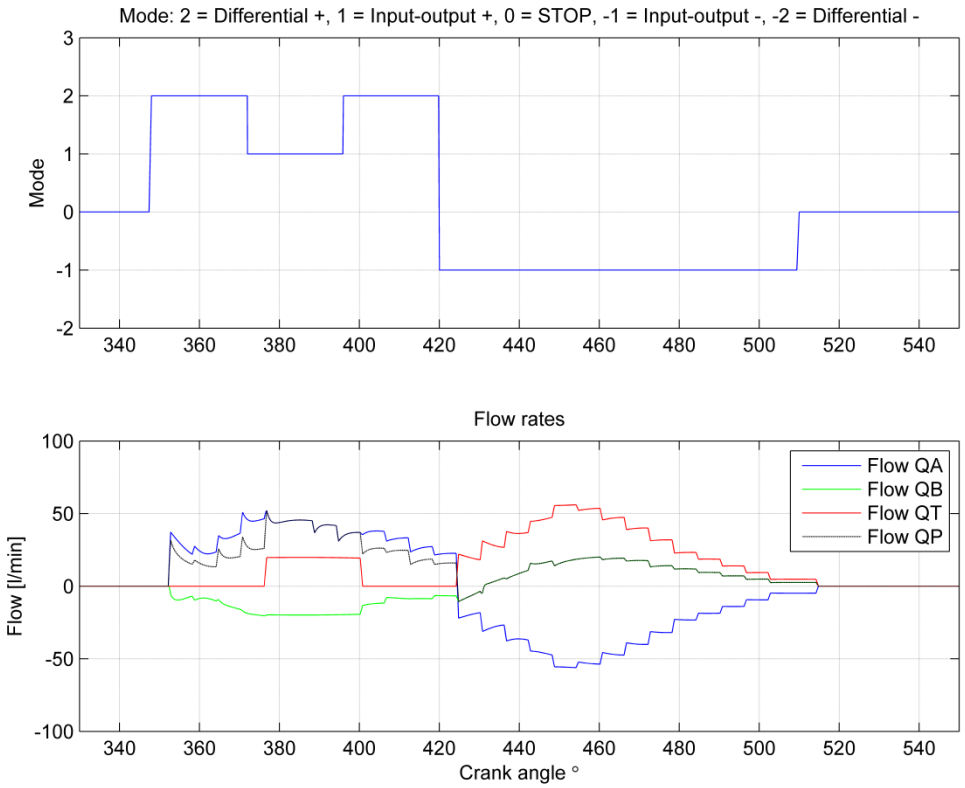

Figure 6.22. *System modes and flow rates.*

As the figure 6.22 shows, during mode 1 the needed flow rate to chamber A has been taken from supply pressure line and flow rate is positive to tank line. During mode -1 flow rate is positive to tank line when fluid flows from A-chamber to tank line. Needed flow rate to B-chamber has been taken from supply pressure line.

Figure 6.23 presents hydraulic cylinder acceleration and system energies. The peak acceleration value is 716 m/s^2 and peak deceleration is 1050 m/s^2. Total input energy value is 174 J, output value is 55 J and consumption value is 119 J.

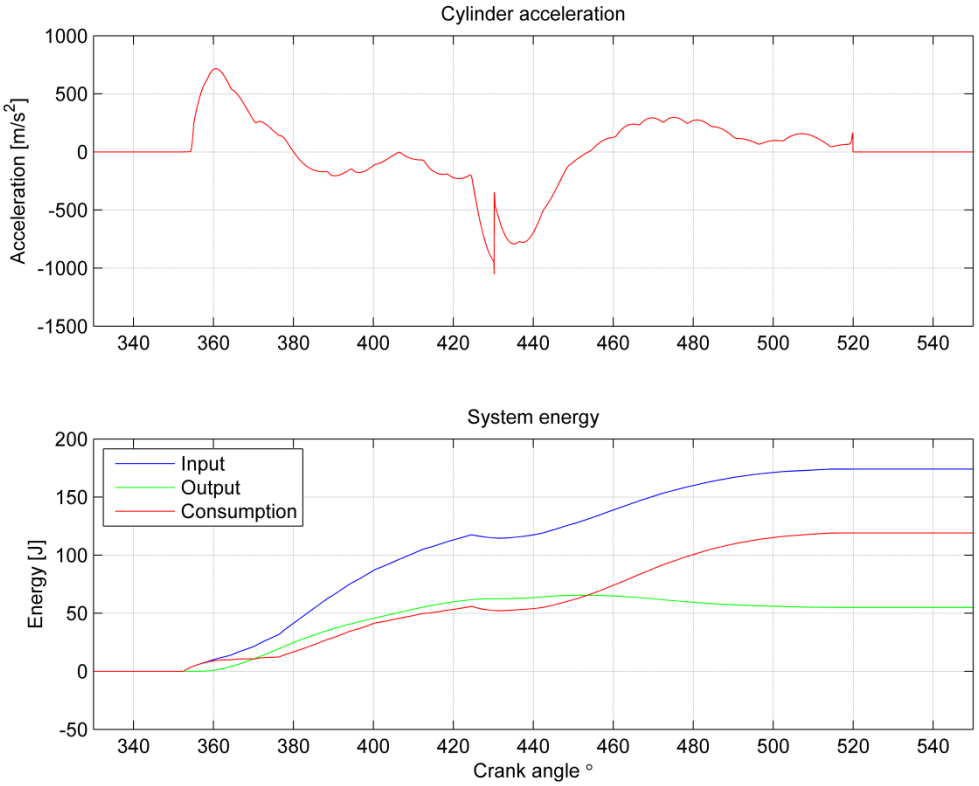

Figure 6.23. *Hydraulic cylinder acceleration and system energies.*

6.3 Simulation results using digital pneumatic valve system

The third simulated system is digital pneumatic valve system. Specific simulation parameters are listed in appendix L. Figure 6.24 shows methane gas mass flow through the valve system, and signals and states of DFCU. Maximum gas flow is 390 g/s.

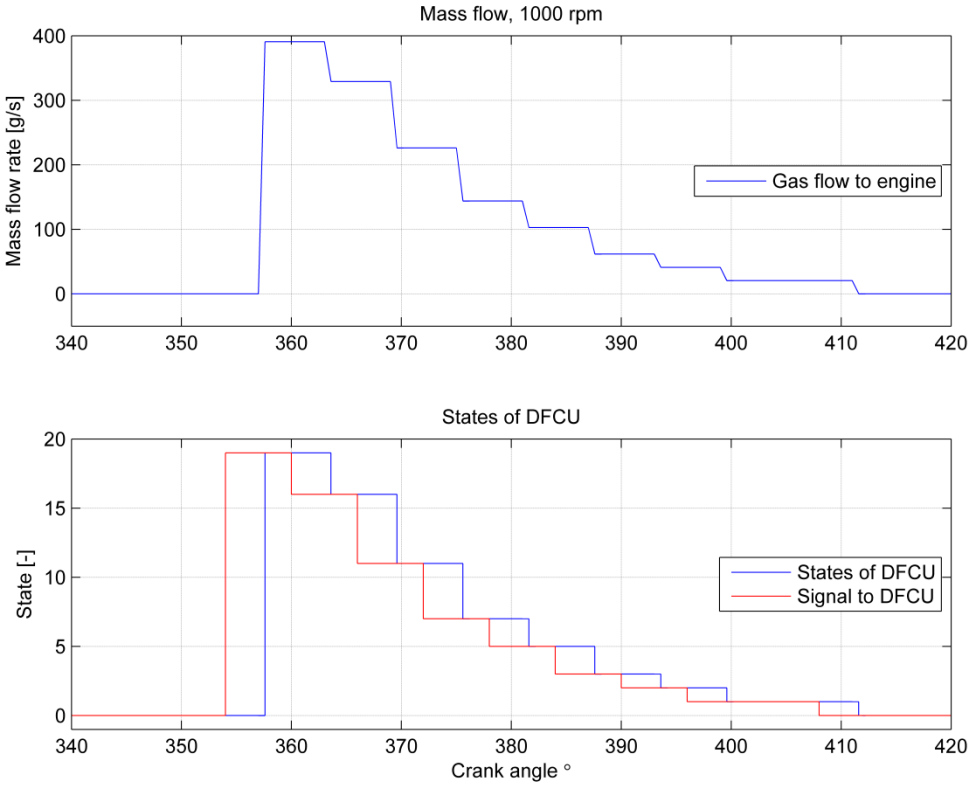

Figure 6.24. *Mass flow and states of DFCU.*

As the figure 6.24 shows, the maximum state of DFCU is 19. The opening signal has been given to the valve at crank angle 354°.

Figure 6.25 presents fed gas amount. Total fed gas amount is 1.34 g.

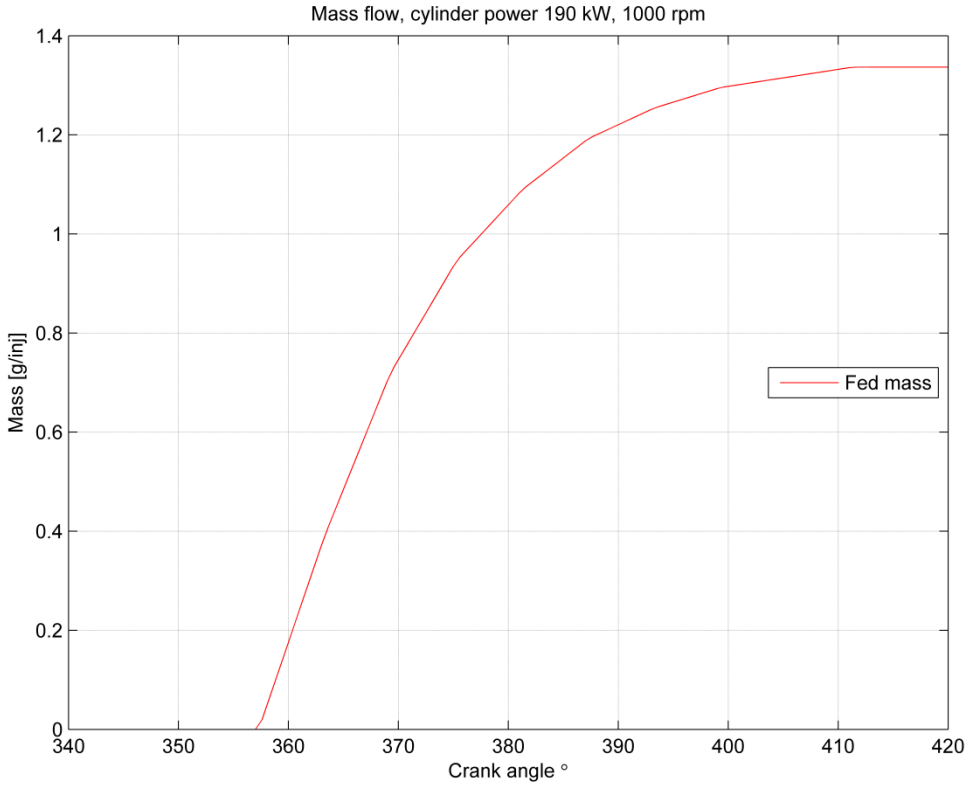

Figure 6.25. *Fed methane gas mass.*

The valve is totally closed at crank angle 412° and the gas feeding is carried out in 10 ms. However, the valves of DFCU should be enough fast with small delay and movement times with enough large flow capacity.

6.4 Comparison of energy consumptions

Energy consumptions for poppet valve using digital and proportional hydraulic and mechanical valve trains are compared. Digital hydraulic energy consumptions are presented in the figures 6.5, 6.10, 6.17 and 6.23. Using proportional valve, differential connection is not used. Mechanical valve train is estimated to consume 0.5 % of total cylinder output power.

6.4.1 Comparison to digital hydraulic valve train

Using digital hydraulic systems, input, output and energy consumptions are listed in the following table.

Table 6.2. *Hydraulic energy consumptions using digital hydraulic systems.*

System (supply pressure)	Input energy [J]	Output energy [J]	Consumption [J]	Output-input ratio
2 X DFCU (30 MPa)	215	85	130	40 %
2 X DFCU (25 MPa)	157	66	91	42 %
4 X DFCU (30 MPa)	192	71	121	37 %
4 X DFCU (25 MPa)	174	55	119	32 %

As the table 6.2 shows, the system with two DFCUs using supply pressure 25 MPa is the most energy efficient. However, different system parameters, for example size of hydraulic cylinder and used flow rate through the DFCU affect to energy consumption values a lot. Also, systems using four and two DFCUs are simulated using different controller and controller parameters. Using supply pressure 25 MPa and four DFCUs, also DFCU-BT is used. Thus, the system using four DFCUs and supply pressure 30 MPa is more energy efficient system than the system using supply pressure 25 MPa.

6.4.2 Comparison to proportional valve train

Using proportional valve, estimated energy consumption can be calculated via the following equation:

$$E_{proportional} = p_p * L_v * A_A + p_p * L_v * A_B \tag{104}$$

In the following table are listed different energy consumptions using supply pressures 25 and 30 MPa and valve lift 15 mm.

Table 6.3. *Energy consumptions using proportional valve.*

Supply pressure [MPa]	Energy consumption [J]
25	280
30	336

Figure 6.26 shows the symbol of 4/3 proportional spool valve.

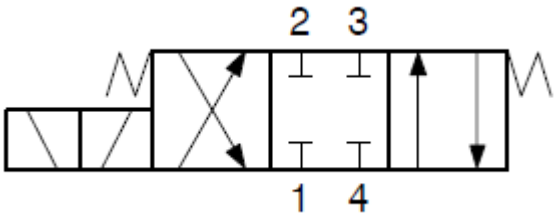

Figure 6.26. *Symbol of proportional valve.*

Using proportional valve, differential connection is not used.

6.4.3 Comparison to mechanical valve train

Mechanical valve train energy comparison is calculated using the estimation that half percent of cylinder output power is consumed for the mechanical valve train. The following equation shows the energy consumption:

$$E_{mechanical} = 0.5\% * 190\ kW * 120\ ms = 114\ J \tag{105}$$

As the equation shows, 114 J of energy is consumed for the mechanical valve train when the crank shaft is rotated 720° using the engine speed 1000 rpm.

6.4.4 Conclusion of energy comparison

Digital hydraulic valve system enables better and smaller energy consumption than proportional valve system. The differential connection has a huge impact on hydraulic energy consumption. As the results show, digital hydraulic system using two DFCUs and supply pressure 25 MPa is the most energy efficient simulated system. However, hydraulic system has of course always more losses than pure mechanical valve train but the main benefit using hydraulic valve train is that valve timings are fully controllable.

6.5 Comparison of velocity error using digital hydraulic systems

In this chapter velocity errors between reference and simulated values have been researched using digital hydraulic systems with two and four DFCUs. Velocity error amounts have been calculated using the standard least-squares estimator which is presented by Slotine and Li [46]:

$$J_{velocity\ error} = \int_{t_1}^{t_2} \left| v_{ref} - v_{sim} \right|^2 dv \tag{106}$$

As the equation shows, amount of velocity error has been found out using square difference of reference and simulated velocities. Table 6.4 shows amount of velocity errors using different values of supply pressures and amount of DFCUs.

Table 6.4. *Comparison of velocity error amounts.*

Amount of DFCUs [-]	Supply pressure [MPa]	Amount of velocity error
4	30	0.01
4	25	0.0106
2	30	0.0175
2	25	0.0179

As the table 6.4 shows, using four DFCUs the velocity error amounts are lower than using two DFCUs. The results show that systems using four DFCUs tracks better velocity reference than systems using two DFCUs.

7 CFD RESULTS

CFD results are done cooperation with CFD experts at Wärtsilä. The following results show CFD analysis of air and gas flow and gas mixing in the port flow for the engine with cylinder power 190 kW. The following table shows the computational methods and boundary conditions for CFD simulations.

Table 7.1. *Computational methods and boundary conditions for CFD simulations using ideal gas and steady state flow. [47].*

Flow solver	STAR-CCM+ 8.04.010
Air pressure at the inlet	0.42 MPa
Air temperature at the inlet	45 °C
Air mass flow	2230 g/s
Methane pressure	0.753 MPa
Methane mass flow	142 g/s
Methane temperature	25 °C
Outlet pressure	0.332 MPa

Uniformity indexes have been defined for different valve lifts. Uniformity index is an indicator how uniform the velocity distribution of the flow is on the section cut. When the value is 1, outflow is fully uniform. The following equation presents the definition of uniformity index:

$$\lambda = 1 - \frac{1}{2A\overline{v}_n} \cdot \int_{outlet} |v_n - \overline{v}_n| dA \tag{107}$$

,where $\overline{v}_n$ is average normal velocity in the outlet plane and A is the outlet cross sectional area. [48].

7.1 Defining the discharge coefficient

For defining the discharge coefficient values at precise valve lifts, the following equation has been used.

$$C_D = \frac{\dot{m}_{real}}{\dot{m}_{ideal}} = \frac{\dot{m}_{real}}{\frac{A_T p_1}{\sqrt{RT}} \left(\frac{p_2}{p_1}\right)^{1/\gamma} \left\{ \frac{2\gamma}{\gamma - 1} \left[1 - \left(\frac{p_2}{p_1}\right)^{\gamma - 1/\gamma} \right] \right\}^{1/2}} \tag{108}$$

In the equation discharge coefficient value C_D has been defined using real mass flow $\dot{m}_{real}$ and ideal mass flow $\dot{m}_{ideal}$ values. The equation (108) is similar to the equation (92) which presents the mass flow equation when the flow is not choked. The flow area parameter A_T has been defined via three different ways, shown in table 7.2.

Table 7.2. *Reference area for defining the discharge coefficient values [47].*

Discharge coefficient	D_T	A_T
1	Cylinder diameter	$A_T = \frac{\pi D_T^2}{4}$
2	Valve head diameter	$A_T = 3\frac{\pi D_T^2}{4}$
3	Valve head diameter	$A_T = 3\pi D_T Lift$

In the equations above the coefficient value 3 should be used because in the system there are three intake valves.

Figure 7.1 presents three different discharge coefficient curves. The curves depend on the definition of flow area A_T.

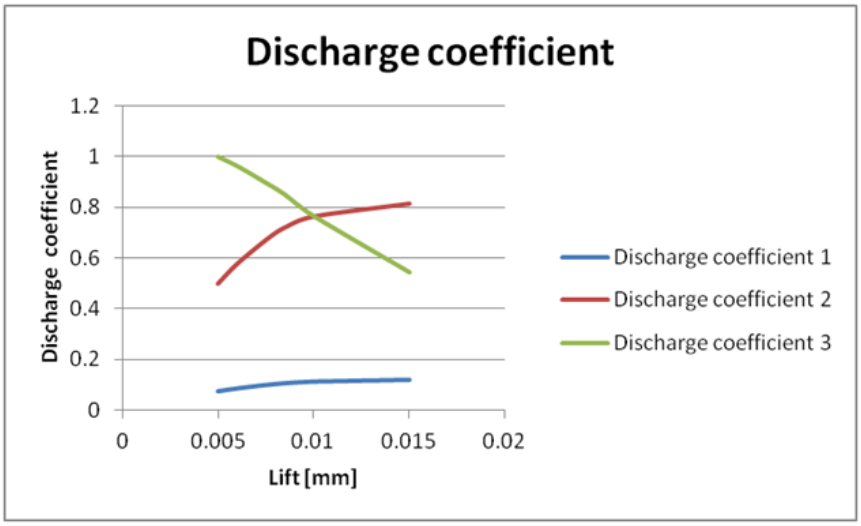

Figure 7.1. *Discharge coefficient curves. [47].*

Table 7.3 shows discharge coefficient values and mass flow rates, $\dot{m}$, using six different poppet valve lifts L_v from 5 mm to 15 mm. Poppet valve head diameter $D_v = 40\ mm$ and cylinder diameter $D_{cyl} = 180\ mm$ have been used.

Table 7.3. *Discharge coefficients and mass flows at precise valve lifts. [47].*

C_{D1} [-]	C_{D2} [-]	C_{D3} [-]	$\dot{m}$ [kg/s]	L_v/D_v [-]	L_v/D_{cyl} [-]	L_v [m]
0.0739	0.4989	0.9978	1.4350	0.1250	0.0278	0.0050
0.0855	0.5770	0.9616	1.6596	0.1500	0.0333	0.0060
0.0995	0.6717	0.8956	1.9321	0.1875	0.0417	0.0075
0.1069	0.7216	0.8489	2.0755	0.2125	0.0472	0.0085
0.1133	0.7649	0.7649	2.2002	0.2500	0.0556	0.0100
0.1208	0.8157	0.5438	2.3464	0.3750	0.0833	0.0150

Discharge coefficient C_{D3} values have been used on the Simulink model to define correct steady-state flow rates.

7.2 Different poppet valve lifts

The following figures show CFD simulation results for gas admission and mixing the gas with air using the valve lift range from 5 mm to 15 mm. Diameters of poppet valves are 40 mm and three valves have been used. For precise lifts, flow velocities and air excess ratios (Lambda) are presented. As the results show, velocity of mixture and air excess ratio depend on valve lift. If valve lift is very small, gas will not flow into the cylinder. However, this depends on the shape of the gas edges. When the air excess ratio is about 2.1, the ratio is optimal. This is also seen in the figure 2.1.

7.2.1 Valve lift 5 mm

Figure 7.2 presents flow velocity at the poppet valve lift 5 mm. The highest flow velocity is achieved just before air flows into the cylinder.

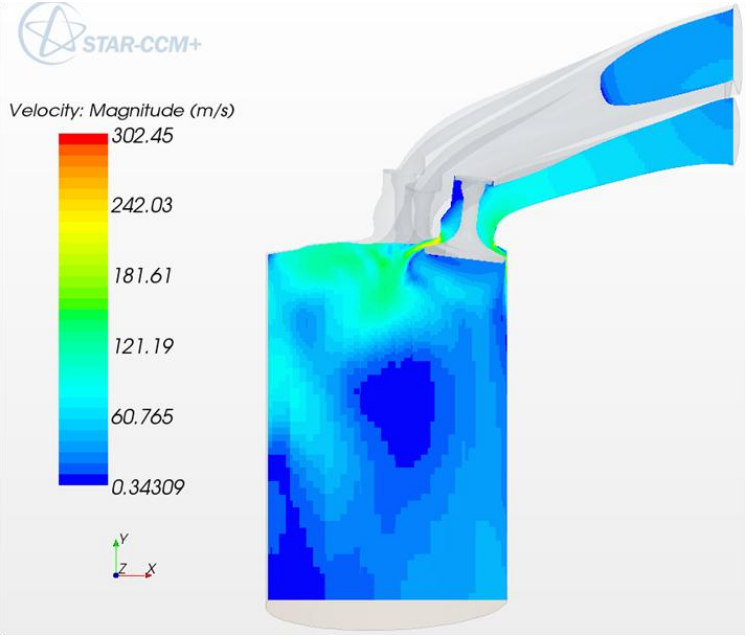

Figure 7.2. *Valve lift 5 mm, side view. [47].*

Figure 7.3 shows that only air flows through the poppet valves at the valve lift 5 mm. The valves are not opened enough that gas would flow into the cylinder. Thus, air excess ratio is 3.

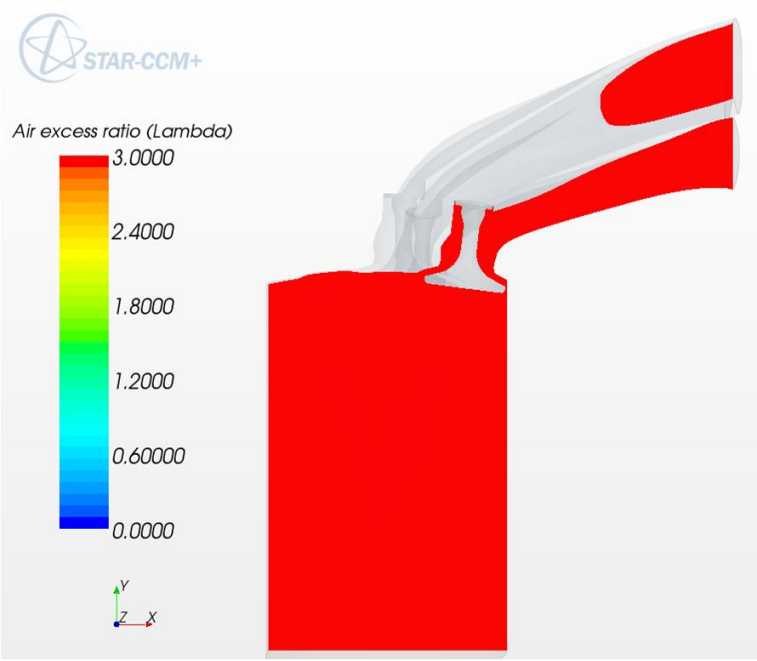

Figure 7.3. *Air excess ratio at poppet valve lift 5 mm. [47].*

Because of the shape of the gas edges and valve lift, cylinder scavenging is possible. The valve should be opened enough much that enough air flow to the cylinder. Howev-

er, too large valve lift should be avoided that gas is not possible to flow into the cylinder.

7.2.2 Valve lift 6 mm

Figure 7.4 presents flow velocity of air-gas mixture when the poppet valve lift is 6 mm. As the figure shows, maximum velocity of mixture is higher than using poppet valve lift 5 mm.

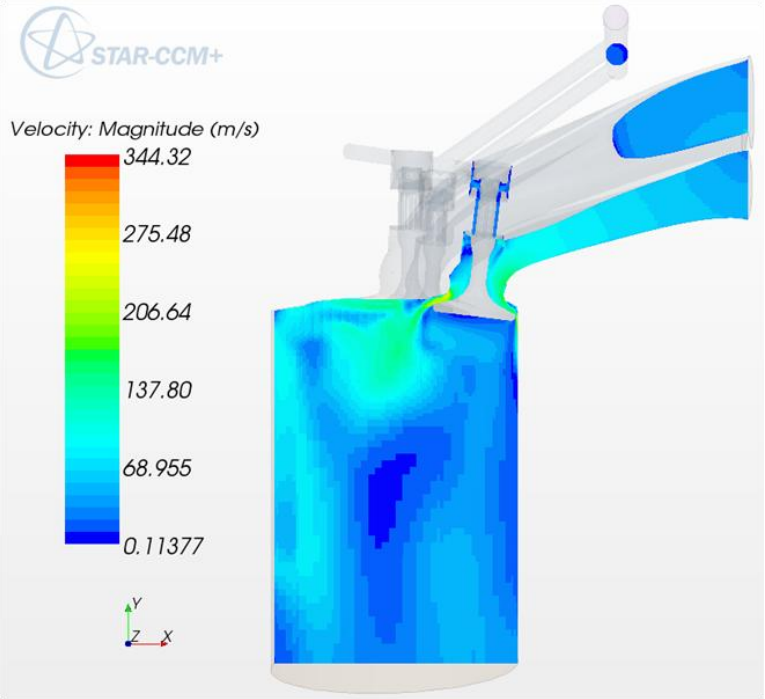

Figure 7.4. *Valve lift 6 mm, side view. [47].*

Figure 7.5 shows the air excess ratio at the poppet valve lift 6 mm. Compared to the valve lift using 5 mm, also methane gas flows into the cylinder.

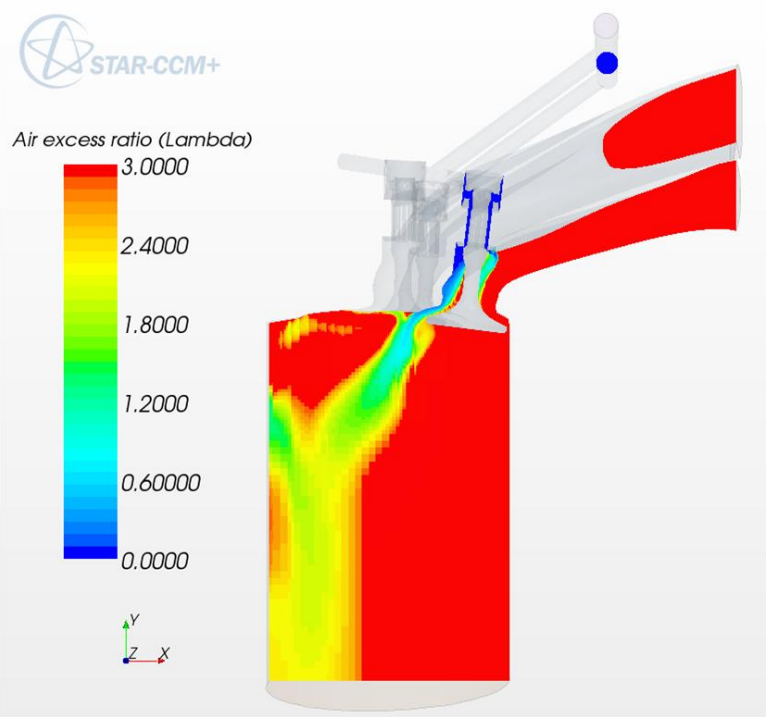

Figure 7.5. *Air excess ratio at poppet valve lift 6 mm. [47].*

As the figure 7.5 shows, methane flows mainly from the left side of the poppet valve. Thus, on the left side of the poppet valve gas mixture is much richer than on the right side. It is also noticeable that gas mixture is not homogenous in the cylinder. For the valve lift 6 mm in steady-state simulation, uniformity index is 0.168 [47].

7.2.3 Valve lift 7.5 mm

Figure 7.6 presents flow velocity of the air-gas mixture when the poppet valve lift is 7.5 mm. In comparison to the previous flow velocity presented in figure 6.4, the maximum velocity value of the gas mixture is higher at valve lift 7.5 mm.

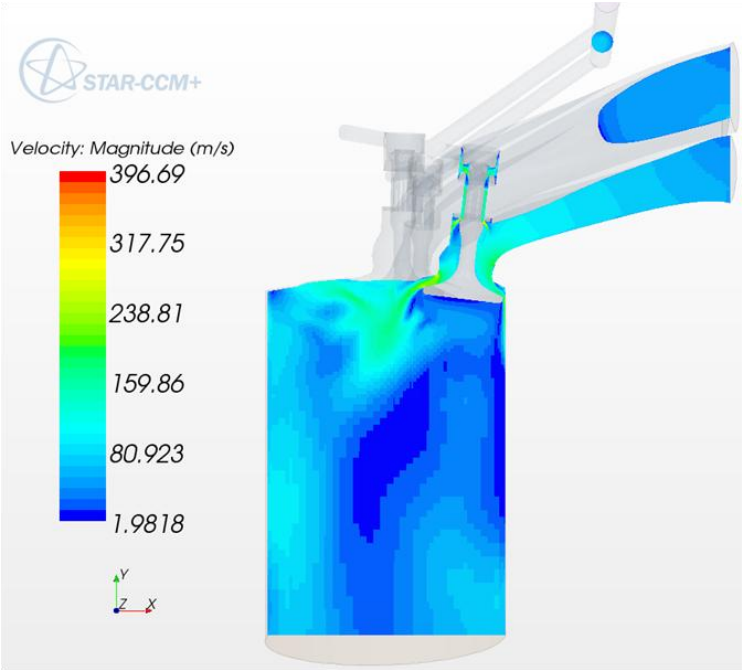

Figure 7.6. *Valve lift 7.5 mm, side view. [47].*

Figure 7.7 shows air excess ratio at the poppet valve lift 7.5 mm.

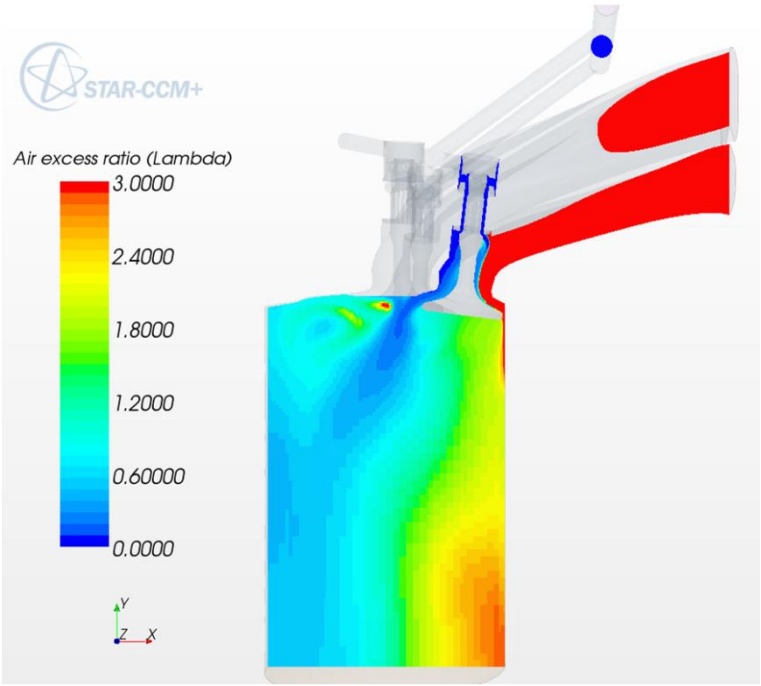

Figure 7.7. *Air excess ratio at poppet valve lift 7.5 mm. [47].*

At the poppet valve lift 7.5 mm in steady-state simulation, uniformity index is 0.168 [47].

7.2.4 Valve lift 8.5 mm

Figure 7.8 presents flow velocity of the air-gas mixture at the poppet valve lift 8.5 mm. Velocity of air-gas mixture is close to the results using poppet valve lift 7.5 mm but the maximum value of velocity is a little bit lower than using valve lift 7.5 mm.

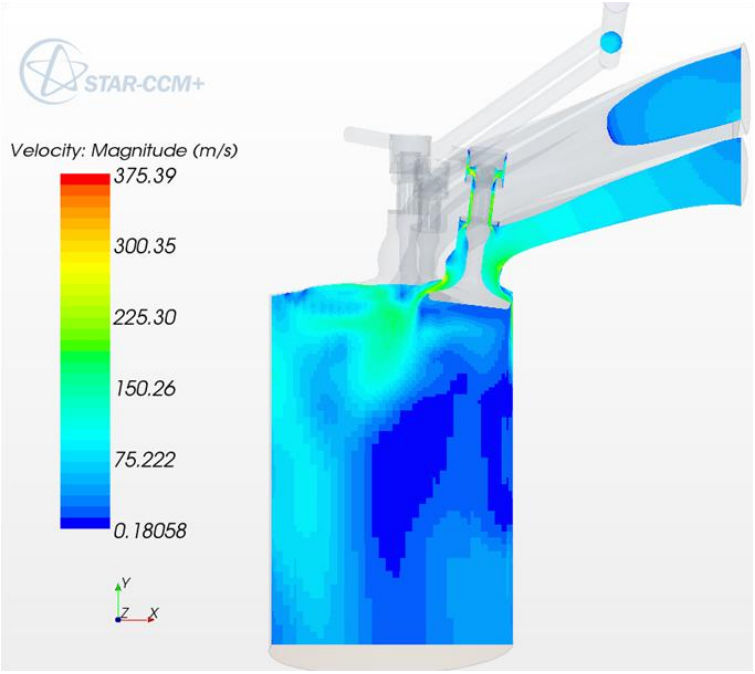

Figure 7.8. *Valve lift 8.5 mm, side view. [47].*

Figure 7.9 shows the air excess ratio at the poppet valve lift 8.5 mm. The figure shows that the area where air excess ratio is 3.0 is larger than using valve lift 7.5 mm. This area is on the right side of the cylinder.

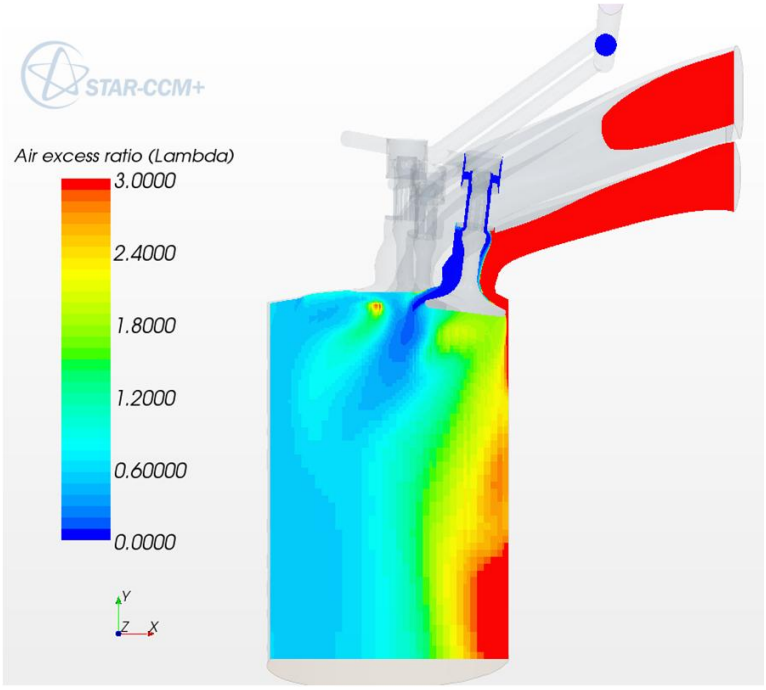

Figure 7.9. *Air excess ratio at poppet valve lift 8.5 mm. [47].*

At the poppet valve lift 8.5 mm in steady-state simulation, uniformity index is 0.075 [47]. Thus, the uniformity index value is lower than at the poppet valve lift 7.5 mm.

7.2.5 Valve lift 10 mm

Figure 7.10 presents flow velocity of air-gas mixture at the poppet valve lift 10 mm. Maximum flow velocity value is higher than using lower poppet valve lifts.

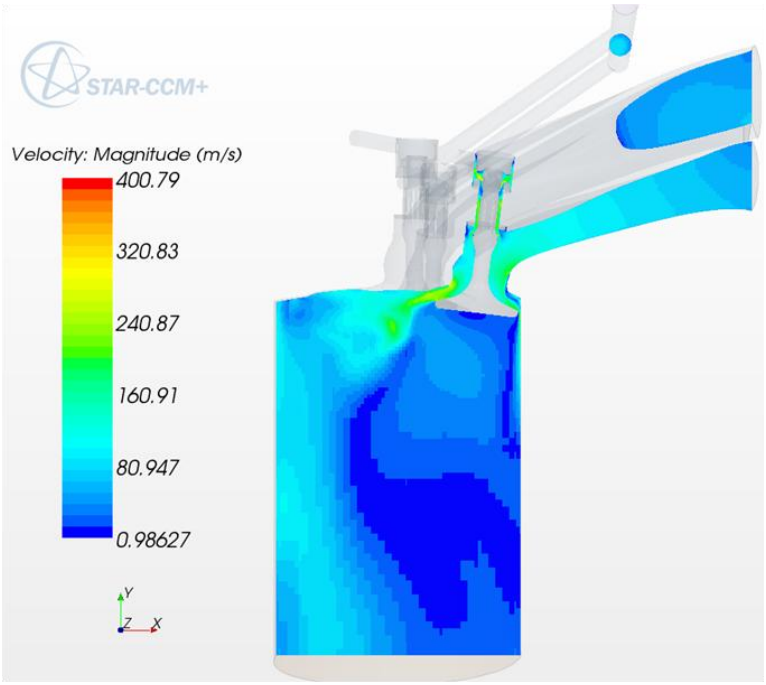

Figure 7.10. *Valve lift 10 mm, side view. [47].*

Figure 7.11 presents the air excess ratio at the poppet valve lift 10 mm. Compared to valve lift 8.5 mm, on the right side of the cylinder where air excess ratio is 3, the area is larger. Also on the top of the cylinder there is obviously area where air excess ratio is 3.

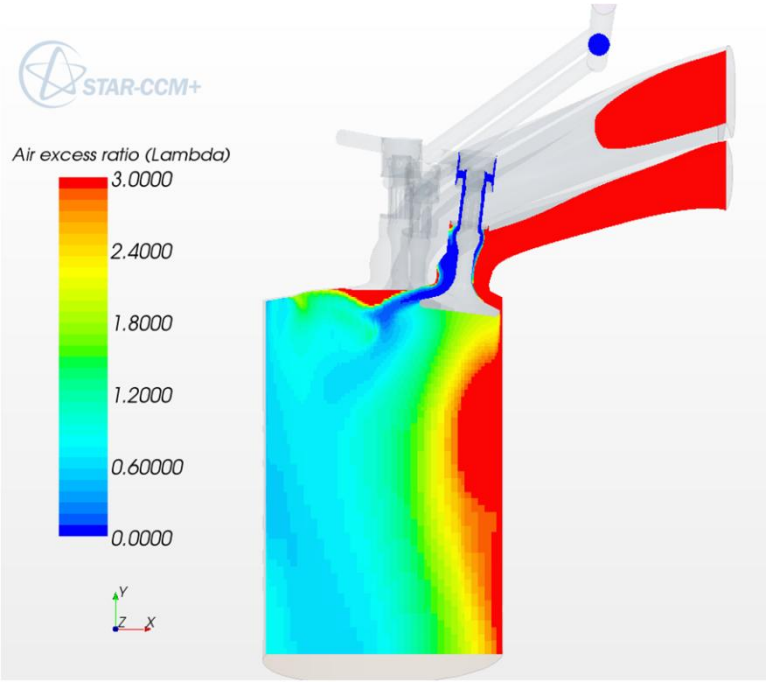

Figure 7.11. *Air excess ratio at poppet valve lift 10 mm. [47].*

At the poppet valve lift 10 mm in steady-state simulation, uniformity index is 0.104 [47]. The value is a little bit higher than using valve lift 8.5 mm but still lower than using poppet valve lift values 6 mm and 7.5 mm.

7.2.6 Valve lift 15 mm

Figure 7.12 presents flow velocity of air-gas mixture at poppet valve lift 15 mm. As the figure shows, maximum velocity value is higher than using lower poppet valve lifts.

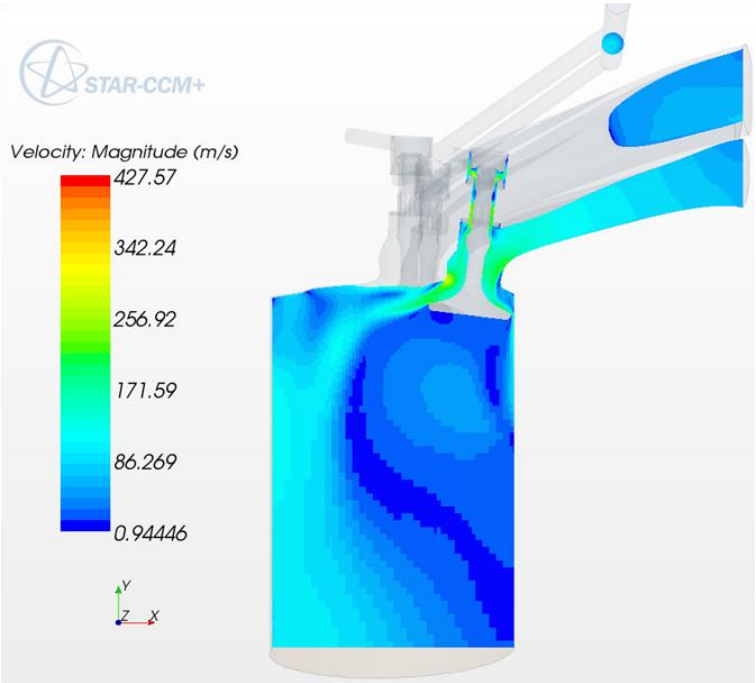

Figure 7.12. *Valve lift 15 mm, side view. [47].*

Figure 7.13 shows the air excess ratio at the poppet valve lift 15 mm. Compared to previous air excess ratio figure, air excess ratio is much lower on the right side of the cylinder.

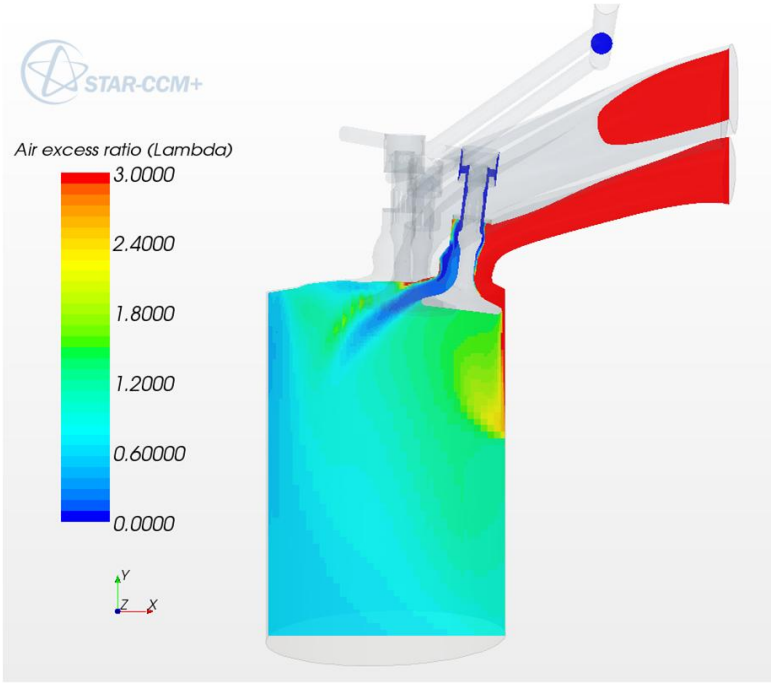

Figure 7.13. *Air excess ratio at poppet valve lift 15 mm. [47].*

As figure 7.13 shows, on the left side of the poppet valve the value of air excess ratio is near zero and on the right side ratio is three. Thus, gas flows still from the left side of the poppet valve and air flows from the right side. For the valve lift 15 mm in steady-state simulation, uniformity index is 0.84 [47]. The value is significantly higher than using lower valve lifts.

7.3 Comparing steady-state flow rates

The following table 7.4 presents steady-state simulation flow rates of Simulink and CFD models at precise valve lifts.

Table 7.4. *Steady-state mass flow rates at precise poppet valve lifts.*

Lift [mm]	Mass flow, Simulink model [g/s]	Mass flow, CFD results [g/s]
5	1430	1435
6	1655	1659.6
7.5	1930	1932.1
8.5	2076	2075.5
10	2204	2200.2
15	2359	2346.4

The following table 7.5 shows the differences between Simulink and CFD steady-state flow rate results. The differences are calculated with the following equation using CFD values as reference values:

$$Difference\ \% = \frac{|Mass\ flow_{CFD} - Mass\ flow_{Simulink}|}{Mass\ flow_{CFD}} * 100\% \quad (109)$$

Table 7.5. *Differences between Simulink and CFD steady-state simulation flow rates.*

Lift (mm)	Difference %
5	0.35
6	0.27
7.5	0.11
8.5	0.02
10	0.17
15	0.54

Average value of difference percent values shown in the table 7.5 is 0.24 % and median value is 0.22 %.

The following figure presents simulated flow rates. Simulated Simulink results are given using valve lift range [0, 15] mm using one millimeter step values. CFD results are given using lift values shown in table 7.5.

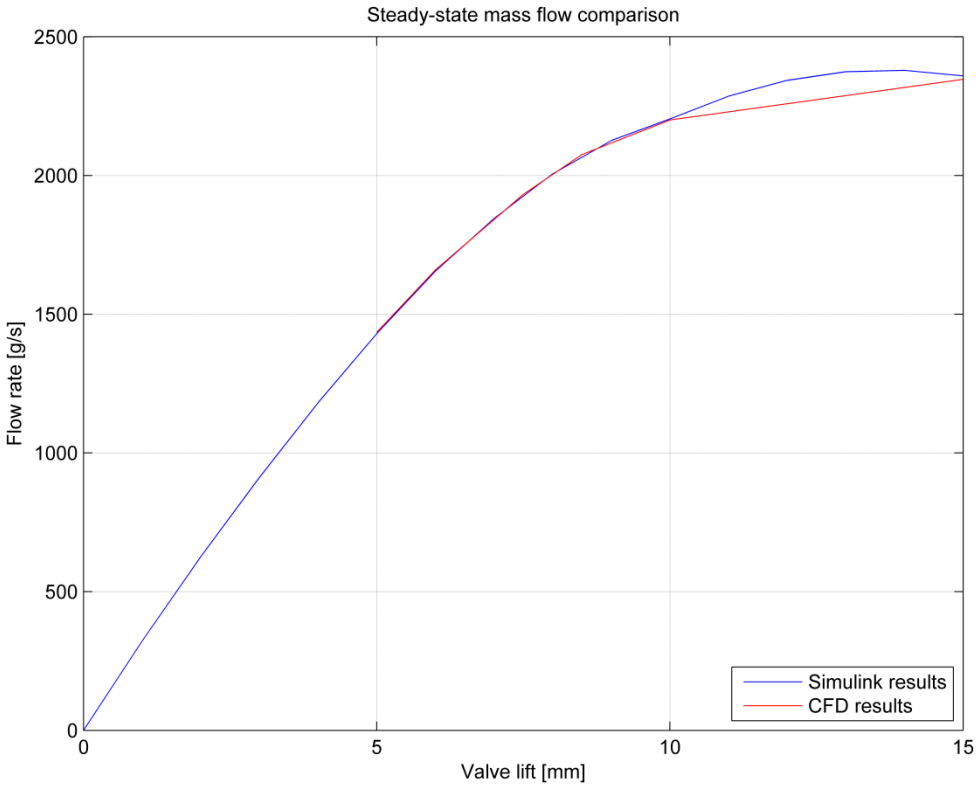

Figure 7.14. *Original Simulink and CFD flow rate results.*

As the figure (7.14) and tables 7.4 and 7.5 show, the simulated results are very similar between lift values [5, 10] mm. Because original high valve lift CFD results are done using two valve lift values, 10 and 15 mm, the curve of CFD result is linear between these valve lifts.

When the original flow rate values are fit to second order polynomial function using Matlab function 'polyfit', the following flow rate equations are given:

$$flow\ rate\ simulink(L_v) = -13.2 * L_v^2 + 355.94 * L_v - 18.65 \quad (110)$$

$$flow\ rate\ CFD(L_v) = -13.23 * L_v^2 + 354.24 * L_v + 5.78 \quad (111)$$

The following figure presents flow rate curves using equations (110) and (111).

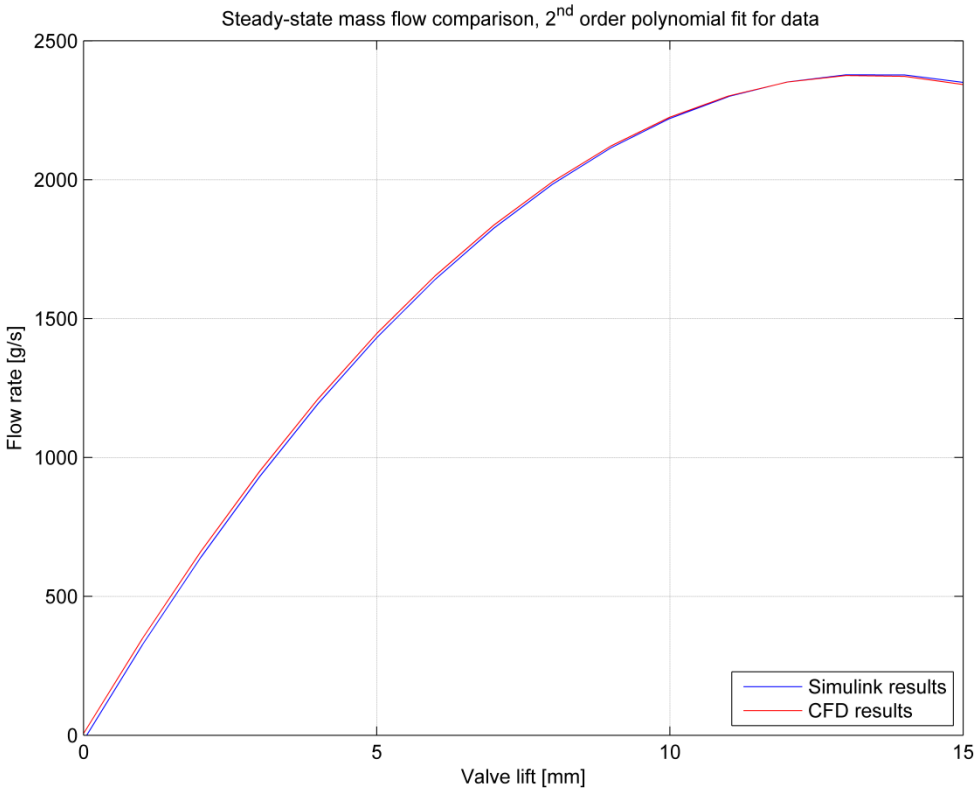

Figure 7.15. *Steady-state mass flow comparison, second order polynomial fit*

As the figure 7.15 and the table 7.5 show, the difference between models is insignificant and using the results, the mass flow rate through the poppet valves can be determined at any valve lift value, accurately.

8 CONCLUSIONS

Methane and natural gases are excellently suited to applications of high compression ratios. However, using gas engine knocking and methane slip exist and these flaws should be avoided. By changing the valve timings and filling the dead volumes of engine are effective ways to reduce blowing gas in overlap period and unburned gas entering the clearance volumes. Gas permeation membrane reduces effectively unburned methane emission but also increases NO_x emissions because of increased combustion temperature.

Single-point injection system enables simpler and often cheaper solution to inject fuel to engine. However, due to continuously increasing environmental demands and more strict emission regulation, multi-point injection is often the only possible way to inject fuel to engine.

Digital hydraulic systems using two and four DFCUs and digital pneumatic system have been modelled and simulated. Hydraulic system enables full controllability of poppet valve train and digital system is more energy efficient than hydraulic system using conventional proportional valve. The main issue of the simulation point of view is to define correct controller parameters for the system that correct amounts of air and gas are fed into the cylinder. As the calculations show, amount of needed air is significantly larger than methane per one cycle. The comparison of steady-state flow rate values show that results of CFD and Simulink models are almost equal and there is in average only 0.24 percent difference between models. Because early Miller cycle is used, ultra fast valves are needed with large flow rate at small pressure difference. In the simulation results, response time from 0.8 ms to 1 ms and nominal flow rate 60 l/min at pressure difference 0.5 MPa have been used using 6 valves per DFCU.

Using digital hydraulic system, reference velocity as the input value for the model-based controller has been used. The main idea of the controllers used in this thesis is to calculate and select the controlling modes which use as less energy as possible and still enables as well as possible the required input references. As the energy comparison results show, using digital hydraulic system, two DFCUs with 25 MPa supply pressure is the most energy efficient system which has been simulated. Digital hydraulic system is also fault tolerant and it is one of the main benefits of the system compared to conventional system using proportional valve. As the results show in the chapter 6.5, the digital

hydraulic system using four DFCUs tracks better velocity reference values than the system using two DFCUs. Amount of velocity error is smaller using four DFCUs.

Digital pneumatic valve system enables precise controllability of gas and the system is fault tolerant. When one big valve is replaced with a number of smaller valves, inertia of the valve is significantly lower, needed amount of energy is lower and the valve is faster. However, total flow rate using a number of smaller valves can be the same than using just one big valve.

The main benefit between the designs of intake air valve with gas flow edges and conventional gas admission valve located to intake manifold is that distance travelled by the gas flow is shorter when grooved intake air valve is used. Because intake air valve should be opened at every intake cycle it is natural choice to integrate gas flow edges to poppet valve.

As the results show, the design of the poppet valve with gas flow edges is a realistic construction and air-gas mixture is possible to feed into the cylinder. The next steps would be to optimize the design of the intake air valve and gas flow edges, and construct the prototype. The simulation results which are presented in the thesis are possible then to verify by using measurement results of the prototype.

REFERENCES

[1] Tajima, H. and Tsuru, D. 2013. Reduction of Methane Slip from Gas Engines by O_2 Concentration Control using Gas Permeation Membrane. SAE Technical Paper 2013-01-2618.

[2] G. Karim and H. Li, Knock in Gas Fueled S.I.Engines. Mechanical and Manufacturing Engineering, University of Calgary, Calgary, Canada T2N 1N4.

[3] Masters of gas engine technology. Twenty-four7, 01/2013. Available: http://www.wartsila.com/file/Wartsila/en/1278531145652a1267106724867-Masters-of-Gas-Engine-Technology.pdf. Cited 17.10.2013.

[4] Haraldson, L,. general manager, alternative NOx solutions, LNG as a fuel for environmentally friendly shipping, retrofit perspective, 33rd motorship propulsion & emissions conference, Copenhagen, 11-12 May 2011, Wärtsilä Corporation.Available: http://www.wartsila.com/file/Wartsila/1278519213998a1267106724867-Wartsila-SP-ppt-2011-LNGretrofit.pdf. Cited 16.12.2013.

[5] General Descriptions, Definitions and Main processes, 4-stroke professionals, presentation, Harry Särs, 6.5.2013.

[6] Modern, highly efficient and flexible combustion engines, 2014, Wärtsilä. Available:http://www.wartsila.com/en/power-plants/technology/combustion-engines/introduction. Cited 7.1.2014.

[7] Antila, E. and Turunen, R. Extreme value engine tests with advanced Miller-cycle (EVE AM), Cycle simulations.

[8] Miller time, the Miller cycle engine explained, 2007, Available: http://www.motivemag.com/pub/feature/tech/Motive_Tech_Miller_Time_-_The_Miller_Cycle_Engine_Explained.shtml. Cited 28.11.2013.

[9] Operational Information, The Miller Cycle and Emissions Reduction. Available: http://www.marinedieselsinfo/2_stroke_engine_parts/Other_info/miller_cycle.htm. Cited 27.8.2013.

[10] Early closing miller cycle internal combustion engine. United States patent 2002026913.

[11] NaturalGas.org, The Combustion of Methane. Available: http://naturalgas.org/overview/combustion/. Cited 17.10.2013.

[12] Oulun yliopisto, Konetekniikan osasto, Polttomoottoritekniikka I, Internal Combustion Engines I, Mauri Haataja, 2010.

[13] Z. Qiang et al, 2013, Experiment Study of the Single Point And Multi-Point Natural Gas Electronic Injection Systems, Applied Mechanics and Materials Vols. 313-314 (2013), pp. 479-483.

[14] Single-point and multi-point injection. Available: http://www.kfz-tech.de/Zentraleinspritzung.htm. Cited 27.8.2013.

[15] Rosli Abu Bakar et al, 2012, Application of Natural Gas for Internal Combustion Engines, Advances in Natural Gas Technology, Dr. Hamid Al-Megren (Ed.), ISBN: 978-953-51-0507-7, InTech, Available: http://www.intechopen.com/books/advances-in-natural-gas-technology/application-of-natural-gas-for-internal-combustion-engines.Cited 7.10.2013.

[16] Heywood, J., Internal Combustion Engine Fundamentals, 1988, ISBN: 0-07-028637-X.

[17] Single injector, single point fuel injection system. United States Patent 4257376.

[18] Multi-point fuel injection module. European patent application 1 304 477.

[19] Fundamentals of Combustion. University of Toronto, Institute for Aerospace. Lecture Notes, subject 6. Available: http://utias.utoronto.ca/~ogulder/ClassNotes6.pdf. Cited 28.11.2013.

[20] Kondo Shigeo, et al. Effect of Pressure and Oxygen Concentration on Quenching Distances Flammable Gases. Nippon Kagaku Kaishi. 7 (1992), pp. 788-792.

[21] Oxygen-enriched air. Membrane Technology and Research, Inc. 39630 Eureka Drive, Newark, CA 94560, 2011. Available: http://www.mtrinc.com/oxygen-enriched_air.html. Cited 16.10.2013.

[22] Meeting on Tuesday 20.8.2013 with Pasi Juppo, Håkan Nynäs, Jonathan Rösgren, Hannu Sillanpää and Harry Särs. Digital hydraulics MSc thesis subject.

[23] SOGAV 250. Solenoid Operated Gas Admission Valve. Product Specification. Available: http://www.woodward.com/EngineAdmissionValves.aspx. Cited 15.8.2013.

[24] Heikkilä, M., Aalto University. Digital hydraulics review, Wärtsilä Corporation, 7.10.2010.

[25] IHA-2570, Digital hydraulics, course material, 2012.

[26] Bibus Solenoid valves 850 series. Matrix Technical Information. Available: http://www.bibus.co.uk/fileadmin/editors/countries/bibuk/product_data/matrix/documents/matrix_technical_information_en.pdf. Cited 7.10.2013.

[27] IHA-2580, Advanced course in digital hydraulics, course material, 2013.

[28] Beater, P., Pneumatic Drives, System Design, Modelling and Control, Springer-Verlag Berlin Heidelberg 2007, ISBN: 978-3-540-69470-0.

[29] Cheung, N.C. et al. Modelling a Linear and Limited Travel Solenoid. University of New South Wales, Australia. Published in: Industrial Electronics, Control, and Instrumentation, 1993. ISBN: 0-7803-0891-3. Pp. 1567-1572, vol. 3.

[30] Nynäs, H., Gas valve, presentation, 10.10.2013.

[31] Bucher Hydraulics Series WS22GD/OD, 2/2 Cartridge Seat Valve, Size 5. Available: http://www.bucherhydraulics.com/31577/Mobile-and-Industrial-hydraulics/Products/Valves/Directional-seat-valves/Cartridge-valves/index.aspx. Cited 23.9.2013.

[32] Conversation with Jukka Myllymäki, Bucher Hydraulics, Sales Nordic Countries, 30.9.2013.

[33] Johnson et al. 2001 Sturman Digital Latching valve, 7th Scandinavian International Conference on Fluid Power, Linköping, Sweden. Cited 17.9.2013.

[34] MathWorks Documentation Center, One-based indexing. Available: http://www.mathworks.se/help/matlab/matlab_external/pass-arrays.html. Cited 10.10.2013.

[35] Metso Develops Controller for Energy-Saving Digital Hydraulic System for Papermaking Equipment Using Model-Based Design, 2013, Available: http://www.mathworks.se/company/user_stories/Metso-Develops-Controller-for-Energy-Saving-Digital-Hydraulic-System-for-Papermaking-Equipment-Using-Model-Based-Design.html. Cited 6.1.2014.

[36] Dorf, C. and Bishop, H. Modern control systems. 12th edition. ISBN-13: 978-0-13-602458-3.

[37] Modelica Language Documents, The Modelica Specifications, version 3.3. Available https://www.modelica.org/documents/ModelicaSpec33.pdf. Cited 4.2.2014.

[38] I. Schepers et al. 2011, A Novel Model for Optimized Development and Application of Switching Valves in Closed Loop Control, International Journal of Fluid Power, Vol. 12, No. 3, pp. 31-40.

[39] Ellman, A. & Piche, R. 1996. A Modified Orifice Flow Formula for Numerical Simulation of Fluid Power Systems. Fluid Power Systems and Technology, ASME

[40] IHA-2600, Modelling and simulation of fluid power systems, course material, 2011.

[41] Meeting on Wednesday 15.1.2014 with Antonino Di Miceli, Jari Hyvönen, Lars Ola Liavåg and Harry Särs. Digital gas admission valve, gas amount, valve timing and CFD.

[42] Wärtsilä W190 intake valve CAD model.

[43] Valve and valve mechanism. Available: http://elearning.vtu.ac.in/P7/enotes/AU51/Unit8-DP.pdf. Cited 17.10.2013.

[44] Pneumatic fluid power, components using compressible fluids, determination of flow rate characterictics. ISO-6358.

[45] Peurala, J. and Saarinen, T. 2013, IHA-2801, hydraulics, special assignment and seminar. Modelling and simulation of mechatronic system with OpenModelica.

[46] Slotine, J. And Li, W. Applied nonlinear control, 1991, ISBN: 0-13-040890-5.

[47] Di Miceli, A. Steady-state simulations of the W190 inlet port flow with digital gas admission presentation.

[48] Othmer et al. 2006. Computation of topological sensitivities in fluid dynamics: cost function versatility.
Available: http://www.fastopt.com/papers/othmeral06.pdf. Cited 6.3.2014.

[49] MAT-45700, Introduction to scientific computing with MATLAB, course material 2013.

[50] Combinations of input vectors. Available: https://raw.github.com/Psychtoolbox-3/Psychtoolbox-3/beta/Psychtoolbox/PsychProbability/CombVec.m.
Cited 10.10.2013.

[51] Create all combinations of vectors. Available:
http://www.mathworks.se/help/nnet/ref/combvec.html. Cited 10.10.2013.

APPENDIX A: DFCU STATE MATRIX

PCM -coded control matrix using 5 valves.

Valve 1	Valve 2	Valve 3	Valve 4	Valve 5
0	0	0	0	0
1	0	0	0	0
0	1	0	0	0
1	1	0	0	0
0	0	1	0	0
1	0	1	0	0
0	1	1	0	0
1	1	1	0	0
0	0	0	1	0
1	0	0	1	0
0	1	0	1	0
1	1	0	1	0
0	0	1	1	0
1	0	1	1	0
0	1	1	1	0
1	1	1	1	0
0	0	0	0	1
1	0	0	0	1
0	1	0	0	1
1	1	0	0	1
0	0	1	0	1
1	0	1	0	1
0	1	1	0	1
1	1	1	0	1
0	0	0	1	1
1	0	0	1	1
0	1	0	1	1
1	1	0	1	1
0	0	1	1	1
1	0	1	1	1
0	1	1	1	1
1	1	1	1	1

APPENDIX B: COMBINATION OF VECTORS

Reference: [49], [50], [51].

CombVec –function is included in Matlab Neural Network Toolbox. However, it was not available straight at Wärtsilä. Combination of vectors generates all possible combinations of input vectors.

Example: Vectors are: a = [1 2], b = [3 4], c = [5 6]
Combinations of these vectors are: d = [1 2 1 2 1 2 1 2; 3 3 4 4 3 3 4 4; 5 5 5 5 6 6 6 6]

The function takes any number of inputs because of using varargin (variable length input argument list) as input.

Code:

```
function Combination = CombVec(varargin)

if isempty(varargin)
    Combination = [];

else

    Combination = varargin{1};

    for i = 2:length(varargin)
        cur = varargin{i};
        Combination = [copyb(Combination,size(cur,2));
copyi(cur,size(Combination,2))];

    end

end

function b = copyb(mat,s)

[mr,mc] = size(mat);
inds    = 1:mc;
inds    = inds(ones(s,1),:).';
b       = mat(:,inds(:));

function b = copyi(mat,s)

[mr,mc] = size(mat);
inds    = 1:mc;
inds    = inds(ones(s,1),:);
b       = mat(:,inds(:));
```

APPENDIX C: FINDING MINIMUM INDEX

Figure C1 shows the graphical idea of finding minimum index block. Input is states of valves and outputs are minimum value of states and zero and one based indexes. The function finds the index and minimum value of input.

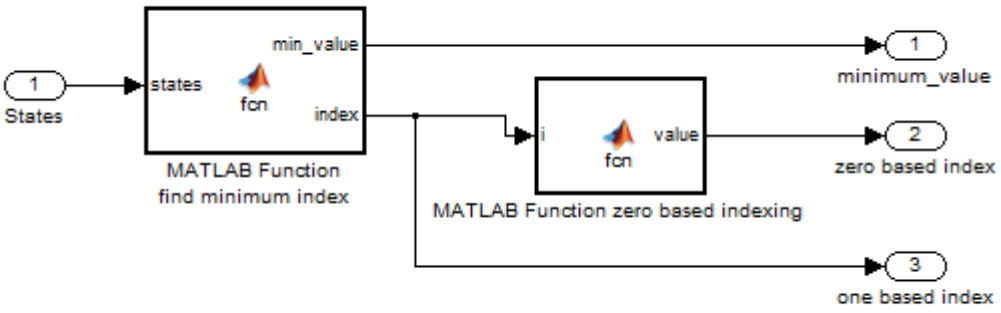

Figure C.1. *Finding zero and one-based indexes and minimum value of state*

Code find index and minimum value:

```
function [min_value,index] = fcn(states)

[min_value,index] = min(states)
```

Matlab function zero based indexing converts input of one-based matrix index to zero-based matrix index. Because zero-based indexing mode is used in selector block in Simulink model, zero based index converter was needed.

```
function value = fcn(i)

i_min = 1;

  value = i - i_min;

  return

end
```

APPENDIX D: POPPET VALVE FORCES AND INITIAL CHAMBER PRESSURES

The initial chamber pressures have been determined using force balance equations:

$$p_{B\ initial} = p_{supply\ pressure} \tag{1}$$

$$p_{A\ initial} = \left(-F_{mass} - F_{air} + F_{spring} + F_{cylinder} + F_{B-chamber}\right)/A_{A-chamber} \tag{2}$$

As the equation (1) shows, initial pressure of B-chamber is supply pressure of the system. Equation (2) shows that initial pressure of A-chamber has been determined using force balance of poppet valve. The following table shows how the forces have been determined.

Table D.1. *Force equations*

Force	Equation
$F_{A\text{-chamber}}$	$p_A * A_{A-chamber}$
$F_{B\text{-chamber}}$	$p_B * A_{B-chamber}$
F_{air}	$3 * A_{gas} * p_{intake\ air}$
$F_{cylinder}$	$3 * A_{valve\ head} * p_{initial\ cylinder}$
F_{mass}	$3 * m_{poppet\ valve} * a_{gravitational}$

Figure D.1 shows force balance of poppet valve. Positive direction is up.

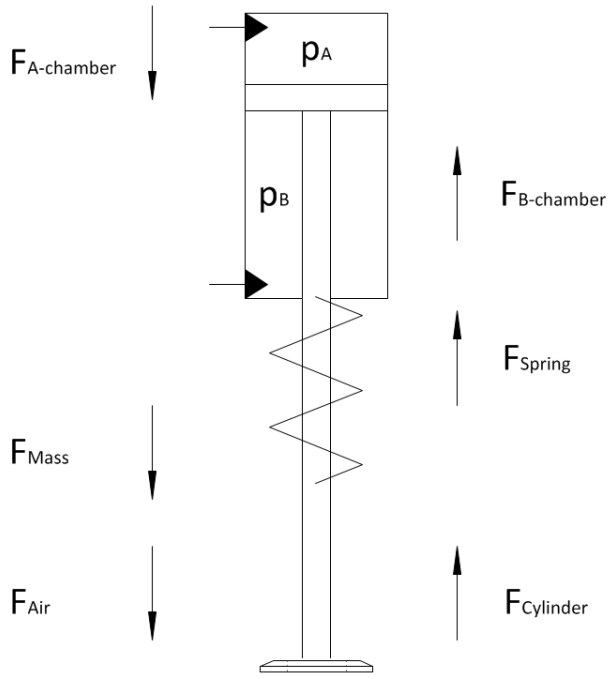

Figure D.1. *Poppet valve force balance.*

APPENDIX E: POPPET VALVE GAS EDGES AND INLET VALVE PARAMETERS

The following table shows gas flow area calculations. Given values are coloured with blue, calculated values with red.

Table E.1. *Determining gas flow area*

Parameter	Value:
Stem diameter:	$D_s = 16\ mm$
Amount of edges:	$a_e = 8$
Distance of curve between edges:	$x_d = 1.8\ mm$
Circuit of circle:	$p = 2\pi\frac{D_s}{2} = 50.265\ mm$
Circle of edge:	$x_c = \frac{p - a_e x_d}{a_e} = 4.483\ mm$
Height of outer edge:	$h_2 = \frac{D_s}{2}\left(1 - cos\left(\frac{180° x_c}{D_s \pi}\right)\right) = 0.312\ mm$
Length of edge:	$s_e = \sqrt{\left(\frac{D_s}{2} - \frac{h_2}{2}\right) 8h_2} = 4.425\ mm$
Area of outer edge:	$A_2 = \frac{h_2}{6s_e}\left(3{h_2}^2 + 4{s_e}^2\right) = 0.924\ mm^2$
Height of inner edge:	$h_1 = 2\ mm$
Area of inner edge:	$A_1 = \frac{h_1}{6s_e}\left(3{h_1}^2 + 4{s_e}^2\right) = 6.804\ mm^2$
Total area:	$A_{total} = A_1 + A_2 = 7.727\ mm^2$
Total area of edge per valve:	$A_{valve} = a_e A_{total} = 6.182 \cdot 10^{-5}\ m^2$

The table E.2 shows used inlet valve parameters in the simulation models.

Table E.2. *Inlet valve parameters using valve head diameter 40 mm*

Inner seat diameter	35.5	mm
Valve head diameter	40	mm
Port diameter	51.6	mm
Seat width	0.9	mm
Seat angle	11	deg
Mean seat diameter	39.1	mm
Stem diameter	7	mm

APPENDIX F: GAS AMOUNT CALCULATIONS

The following table shows gas admission quantity when cylinder power is 190 kW, speed of engine is 1000 rpm and efficiency of engine is 47%. Given values are coloured with blue, calculated values with red.

Table F.1. *Gas amount calculations*

Engine data								Gas properties		
Configuration	Cylinders	Power/cyl	Speed	Efficiency	Engine power	Required input/cylinder		LHV	Normal density	Admission quantity
1=L, 2=V	no	kW	rpm	%	kW	kWh	MJ	MJ/m^3	kg/m^3	g/inj
2	8	190	1000	47,0 %	1520	404,3	1455	30	0,816	1,3195

APPENDIX G: HYDRAULIC SIMULATION MODELS, COMMON PARAMETERS

Table G.1. *Poppet valve and gaseous parameters*

Parameter	Value	Unit
Gas pressure	0.58e6	Pa
Intake air pressure	0.5e5	Pa
Cylinder pressure	0.332e6	Pa
Density of methane	0.816	kg/m^3
Density of air	1.3	kg/m^3
Kappa constant to air	1.4	-
Kappa constant to methane	1.32	-
Methane temperature	298.15	K
Air temperature	318.15	K
Mass of one poppet valve	1	kg
Initial spring force of poppet valves	2700	N
Poppet valve spring coefficient	120	N/m

Table G.2. *Shape of gas edge*

Y	0	0	0	0.3	1	1	1	1	1	1
X	1/15	2/15	5/15	5.5/15	6/15	7.5/15	8.5/15	10/15	13/15	15/15

Table G.3. *Hydraulic system parameters*

Parameter	Value	Unit
Bulk modulus of oil	1200e6	Pa
Hydraulic cylinder piston diameter	26e-3	m
Piston rod diameter	20e-3	m
Dead volumes of cylinder (A and B side)	0.1e-3	m^3
DFCU flow rate	60	l/min
Nominal pressure difference	0.5e6	Pa
Number of valves per DFCU	6	-

Table G.4. *Friction and damper model parameters*

Viscous friction coefficient	8 % * Supply pressure * Area of A-chamber
Static friction	8 % * Supply pressure * Area of A-chamber
Coulomb friction	70 % * Static friction
Velocity of minimum friction	8 mm/s
Tanh parameter	5000
Position of damper	3 mm
Damping factor	4500 Ns/m

APPENDIX H: SPECIFIC SIMULATION PARAMETERS, 2 X DFCU, SUPPLY PRESSURE 30 MPA

Table H.1. *Controller parameters*

Parameter	Value	Unit
Controller sample time	1e-3	s
Controller time constant	1e-3	s
Valve switching cost	0	-
Short-circuit cost	2/60000	-
Position controller gain	124	.
Minimum velocity controller	-2	m/s
Maximum velocity controller	2.1	m/s

Table H.2. *System parameters*

Parameter	Value	Unit
Delay of valve	0.8e-3	s
Movement time	0.2e-3	s
Sticking time	0.1e-3	s
Supply pressure	30e6	Pa
Tank pressure	0e6	Pa
Maximum area of gas edge per poppet valve	0.64e-4	m^2

APPENDIX I: SPECIFIC SIMULATION PARAMETERS, 2 X DFCU, SUPPLY PRESSURE 25 MPA

Table I.1. *Controller parameters*

Parameter	Value	Unit
Controller sample time	1e-3	s
Controller time constant	0.5e-3	s
Valve switching cost	0	-
Short-circuit cost	2/60000	-
Position controller gain	147	.
Minimum velocity controller	-2.0	m/s
Maximum velocity controller	2.2	m/s

Table I.2. *System parameters*

Parameter	Value	Unit
Delay of valve	0.8e-3	s
Movement time	0.2e-3	s
Sticking time	0.1e-3	s
Supply pressure	25e6	Pa
Tank pressure	0e6	Pa
Maximum area of gas edge per poppet valve	0.64e-4	m^2

APPENDIX J: SPECIFIC SIMULATION PARAMETERS, 4 X DFCU, SUPPLY PRESSURE 30 MPA

Table J.1. *Controller parameters*

Parameter	Value	Unit
Low-pass filtering, controller Ts sample time	0.1e-3	s
Controller sample time	1e-3	s
Low-pass filter time constant (load force LP filter)	1e-3	s
Controller time constant	1e-3	s
Pressure error coefficient	1e-16	-
Switching coefficient	19500	-
Maximum pressure	30e6	Pa
Minimum pressure	2e6	Pa
Reference pressure difference	2e6	Pa
Force threshold	100	N
Velocity threshold	200e-3	m/s
Position controller gain	126	-
Minimum velocity controller	-1.7	m/s
Maximum velocity controller	1.6	m/s

Table J.2. *System parameters*

Parameter	Value	Unit
Delay of valve	0.7e-3	s
Movement time	0.1e-3	s
Sticking time	0.05e-3	s
Supply pressure	30e6	Pa
Tank pressure	0e6	Pa
Maximum area of gas edge per poppet valve	0.62e-4	m^2

APPENDIX K: SPECIFIC SIMULATION PARAMETERS, 4 X DFCU, SUPPLY PRESSURE 25 MPA

Table K.1. *Controller parameters*

Parameter	Value	Unit
Low-pass filtering, controller Ts sample time	0.1e-3	s
Controller sample time	1e-3	s
Low-pass filter time constant (load force LP filter)	1e-3	s
Controller time constant	1e-3	s
Pressure error coefficient	9e-16	-
Switching coefficient	14000	-
Maximum pressure	25e6	Pa
Minimum pressure	2e6	Pa
Reference pressure difference	2e6	Pa
Force threshold	100	N
Velocity threshold	200e-3	m/s
Position controller gain	127	-
Minimum velocity controller	-1.9	m/s
Maximum velocity controller	2	m/s

Table K.2. *System parameters*

Parameter	Value	Unit
Delay of valve	0.7e-3	s
Movement time	0.1e-3	s
Sticking time	0.05e-3	s
Supply pressure	25e6	Pa
Tank pressure	0e6	Pa
Maximum area of gas edge per poppet valve	0.62e-4	m^2

APPENDIX L: SPECIFIC SIMULATION PARAMETERS, PNEUMATIC SYSTEM

Table L.1. *System parameters*

Parameter	Value
Number of valves on DFCU	5
Sample time	1 ms
Delay of valve	0.5 ms
Movement time of valve	0.1 ms
Sticking time of valve	0.1 ms
Throttle sizes	[7 9.9 14 19.8 28] mm
Mass flow pressure coefficient	[6.272 12.55 25.09 50.18 100.4]*10^{-8} m^3/s*Pa
Proportional controller gain	14000